CZECH TECHNICAL UNIVERSITY IN PRAGUE
FACULTY OF CIVIL ENGINEERING

Characterization and Development of Unconventional Natural Thermal Insulation Materials

Charakterizace a vývoj netradičních přírodních tepelně izolačních materiálů

HABILITATION THESIS COLLECTION OF PUBLISHED SCIENTIFIC PAPERS

Miloš Jerman

Praha, 2024

Acknowledgement

I would like to sincerely thank my colleagues for creating a productive and intellectually stimulating environment, as well as for their valuable insights and comments throughout this work. In particular, I would like to thank Professor Robert Černý for his professional support and guidance.

Abstract

The habilitation thesis consists of a set of five published scientific articles. All articles are devoted to experimental methods for obtaining a complete set of material characteristics. In the presented articles, mainly thermal insulation materials, whether commonly used as polystyrene, mineral wool, calcium silicate, various types of aerated concrete, aerated concrete, and plaster, are studied. Next, natural materials with a low or even negative carbon footprint are introduced and a newly developed thermal insulation board is presented in the final article. The experimental methods are described in detail in the papers presented and the most interesting findings are described in the commentary. Material properties were measured beyond current standards, which is particularly important for a more detailed analysis and understanding of some phenomena. The experimental results showed that the pore size distribution curve affects many material properties, especially the liquid water transport properties. The water contained in the pore structure affects other properties such as frost resistance and thermal and moisture conductivity. Experimental results show that the thermal conductivity of a material fully saturated with water is up to six times higher than in the dry state and that the thermal conductivity increases by up to 50% when the temperature of the sample is increased from 2 °C to 40 °C. When the linear hygric expansion coefficient was determined, it was found that the greatest longitudinal changes occur in areas close to zero, which are not accounted for in the standard. The test methods have provided important insights into the properties of the materials, which are crucial in several respects. Firstly, for the correct design of the building structure as a whole, then in scientific studies in the field of materials engineering, in the certification of building materials, and last but not least in the production and optimization of manufacturing processes of new materials and in the targeted development of new materials for special building applications. With these findings, the thesis contributes to the extension of the current knowledge in the field of characterization of thermal insulating building materials. At the same time, it has been demonstrated from a practical point of view that it is possible to successfully use residues from agricultural production for the production of environmentally friendly building materials.

Keywords: hygric properties, thermal properties, thermal insulation materials, biomaterials

Abstrakt

Habilitační práce je tvořena souborem pěti uveřejněných vědeckých článků. Všechny články se věnují experimentálním metodám pro získání kompletní sady materiálových charakteristik. V předložených článcích jsou studovány především tepelně izolační materiály, ať běžně používané jako jsou polystyreny, minerální vlny, kalcium silikát, různé druhy pórobetonu, pěnobeton a omítky. Dále přírodní materiály s nízkou nebo dokonce zápornou uhlíkovou stopou a v závěrečném článku je představena nově vyvinutá tepelně izolační deska. Zkušební postupy jsou podrobně popsány v předložených článcích, v komentáři jsou popsány nejzajímavější poznatky. Materiálové charakteristiky byly měřeny nad rámec platných norem, což je důležité především pro detailnější analýzy a pochopení některých jevů. Na základě experimentálních výsledků bylo prokázáno, že mnohé materiálové charakteristiky jsou ovlivněny distribuční křivkou pórů, zejména transport kapalné vody. Voda obsažená v porézní struktuře ovlivňuje další vlastnosti, jako například mrazuvzdornost, tepelnou a vlhkostní vodivost. Experimentální výsledky ukazují, že tepelná vodivost materiálu plně nasyceného vodou je až šestkrát vyšší než v suchém stavu, že tepelná vodivost stoupne až o 50 % pokud se teplota vzorku zvedne ze 2°C na 40 °C. Při stanovení součinitel délkové vlhkostní roztažnosti bylo prokázáno, že k největším délkovým změnám dochází v oblastech blízkých nule, které ovšem norma nijak nezohledňuje. Prostřednictvím zkušebních metod byly získány důležité poznatky o vlastnostech materiálů, které jsou klíčové hned z několika hledisek. Jednak pro správný návrh konstrukce jako celku, při vědeckých studií v oblasti materiálového inženýrství, pro certifikaci stavebního materiálu, v neposlední řadě při výrobě, optimalizaci výrobních postupů nových materiálů, při cíleném vyvíjení nového materiálu pro speciální stavební použití. Těmito zjištěními práce přispívá k rozšíření současného poznání v oblasti charakterizace tepelně-izolačních stavebních materiálů. Zároveň z hlediska praxe bylo prokázáno, že je možné úspěšně využít zbytky ze zemědělské výroby pro produkci ekologicky šetrných stavebních materiálů.

Klíčová slova: vlhkostní vlastnosti, tepelné vlastnosti, tepelně izolační materiály, přírodní materiály

Table of Contents

1. Introduction

The favorable conditions that prevail on our planet should by no means be taken for granted. Due to the Earth's favorable distance from the Sun, water on our planet is found in three states. This is one of the many prerequisites for life. Just to give you an idea, the temperature on Venus does not drop below 400 °C, whereas on more distant Mars, the temperature drops well below freezing, down to -60 °C on average. For the last fifteen thousand years, the climate on Earth has been relatively favorable and stable [1]. From the last ice age to the 18th century, the average temperature stabilized at 14 °C. Around the year 1750, fossil fuels began to be burned and the average temperature has increased by 1 °C since then due to human activity. The question is whether this is due to rising CO_2 levels, human population growth, rainforest clearance, swamp drainage, land reclamation, intensive agriculture, etc. In short, the Earth is demonstrably warming due to human activity. One of the biggest polluters of the environment is the construction industry.

The construction industry contributes significantly to overall environmental pollution, whether it is the extraction and consumption of primary resources, the production of greenhouse gases in the production of building materials, the transportation of individual components to the construction site, the construction process, as well as the energy spent on the operation of the building, its maintenance, heating, water heating, and lighting. It also includes the disposal of the building, the disposal of materials in landfills, and so on. As can be seen, there is great scope for achieving energy savings in all phases of the building life cycle. The land take associated with the construction of large, low-rise buildings, where, for example, large warehouses are being built on high-quality black soil around Prague, should not be overlooked [2].

This work focuses primarily on thermal insulation materials that can significantly reduce heating costs and thus partially reduce a building's carbon footprint. Due to legislative requirements, thermal insulation materials are becoming an integral part of buildings. ETICS (External Thermal Insulation Composite System) is commonly used. Today there are many very efficient synthetic materials with low thermal conductivity. One of them is polystyrene, which has a low thermal conductivity coefficient and its

major advantage is its low cost. Mineral wool is a time-tested effective thermal insulation and although more expensive than polystyrene, it is popular for its longer life. Mineral wool and polystyrene are the two most commonly used thermal insulation materials with a thermal conductivity of approximately 0.04 W MK [3]. Slightly better values are achieved by other synthetic materials such as phenolic foams or polyurethane insulation. The best values are achieved by highly efficient thermal insulations such as vacuum boards with 0.008 $W \cdot m^{-1} \cdot K^{-1}$ [4–6] and aerogel with 0.015 $W \cdot m^{-1} \cdot K^{-1}$ [7].

The above materials are made from non-renewable resources and have a carbon footprint on the environment. In addition to these synthetic thermal insulations, purely natural growing materials can also be used.

These are still perceived as alternative materials, yet they can be used for many purposes, such as building materials, acoustic insulation, thermal insulation, or as roofing. A major advantage of plant-based materials is their low ecological burden and especially their renewability [8]. Plant-based materials absorb large amounts of CO_2 during their growth by photosynthesis, and for many biomaterials, CO_2 emissions can exceed CO_2 emissions during processing, reprocessing, and production. This is of course true for plant materials. In addition to these, materials of animal origin such as sheep's wool can also be used [9].

Another advantage of natural materials is that they can create a favorable microclimate indoors. An example is sheep wool. It can absorb toxic substances and not release them further into the air. It has been shown that 1 kg of sheep wool absorbs 49.80 g of formaldehyde [9,10].

The proposal must meet a number of legislative requirements and demands. It must guarantee mechanical resistance and stability, fire safety, hygiene, and protection of health and the environment, be safe to use, protect against noise and, of course, be energy-efficient throughout its lifetime [11]. It must ensure efficient construction, durability, and trouble-free operation. In order to meet all the above criteria, the design must be carefully developed taking into account the orientation of the building in relation to the cardinal points, altitude, and location. Detailed analysis is required when designing more complex structures. Steady-state analysis alone cannot be relied upon;

water suction, water vapor accumulation, and cross effects between heat and moisture transfer must be taken into account. In this context, it should be noted that nowadays it would be quite difficult even for a very active and responsible designer to collect sufficient data for a more accurate analysis of the hydrothermal and mechanical properties of building envelope systems. Complete data are not available in many cases [12–14]. This was the main reason for writing the first two articles, where the above parameters for thermal insulation materials and two types of autoclaved concrete are determined in detail.

The thermal and humidity behavior of the structure can be verified using numerical models. The accuracy of the numerical model outputs strongly depends on the quality of the input parameters, which are the material characteristics. The material characteristics are the focus of this paper. After all, material characteristics are also used to compare competing products with each other and therefore must be measured objectively, without distortion and using the correct test procedure.

In short, the principles of materials testing must be followed. Tests must be carried out under defined conditions and in a defined manner, preferably using a test standard. The test standard generally defines the size of the sample, the number of tests, and the method of sampling, and it defines the measurement conditions, i.e., temperature and relative humidity, the age of the sample, if any, and many other factors. The standard also defines on which instruments the tests are to be carried out, how and at what intervals the test instruments are to be calibrated, the qualifications of personnel, and certification. Everything that has to be met for a material to be certified. The standard test is quite costly to perform, but the result is relatively accurate and can be used primarily to assess the quality of the tested material and as an input parameter for numerical analyses. Several types of tests must, of course, be carried out for one material.

Standard results provide valuable information about the material but are often insufficient for detailed numerical analyses to assess the behavior of the structure as a whole. In some cases, the results obtained by standard procedures do not cover the full range of material behavior. There are several examples of this: in determining the coefficient of moisture expansion, it has been shown that the greatest length changes

occur when the material moisture content is close to zero. However, this fact is not reflected in the standards. Neglecting these effects can lead to cracking of the structure.

In order to make the input parameters for the computer standards complete, tests beyond the current standards are required. Several examples can be given: individual parameters are in many cases given as constants, e.g., thermal conductivity coefficient. For aerated concrete, according to EN 73 1353, the thermal conductivity coefficient is measured in the dry state at a mean temperature of 10 °C [15]. However, this parameter is dependent on both temperature and humidity. The thermal conductivity of materials increases with increasing temperature and humidity and should be taken into account. Another example is resistance to freezing and thawing. This is determined for the extreme case, i.e., for water-saturated samples. This result is certainly valuable, but on the other hand, with proper design and maintenance of the building structure, this condition is unlikely to occur. Of more interest in assessing the service life of the structure is how the material will resist cyclic frost action under different moisture conditions.

2. Aims of the work

The primary aim of the work is to supplement missing technical information regarding the behavior and properties of construction materials, particularly thermal insulation materials. Furthermore, the goal is to obtain a complete set of material characteristics that will provide essential information to assess the overall durability of a structure, prevent potential failures, and enable the comparison of different materials. Additionally, based on the data obtained, it will be possible to evaluate alternative applications for the given materials. In order to achieve this objective, it is necessary to determine all material properties beyond the scope of current standards. The main objectives can be summarized as follows:

- To present measurements of the complete set of parameters for heat and moisture transport and accumulation in selected thermal insulation materials, with respect to their moisture content.
- To determine the freeze-thaw resistance of selected materials, again beyond the scope of current standards. The value set by the standards applies to fully saturated conditions, which should not occur in real structures. Additionally, it is essential to investigate how the material will react to cyclic freeze-thaw loading at lower moisture levels.
- To assess the impact of cyclic wetting and drying on the coefficient of moisture-induced linear expansion. Current standards do not specify this parameter across the full moisture range, and information regarding the behavior of materials at near-zero moisture levels could be crucial.
- To determine a complete set of material characteristics for new natural materials with low carbon footprints.
- To develop a new thermal insulation material from rapeseed straw without the use of adhesives, utilizing the self-bonding properties of lignin. A sub-objective is to design and evaluate the production process, particularly the effect of steaming temperature on the adhesive properties of lignin.
- To determine the thermal, moisture, and mechanical properties of the newly developed materials.

3. Comprehensive characterization of material properties

3.1. Basic physical properties

Basic physical properties include bulk density, matrix density, and porosity. For their determination, it is sufficient to know only the dimensions of the samples and their mass. Several methods exist for measuring these properties. For example, for autoclaved aerated concrete, the standard states that the bulk density is determined by the ratio of the mass to the volume of the test sample. The volume of each sample is calculated from its dimensions. The test pieces are dried at 105 ± 5 °C. The required number of solids, flatness requirements, and other conditions are given in EN 678 [16]. Another method is the vacuum saturation method using Archimedes' law. This procedure determines the bulk density of hardened concrete according to EN 12390-7 [17]. The vacuum saturation method is used to determine the density, bulk density, and open porosity of natural stone masonry units according to EN 772-4 [18]. In general, the vacuum saturation method is suitable for materials with open porosity. For materials with closed porosity, such as foamed glass or even aerated concrete, where both open and closed porosity is present, it is appropriate to use, for example, the pycnometric method for density determination. The principle of the gas pycnometric method is that a gas atom, usually helium, is small and penetrates all parts of the solid. If the solid has a closed porosity, it should be suitably prepared for the test, e.g., by grinding. The prepared body, i.e., dried and tempered, is placed in the chamber of the pycnometer. The density of the material to be tested is determined by the volume of inert helium which penetrates the structure of the material at a given pressure. See [19,20] for details. This is a standard procedure used, for example, for the determination of the density of plastics in EN ISO 1183-3 [21].

For fine-grained materials with complex pore structures, helium pycnometry should provide more accurate matrix density values than the vacuum water saturation method, despite the smaller sample size, because small helium molecules can penetrate even the smallest pores of crushed samples. Despite this assumption, the porosity of the autoclaved aerated concrete (AAC) measured in the second submitted paper using

vacuum saturation came out higher. This exception was probably due to the complex porous system of the studied AAC.

Measurements of the basic physical properties are presented in four of the five articles submitted, where the measurement methods are described in detail. For materials with closed porosity, a helium pycnometer was used. Materials with open porosity can be measured using Archimedes' law. For cellulosic materials, the bulk mass was determined from the mass and dimensions of the solids.

The basic physical properties have a direct influence on material behavior and directly affect other material properties. In general, the greater the porosity, the lower the thermal conductivity and the better the thermal insulation properties of the material. Conversely, dense materials have better mechanical properties. Porosity can be open or closed, or a combination of both. Open porosity is related to the transport of liquid water and water vapor. Water in open pores changes the material properties, increases thermal conductivity, and affects frost resistance. Water may contain various chemicals, e.g., salts, sulfates, chlorides, etc. These substances can then cause corrosion, etc.

Determination of the total pore content would not be sufficient. For a comprehensive understanding of the material, it is necessary to know the pore size and its volume distribution, i.e., the pore distribution curve. Pores can have different sizes and different shapes. Different materials can have a wide range of pore sizes, from gel pores on the order of nm to macropores visible to the naked eye. The representation of individual pores then influences the transport processes and other functional properties of the material as a whole. In order to detect the full range of pores, it is necessary to combine several methods.

The Mercury Intrusion Porosimetry (MIP) method was used in the presented papers. It works on the principle that a non-wetting liquid is forced into the test sample. Since the liquid is non-wetting, it needs to be pressurized to occupy and penetrate smaller capillaries. The measurement range is from a few nm to hundreds of µm. The actual experiment is described in the second and third submitted papers, where it is also described in detail [20,22].

The porosity of AAC determined by MIP was three to six times lower than the total open porosity measured by the water vacuum saturation method Since MIP can only identify pores below 100 µm, the difference can be attributed to pores of higher radii [20]. This is confirmed by SEM analysis.

As can be seen, each method has its specifics and limitations, and therefore, for a material with a complex porous structure, these methods must be combined to fully describe the porous system.

The main findings concerning the basic physical properties are mainly related to aerated concrete AAC due to its interesting porous structure.

- AAC is a very interesting material in terms of porous systems. It contains very bulky pores resulting from the foaming of the fresh mix. However, the matrix surrounding these voids is also porous. It consists mainly of tobermorite, ($Ca_5Si_6O_{16}$*4(H_2O). It can therefore be said that aerated concrete contains 2 porous systems. To detect them, several methods need to be combined, as was done in the second paper. The total porosity came out differently using the vacuum saturation method (Selected paper 2).
- The matrix density measured by the MIP method differed from that measured by the vacuum saturation method by up to 20%. This is because the large pores on the sample surface are infiltrated by the inherent hydrostatic pressure of mercury and are not recorded in the measurement (Selected paper 2).
- The use of the vacuum saturation method for bulk and matrix density determination is not suitable for cellulosic materials, which are discussed in selected papers 4 and 5, but is suitable for calcium silicates, concretes, mortars, and inorganic materials.

3.2. Length changes

The properties of some materials may change over time. The changes can be different and can be caused by chemical processes such as pozzolanic reactions in concrete, carbonation of concrete, intrusion of foreign reactive substances into the structure, and many others. Changes can also be caused by physical processes such as exposure to frost cycles, temperature changes, or wetting and drying. Length changes

are important in determining the compatibility of two materials. When two materials interact, undesirable stresses and subsequent cracking of the structure may occur due to different longitudinal moisture content or longitudinal thermal expansion coefficients. It is these length changes that are the subject of the third paper presented.

For example, for aerated concrete, standard ČSN EN 680 [23]: For autoclaved aerated concrete, standard ČSN EN 6806: the determination of drying shrinkage of autoclaved aerated concrete applies. According to this standard, the results are given in the product catalogues, but it should be noted that this standard has its limits. The total shrinkage value is the relative change in length caused by drying from a saturated state to a constant length under defined climatic conditions, the relative change in length between a humidity of 30% and 6% by weight. However, it has been found that the greatest length changes occur at low humidities with relatively small changes in moisture content. Such low moisture contents can occur when the material is exposed to higher temperatures, e.g., when it is near a heating element.

Length changes of mortars and aerated concrete were measured beyond the scope of applicable standards. Manufacturers report standard results in their product catalogs, specifically the relative length change between 30% and 6% moisture levels. This change typically does not exceed 0.2 mm/m. This is consistent with results published by the author [23,24], but the largest length changes occur at different moisture levels that are not accounted for by the standard.

- The greatest changes in length occur at humidity values close to zero (Selected paper 3).
- The coefficient of longitudinal moisture expansion can be expressed as a hyperbolic function (specific equations for the materials studied are given in the submitted documents (Selected paper 3).
- In the second cycle, the linear hygric expansion coefficient over the whole range of moisture content was about two times lower than in the first cycle (Selected paper 3).
- The conventional reference shrinkage and total shrinkage specified in EN 680:2005 were found to not be suitable for a basic practical assessment of

hygro-mechanical effects on the AAC elements in building structures, the first leading to an underestimation and the second to an overestimation of hygric strain in most practical cases (Selected paper 3).

- A permanent change was observed between the first and second cycles for both the aerated concrete and the plaster. This can be explained by carbonation or shrinkage of chemical origin. The plaster may also have been affected by pozzolanic reactions. Both carbonation and pozzolanic reactions are irreversible processes during which dimensional changes can occur. No significant changes occurred during the subsequent cycles (Selected paper 3).

3.3. Determination of resistance to cyclic freezing and thawing

The essence of the freeze resistance test is to monitor the loss of weight and strength of the tested samples due to freezing cycles. There are many standards for determining freezing resistance; each type of material can be said to have its own standard. For example, concrete CSN 73 1322 [26], mortars CSN 72 4522, tiles, etc. Although there are many standards, the principle is almost always the same. As already mentioned, the weight loss and strength of the test bodies are monitored. These are in most cases fully saturated with water. The standards then mainly regulate the dimensions of the test samples and the cyclic loading temperatures. On the one hand, this is fine; the test samples are exposed to worse conditions in the laboratory than in the real structure; on the other hand, when the building is used responsibly, the moisture content in the real structure will be significantly lower than the moisture content required by the standard. And since it is possible to estimate the moisture content based on PC simulations, it is useful to determine the frost resistance for different moisture conditions. A concrete example is the frost resistance test of aerated concrete. According to EN 15304 [27], the aerated concrete block is immersed in water for 48 hours. The block is then placed in polythene bags for 24 hours to equilibrate the moisture, and then test specimens are cut. The test set consists of 12 test blocks with an edge of 100 ± 2 mm, 6 blocks being a reference, and 6 test blocks. These are then subjected to cyclic frost loading.

The standard procedure has been modified in the second selected paper. After cutting the test samples from the block, the entire test set was dried in an oven at 100 °C and the dry mass was determined. Then three variants were prepared for freeze-thaw resistance testing. The first variant consisted of a set of dried samples, i.e., with zero moisture content, and the second variant consisted of a set of blocks with 10% moisture by mass. The cubes forming the third set were immersed in water for 48 hours and then placed in polyethylene bags for 24 hours to equalize the moisture content. Their moisture content by volume was then determined [20].

The test samples were placed in freezer boxes and subjected to freezing cycles. The freezing and thawing cycle was set according to EN 15304 [27], according to which the test bodies must be frozen in air at a temperature of -15 ± 2 °C. The spacing between the frozen bodies must be at least 50 mm. The temperature in the center of the test pieces shall reach 0 °C within 3 ± 1 hours and shall be checked on the control body before the test is started. The total freezing time shall be at least 8 hours until a freezing temperature of -15 ± 2 °C at the center of the test pieces is reached [20].

Reference samples with the appropriate moisture content were stored in polyethylene bags in the laboratory environment for the duration of the freeze test.

Strength and weight losses were determined after the freezing cycles. The compressive strength was determined on an ED 60 apparatus according to EN 679 [28] on all test pieces. The calculation of compressive strength loss was carried out according to EN 15304 [27].

The weight loss is determined from the difference between the original weight and the final weight determined directly on the frozen test pieces. The weight loss was calculated on the dried test pieces.

Determination of frost resistance was the subject of selected paper 2, devoted to aerated concrete. Based on the results, it can be argued that freezing cycles have a negligible effect on dry bodies. The losses in mass and strength are minimal, almost negligible for both 25 and 50 cycles. At 10% moisture, higher weight and strength losses are already observed, but it can still be said that these results are favorable after 25 cycles. Porous concrete P 1.8 300 was the worst performer, with a strength loss of 16.3%

after 50 cycles. For 40% moisture by volume, the best result was obtained for aerated concrete P 4-500, with a weight loss of 1.5%, which is several times better than the other two materials. This can be explained by the favorable pore distribution of P 4-500. Compared to the other porous concrete materials studied, it contains the least number of pores with a size above 100 µm, which are critical in terms of frost resistance because water already freezes in them at temperatures close to zero. However, water can hardly freeze in the gel pores, for this it would require a temperature of -78°C. The ice in the capillary pores then pushes the previously unfrozen water out, and the value of the above pressure depends on the cross-section and length of the capillaries [29].

Main findings:

- On dry silicate materials, freezing cycles have a minimal effect on service life (Selected paper 2).
- The freeze resistance is strongly influenced by the pore distribution curve. AAC 4 - 500 had the most gel pores and therefore demonstrated the highest resistance to freeze cycles (Selected paper 2).
- On the other hand, materials with pores larger than 100 µm resisted freezing cycles poorly (Selected paper 2).

3.4. Liquid water transport

3.4.1. Water absorption coefficient

The transport of liquid water in a material can be described in several ways. Probably the simplest is the determination of the water absorption coefficient. This expresses the ability of the body to carry liquid water above the waterline. The principle of determining the coefficient is the same for almost all materials. The body is coated on four sides with a waterproof and vapor-proof layer and the front of the sample is immersed in the liquid approximately one to two millimeters below the surface. Standard procedures for specific materials vary in particular in the dimensions of the test bodies or in the time periods for reading the water weight increments. For example, EN 1015-18 [30] applies to masonry mortars. In this case, a block with dimensions of 40 × 40 × 160 mm is used as the test body. This is waterproofed on the longitudinal walls and provided with a vapor barrier to ensure one-dimensional water transport. The test block is divided transversely

into two halves. The dried and prepared test body is immersed with the fracture face in the liquid and the cumulative water gain is measured after 10 and 90 minutes. A third and final weight measurement is made. The body shall then be broken lengthwise, and the height of the soaked water measured to the nearest 1 mm.

A similar principle is used in the EN ISO 15148 standard [31]. Compared to the previous procedure, the contact area is considerably higher, at least 50 cm^2. For higher accuracy, the standard recommends an area of at least 100 cm^2. The weight gain is measured after 5 minutes when the sample is removed from the water, surface-dried, weighed, and then partially re-immersed in water. Subsequent weighing occurs after 20 minutes, and then after 1 h, 2 h, 4 h, 8 h, and 24 h. The cumulative weight gain over time is determined from the weight gains relative to the sample area, and the water absorption coefficient is evaluated.

Manual measurements of weight gain lead to a larger measurement error due to water loss and time delay. This is especially true for materials with higher and faster absorption rates. The resulting value of the absorption coefficient may come out smaller than in the case of automatic measurement [32].

The principle described above was also used in the presented papers. Compared to the standards, the weight gain was monitored continuously. The test specimen was first dried and conditioned according to the standard requirements, then waterproofed and vapor-sealed using epoxy resin. In contrast to the standard procedure, it was immersed face down in water using a suspension device connected to a digital balance. The weight gain of the water is thus recorded automatically at freely adjustable intervals.

3.4.2. Moisture diffusivity

Moisture diffusivity as a function of moisture content is another way of expressing the transport of liquid water. It is possible to determine the average moisture diffusivity coefficient or the moisture conductivity as a function of humidity. This is determined from moisture profiles obtained at different time periods. Long prism-shaped samples are used to measure moisture profiles. One end of the prism is in contact with water. In order to measure the transmission in only one direction, it is necessary to prevent the evaporation of water on the other four walls. From the obtained moisture profiles, the

moisture conductivity coefficient is calculated as a function of moisture content using the Boltzmann-Matan method [34,35]. The method is described in the first and second submitted papers and has been further described in detail in [33].

Main findings from the submitted articles:

- Hydrophilic materials such as calcium silicate, special mineral wools, and other materials achieved extremely high water absorption coefficient values (Selected paper 1).
- As expected, materials with predominantly closed porosity, such as polystyrene, showed the lowest values of the absorption coefficient (Selected paper 1).
- For aerated concrete, foam concrete, and other mineral materials, water transport is due to capillary forces. This is not the case for fibrous materials. There, transport occurs in the cavities between the fibers (Selected paper 1,2).
- The moisture conductivity increases with the moisture content of the material. The difference between the dry and saturated state is at least an order of magnitude. For example, in aerated concrete, the moisture conductivity coefficient is up to an order of magnitude higher than in the dry state at higher moisture contents. Hydrophilic materials such as mineral wool or calcium silicate are similar (Selected paper 1,2).
- It makes a difference whether the transport is perpendicular or parallel to the fibers. This has been observed for hydrophobic mineral wool. A higher value was measured in the fiber direction than in the perpendicular direction (Selected paper 1).
- The liquid water transport rate is strongly influenced by the pore distribution (Selected paper 2).
- It also depends on the layout of the experiment, whether it is vertical or horizontal. If we compare the average moisture conductivity coefficient calculated from the water absorption coefficient and the same coefficient obtained from moisture profiles obtained in the horizontal position, the value may vary considerably for some materials. If the material contains a significant amount of macropores, water is no longer transported by capillary forces and, in

the vertical position, transport is considerably slowed down by gravity (Selected paper 2).

3.5. Water vapor transport properties

The ability to transmit water vapor through the material is characterized by the water vapor diffusion resistance factor [-], the water vapor diffusion coefficient D [m^2 s^{-1}], and the water vapor diffusion permeability δ [s]. The bowl method was used to determine the diffusion properties, which proved to be accurate and reliable in practice. It is based on the one-dimensional diffusion of water vapor through the sample and consists of measuring the diffusion flux of water vapor through the sample, knowing the partial pressures of water vapor in the air below the sample and the specific surface area of the sample above the sample according to ČSN EN ISO 12572 [34]. The sample is airtight in a tray filled with a solution of known relative humidity. The sample pan is weighed periodically, and the observed weight loss or gain is plotted on a graph according to the time of weighing. When the curve reaches a straight line, the measurement is considered complete. The calculation is given in four of the five articles presented. In 2017, this standard was changed. For vapor-permeable materials, the air resistance on the bottom and top surfaces of the specimen cannot be neglected. Therefore, the thickness of the air layer below the sample and the water vapor permeability at a certain temperature had to be newly taken into account [34]. This is explained in more detail in the fourth paper and in the fifth paper [35,36], this procedure is also used.

Diffusion properties are most often determined in two variants, namely in a dry cup and a wet cup. A significant difference can be observed between the two variants. The value for the dry cup is significantly higher. This trend can be observed in all the submitted papers. The most significant difference was observed for the porous concrete. In the case of the dry cup, autoclaved aerated concrete came out with three times higher values than in the case of the wet cup. Similar results were obtained for polystyrene, where it is approximately twice as high. This is due to the fact that the water vapor transport measured during the experiment partly takes into account the hydrodynamic transport of capillary condensed water in the porous system of the measured material.

Main findings:

- The ability of a material to transmit water vapor is closely related to the nature of the porous system. A material with open pores larger than 100 µm conducts water vapor better than material with smaller pores. In this type of pore, the water vapor transport was faster than in smaller pores due to the relatively lower importance of friction on pore walls (Selected paper 2).
- In the wet cup experimental design, this value is approximately twice as high as in the dry cup design. The apparent reason for this finding was that the water vapor transport parameters measured in the wet-cup setup partially also included hydrodynamic transport of capillary condensed water in the pore system, in addition to the bulk water vapor diffusion (Selected paper 1, 2, 4, 5).

3.6. Sorption isotherms

The ability of a material to absorb water vapor from the air is referred to as moisture sorption. It is the accumulation of water in a gaseous state. If water is bound to the material by intermolecular van der Waals forces, it is adsorption. In this case, water vapor molecules are attracted to the solid molecules of the material. If the water vapor is absorbed into the porous structure of the material by diffusion, it is absorption. If the absorption of moisture involves chemical bonds, it is chemisorption. Standard procedures are simplified and focus primarily on the maximum amount of water vapor that can be absorbed by a body at a relative humidity of 98%. The standard CSN 77 0940 for the design of moisture sorption isotherms has been withdrawn without a replacement. The sorption properties of thermal insulation materials are dealt with in standard EN ISO 16536 [37]: Thermal insulation products for use in construction - determination of long-term moisture diffusion.

In determining the sorption isotherms, the equilibrium sorption moisture at which the mass stabilizes is sought. Sorption isotherms were measured in the four papers presented and in all cases the desiccator method with saturated salt solutions was used.

Sorption isotherms can be obtained using the DVS Advantage 2 instrument, which measures mass gain and loss using highly sensitive scales accurate to 10 µg. The test samples must be dried in a vacuum oven before measurement. The individual samples

are suspended from one arm of the balance, the position of which is controlled by an optical sensor.

An electronic humidity controller provides partial water vapor pressure around the sample by mixing dry air with fully saturated air. The relative humidity profiles can be freely selected from 0 to 98% and the experiment can be performed at any temperature [38].

Sorption isotherms are presented in four of the five articles. For natural materials, desorption was also measured and was no longer reported in the fourth paper.

Main findings:

- Mineral wool has the lowest values regardless of whether the fibers are hydrophilic or hydrophobic (Selected paper 1).
- In contrast, the natural thermal insulation wools mentioned in the fourth article, as well as the rapeseed wool mentioned in the fifth article, reach relatively high values (Selected paper 4,5).

3.7. Thermal properties

Thermal properties include thermal conductivity and specific heat capacity. Thermal conductivity is a physical property that expresses the ability of a material to conduct heat. The specific heat capacity determines the heat required to heat 1 kg of material by 1 °C.

Heat transfer and heat storage are very important material properties that are essential for a proper building design. However, the thermal conductivity coefficient tends to increase with increasing temperature and humidity, which is often neglected in building behavior simulation [39]. Usually, the declared value obtained under standard conditions of 10 °C or 23 °C and a relative humidity of 50% according to ISO 10456 [40] is used.

The thermal conductivity is usually indicated as the standard value measured under dry conditions. However, it was found that ambient temperature and humidity of the environment are important parameters that affect the thermal conductivity of the building materials [41].

According to EN 12667 [42], it should be measured via a stationary method. The measurement conditions are specified in EN ISO 10456 [40] or in the Czech standard CSN 72 7012 [43].

An interesting problem is the determination of the thermal conductivity coefficient at higher humidity. In addition to heat transport, there is also moisture transport, and therefore, such an experiment can take several dozen hours to reach a steady state. It has been shown that the measurement time increases with sample thickness and moisture content. The thickness must be representative of the material. The smaller the temperature difference between the plates, the smaller the moisture transport and the shorter the experiment time. However, the smaller the heat flux, the higher the measurement uncertainty.

ISO 10051 proposes a method for estimating the moisture-dependent thermal conductivity coefficient in Annex C [44]. The standard assumes a linear relationship between moisture content and thermal conductivity. All these results can be derived from the results presented in the submitted articles, where the thermal conductivity coefficient was measured as a function of moisture content and temperature.

In the presented work, the thermal properties were measured by a non-stationary method as a function of humidity and temperature using the ISOMET 2104 instrument. The measurement is based on the analysis of temperature response to generated heat flow pulses. The heat flow is induced by electric heating using a resistor heater that has direct thermal contact with the surface of the sample. The accuracy guaranteed by the manufacturer is 5% of reading +0.001 $W \cdot m^{-1} \cdot K^{-1}$ in the range of 0.015–0.7 $W \cdot m^{-1} \cdot K^{-1}$ and 10% of the reading in the range of 0.7–6 $W \cdot m^{-1}\ K^{-1}$ [45].

The thermal conductivity coefficient of the most common materials, such as polystyrene or mineral wool, was measured in the first paper presented and its value in the dry state was approximately 0.04 $W \cdot m^{-1} \cdot K^{-1}$. For the environmentally friendly thermal insulation materials presented in the fourth and fifth papers, the dry value of the thermal conductivity coefficient was approximately 11 to 39% higher. However, these are still favorable values. For aerated concrete, the thermal conductivity coefficient came out to be approximately 0.08 $W \cdot m^{-1} \cdot K^{-1}$, which is twice the value of thermal insulation

materials; on the other hand, it is a structural material capable of carrying mechanical loads [20].

A sharp increase in thermal conductivity with increasing humidity was observed for all materials. In the case of hydrophilic mineral wool, this was several times higher, similar to the other absorbent materials.

Thermal conductivity also increased with increasing temperature, but not as dramatically as with increasing humidity. In the fourth paper presented, the thermal conductivity coefficient was measured over a temperature range from 5 °C to 35 °C. The difference between the thermal conductivity values was approximately 30%.

The specific heat capacity was measured in the dry state and the values as a function of humidity were calculated using the mixing rule given in the submitted articles.

Main findings:

- The thermal conductivity of all materials increased very quickly with increasing moisture content (Selected paper 1, 2, 4, 5).
- The dependence on thermal conductivity was less pronounced than on moisture content. In the temperature range of 2 – 40 °C, its increase was up to 50 % only for AAC, and for biomaterials, the difference was even smaller (Selected paper 2,4).
- The thermal conductivity of common materials such as mineral wool and polystyrene, measured in the first submitted paper, was less than 0.04 $W \cdot m^{-1} K^{-1}$. (Selected paper 1)
- The natural thermal insulation materials presented in the fourth paper showed a higher thermal conductivity coefficient of approximately 11 to 36% than conventional insulations such as polystyrene or mineral wool (Selected paper 1, 4).
- Compared to conventional thermal insulation materials, the thermal conductivity coefficient of aerated concrete had twice the value. This is due to its higher bulk density (Selected paper 1, 2).

4. Natural thermal insulation materials and their properties

Although natural plant or animal materials have a significantly lower carbon footprint than conventional synthetic materials [46–49], they are still seen more as an alternative and are not very popular in the construction market. There are several reasons for this. The first is the distrust towards new, previously unknown materials rather than the commonly used synthetic materials. Another factor is the low resistance of natural materials to biocorrosion. Of course, the higher price of natural thermal insulation compared to mass-produced products is also a major factor.

For new materials to become established on the market, their properties and advantages and disadvantages need to be independently identified so that they become known to the professional and wider public, optimizing new natural materials during production. Knowledge of the properties of the materials detailed in the first part of this thesis plays a key role in optimizing the production of new composite materials.

The next step is to refine these materials and optimize their properties, if they were natural composite materials such as hempcrete, to determine the optimum proportion of each component to increase resistance to biodegradation.

In theory, natural materials could also be used for special applications such as building desalination. In this case, the high moisture conductivity of the material plays a key role.

Jute, flax, and hemp fibers can have a wide range of applications. They can serve as reinforcement in composite materials and can improve the tensile strength of geopolymers [50].

Two articles are devoted to natural thermal insulation materials. In the first, thermal insulation made of hemp, flax, jute, wood fibers and sheep wool was tested. These insulation materials are already available on the market, but their share is very low. One reason for this may be ignorance of the material's properties in relation to humidity and temperature. For this reason, it was decided to write a fourth article.

The fifth article is devoted to the research and development of thermal insulation made of rapeseed straw. The fibers were prepared in laboratory K 123 of the Faculty of Civil Engineering, and the effect of delamination and temperature was tested.

4.1. Hemp

Hemp (*Cannabis sativa*) is a very well-known and often studied material in scientific workplaces. Substances extracted from hemp seeds have been used to treat malaria, rheumatism, and other diseases for several thousand years BCE). The cannabis plant consists of the root, the stem, and the fruiting tops, which in female plants ripen into cannabis seeds after pollination. The stem of the plant is mainly used for construction purposes. The fibers of the stalk are used to make ropes and cordage or can be woven into a relatively high-quality canvas [51,52]. Hemp fibers are also used for thermal insulation. This is used to insulate attics and inter-roof spaces.

Hemp shives are obtained from the stem of the plant. This can be used in the production of hempcrete. Air lime with pozzolanic admixtures is most commonly used as a binder for hempcrete. Hemp shavings are used as a filler. Since conventional cement-based concrete carries a significant environmental burden, hempcrete is widely studied. The advantages of hempcrete include a low water vapor diffusion resistance factor [53,54], good thermal insulation properties, and moisture control ability [55]. On the other hand, a major disadvantage is the long setting and hardening time [56,57], and probably the biggest disadvantage is the low strength. In most papers dealing with hempcrete, the compressive strength has not exceeded 1 MPa [57,58].

In addition to the aforementioned shive, it is possible to use hemp fibers for thermal insulation. They can be used similarly to mineral wool as inter-roof insulation, or for insulation of floors and ceilings. However, its further use needs to be assessed very carefully, and it is necessary to know its material characteristics in relation to humidity and temperature. These measurements were carried out in the fourth selected paper. [35]. Based on the research, it can be stated that the bulk density ranges from 30 to 100 $kg \cdot m^{-3}$, and the thermal conductivity coefficient reaches a value common for thermal insulation materials of 0.04 $W \cdot m^{-1} \cdot K^{-1}$. One advantage could be a higher specific heat capacity of 1600 $J \cdot kg^{-1} \cdot K^{-1}$ [52].

4.2. Flax

Flax (*Linum usitatissimum*) is an annual herb growing in mountain and foothill areas. In our region, it is cultivated mainly for fiber and oilseeds. The oil from the seeds is used as a film-forming agent in paints. The fibers were used for weaving cloth. The fibers can be used to make composite materials along with epoxy resin and other fibers. These composites have applications in the automotive industry [59]. Flax fibers alone can be used to produce thermal insulation material. Other fibers can be added to flax fibers, for example from recycled materials, bast fibers, and so on. The resulting fibrous thermal insulation must be treated with fire and anti-fungal agents. Natural soda impregnation shall be used. The resulting flax wool can be used as inter-roof or floor insulation. In general, flax fibers can be used to produce thermal insulation with a bulk density of 5 to 100 $kg \cdot m^{-3}$ with a thermal conductivity coefficient of 0.035 to 0.075 $W \cdot m^{-1} \cdot K^{-1}$ in the dry state, and a relatively high specific heat capacity of 1550 $J \cdot kg^{-1} \cdot K^{-1}$ [60]. As this type of insulation cannot carry mechanical loads, it is mainly used as a filling material. One of its disadvantages is its flammability, and the fibers have to be treated with flame retardants [61].

4.3. Jute

Jute (*Corchorus*) needs specific conditions for its growth, especially nutrient-rich soils, air temperatures between 15 and 32 °C and, above all, high humidity. These tropical conditions are provided in India, Bangladesh, China, Thailand, and Vietnam where Jute is grown and exported worldwide. During its growth, the jute plant can reach a height of up to 3.5 m. The fibers of the jute tree are used to make coarser fabrics, most notably jute sacks. In the construction industry, mainly recycled fabric obtained from jute sacks is used. Geotextiles or thermal insulation materials are made from recycled jute fabric. These can then replace conventional thermal insulation or composite materials based on jute fibers and polymers. N. M. Ali has experimentally fabricated and tested a number of composite materials based on jute and polyesters. Materials with bulk weights ranging from 180 $kg \cdot m^{-3}$ to 600 $kg \cdot m^{-3}$ were obtained. Materials with the lowest bulk density showed a very favorable thermal conductivity coefficient of 0.03549 $W \cdot m^{-1} \cdot K^{-1}$, while materials with higher bulk density showed excellent acoustic properties [62]. The thermal conductivity coefficient of jute wool with a bulk mass of 20 $kg \cdot m^{-3}$ at 10 °C

was 0.04 $W \cdot m^{-1} \cdot K^{-1}$ and 0.045 $W \cdot m^{-1} \cdot K^{-1}$ at 30 °C [63]. Thermal moisture material characteristics for thermal insulation made of Jute were determined in the fourth paper presented [35].

4.4. Sheep wool

Unlike the above materials, sheep's wool is of animal origin. It is a renewable and recyclable material. It is estimated that there are approximately 1.3 billion sheep in the world [51] and 174,196 sheep were registered in the Czech Republic in 2022 [64]. An adult sheep produces 2.5 to 5 kg of wool per year [51].

The sheep herds also serve to maintain the landscape, grazing mountain meadows and helping to restore the mountain flora. They thus maintain the ecological stability of the landscape and nature. The Merino sheep breed produces the highest quality wool, and most are currently bred in New Zealand and Australia. In the Czech Republic, sheep are bred with coarser wool, unsuitable for the textile industry but fully sufficient for building purposes for thermal insulation. In the past, sheep's wool was widely used in timber buildings. Ropes woven from strands of wool wrapped with thread were used to fasten windows and seal joints. The bulk density of the strings is 196 $kg \cdot m^{-3}$ [51].

Sheep's wool has a characteristic smell and positively affects the human psyche. Another advantage is that it regulates indoor humidity due to its high hygroscopicity [13,38]. It can absorb moisture from the air or, conversely, if the humidity is reduced, it can release it into the environment. This is confirmed by the results of scientific articles where sorption isotherms have been measured, and it has been shown that at a relative humidity of 95%, the moisture content of sheep wool reaches 30% [65].

Sheep wool can also be used as protection against impact noise in the form of compressed felt strips [18]. Sheep's wool as thermal insulation is produced in various bulk densities, usually ranging from 10 to 30 $kg \cdot m^{-3}$. However, values of bulk density that are too low are not suitable in terms of thermal conductivity. Ye et al. showed that sheep wool with a bulk density of about 10 $kg \cdot m^{-3}$ has a thermal conductivity coefficient of 0.065 $W \cdot m^{-1} \cdot K^{-1}$, whereas when the bulk density increases above 20 $kg \cdot m^{-3}$, the coefficient drops below 0.04 $W \cdot m^{-1} \cdot K^{-1}$ [66]. The thermal conductivity coefficient is also temperature-dependent. Sheep's wool with a bulk density of 20 $kg \cdot m^{-3}$ showed a

thermal conductivity coefficient of 0.05 $W \cdot m^{-1} \cdot K^{-1}$ at 40 °C and decreased to 0.038 $W \cdot m^{-1} \cdot K^{-1}$ at 10 °C [65]. A similar trend was observed in the fourth submitted paper [35], where the complete thermal moisture characteristics of selected sheep wool are measured. In general, the thermal conductivity coefficient is around 0.04 $W \cdot m^{-1} \cdot K^{-1}$.

5. Newly developed thermal insulation board made of rapeseed straw without binder

Due to global sustainability development, low-carbon bio-composites from agricultural wastes are in great demand. Using them, it is possible to produce thermal insulation boards that reduce the heat loss of buildings through heat transfer [67]. Wood fibers are undoubtedly the most important lignocellulosic raw material for the production of natural thermal insulation boards. Recently, the demand for non-wood lignocellulosic fibers has increased due to the global scarcity of forest resources as well as economic and environmental considerations [68,69].

Wood particles may be replaced by agricultural residues such as stalks, leaves, stems, or straw, which are abundantly produced annually by locally available crops for alternative fiberboards [4]. Annual plants represent a good opportunity to reduce the carbon footprint and replace non-renewable materials because the storage of carbon dioxide in fast-growing bio-based material is a key part of sustainable development [36,70].

Another benefit is their easy biodegradability, development of a low-carbon economy, and non-toxic nature. With increasing concern over health issues and biomass conservation, the fiberboards from agriculture residues with or without adhesive are under intensive investigation [71]. Many plants can be used for construction or thermal insulation purposes [72]. Sources of such materials may include, for example, straw, hemp-shive, flax fiber, etc. This biomass is an agricultural by-product and is a significant source of renewable energy. Certain adhesives are needed for particleboard production. The most commonly used adhesives are formaldehyde-based, phenol formaldehyde (PF), resorcinol formaldehyde (RF), melamine formaldehyde (MF), and urea formaldehyde (UF)[73]. Urea-formaldehyde-modified adhesives such as MUF (melamine-urea-formaldehyde adhesives) are also used [70,74]. Another option is polyvinyl acetate adhesives (PVAC) [75,76]. However, these types of adhesives are not harmless [57]. Therefore, this project aims to use the self-adhesive ability of lignin contained in plants to create a thermal insulation board without a binder [36].

Internal bonding is a key factor in reflecting the interior self-bonding quality between fibers. Lignin is characterized by a highly branched, amorphous, three-dimensional structure. Under certain conditions, and at temperatures between 100 °C and 200 °C, lignin softens and allows its molecules to deform in cell walls. This phenomenon has many advantages and disadvantages. Elucidation of this process can lead to the efficient production of self-adhesive fiberboards.

Lignocellulosic materials are widely studied to achieve self-bonding materials without synthetic binders. Bonding is caused by lignin plasticization, lignin polycondensation, and hemicellulose reactions, among others, at high temperature [69,77]. Internal bonding without additional adhesive is mainly due to hydrogen bonding - binding between fibers, condensation reaction in lignin and lignin-polysaccharides cross-linking reaction, lignin polycondensation and hemi-reaction, among others, at high temperature and steam [36,71].

Rapeseed straw was selected as the source of lignocellulosic fibers. Rapeseed (*Brassica napus* L.), a yellow-flowered plant cultivated for its seeds that yield edible oil, presents one of the suitable alternatives that do not face problems related to the cultivation of hemp. In the Czech Republic, rapeseed was grown on 379,632 hectares in 2023 and 344,073 hectares in 2024 [78]. The yield of rapeseed is approximately 34.5 t/ha [57], and it therefore represents an abundant and available raw material for further processing. In addition to the fact that rapeseed straw is a renewable source and can be grown locally, its application has many other beneficial aspects. As a fast-growing plant, rapeseed provides a promising opportunity to radically decrease the carbon footprint of building materials [46]. This material is 100% recyclable, and its straw is considered a waste product resulting from the harvest of the seed part. Compared to other types of straw, rapeseed straw contains a high content of cellulose and a relatively low amount of wax on its surface [57,79].

The main objective of the last presented paper is to study the softening of lignin and the subsequent development of glycosidic bonds. The development of these chemical bonds can be influenced by several factors, firstly during pulping and secondly during the production of fiberboards.

Based on the experiments described in the fifth and final article, the above assumptions were confirmed. The lignin released from the rapeseed fibers indeed acted as an adhesive. Four steaming temperatures were investigated: 100, 140, 180, and 200 °C. The steaming temperature had the greatest effect on tensile strength. Samples produced at 200 °C showed the highest tensile strength and the least swelling due to moisture gain. Since the samples produced at 180 °C showed only slightly worse properties, 180 °C was determined to be the optimum temperature with respect to energy consumption [36].

6. Selected publications of the author and their contribution to practical testing and development of new materials

In this section, five selected papers will be presented in turn, focusing on the material characteristics of building materials, both common materials for special applications and newly developed thermal insulation materials with a low carbon footprint.

Detailed thermal versus moisture properties are particularly useful to know for newly developed materials or materials intended for hazardous environments such as internal thermal insulation. There, the applicability of each material needs to be very carefully verified and this cannot be done without knowing the thermal and moisture properties.

In particular, the effect of humidity and temperature on the material properties is often underestimated. In product catalogs, the thermal conductivity is often given only as a constant, and the same applies to other parameters. However, thermal and humidity parameters increase with increasing humidity and also change with increasing temperature. Parameters can also change over time as the material is exposed to a changing environment.

Accurate and unbiased determination of material characteristics is an important step in the research and development of new materials. It was found that material characteristics are affected by the porous system. The pore distribution has a direct effect on the transport of liquid water and water vapor. It influences frost resistance. This finding can particularly be used by material manufacturers to optimize the properties of the composite material by changing the manufacturing process to influence the pore distribution curve. Through targeted changes in the pore system, they can influence the transport properties and thus increase the resistance to frost cycles.

Selected paper 1 – Energy and Buildings

Jerman, M., Černý, R., ***Effect of moisture content on heat and moisture transport and storage properties of thermal insulation materials*** – 2012

In this paper, the basic physical moisture and thermal properties of selected thermal insulation materials are measured in dependence on moisture content. These data can be utilized for both scientific and practical purposes. Incidentally, this article has been cited 191 times from its publication until the end of 2023.

Contribution to practical use: The obtained parameters are useful for other application research. The obtained data can be considered a step toward the establishment of a material database for thermal insulation systems which is currently not available, and which should serve for hydro-thermo-chemo-mechanical models, making it possible to perform complex durability and reliability-based studies of building constructions involving thermal insulation in various applications.

Energy and Buildings 53 (2012) 39–46

Contents lists available at SciVerse ScienceDirect

Energy and Buildings

journal homepage: www.elsevier.com/locate/enbuild

Effect of moisture content on heat and moisture transport and storage properties of thermal insulation materials

Miloš Jerman, Robert Černý*

Department of Materials Engineering and Chemistry, Faculty of Civil Engineering, Czech Technical University in Prague, Thákurova 7, 166 29 Prague 6, Czech Republic

ARTICLE INFO

Article history:
Received 11 May 2012
Received in revised form 18 June 2012
Accepted 4 July 2012

Keywords:
Thermal insulation materials
Thermal properties
Hygric properties
Moisture content

ABSTRACT

Computational models of heat and moisture transport are frequently used in calculating energy gains and losses in buildings. However, any model can provide reliable information only in the case that the quality of input data is adequate. This is not always true because the standard lists of thermal and hygric parameters given by the producers as well as the material databases included in the simulation tools are usually far from complete. In this paper, we present the measurements of complete sets of heat and moisture transport and storage parameters of selected thermal insulation materials in dependence on moisture content. Two common thermal insulation materials, namely hydrophobic mineral wool and expanded polystyrene, are selected as reference materials. Two types of hydrophilic mineral wool and an autoclaved-aerated-concrete thermal insulation board are the representatives of prospective materials which appeared on the market within the last couple of years. The studied material parameters include bulk density, matrix density, porosity, saturation moisture content, thermal conductivity, specific heat capacity, moisture diffusivity, water vapor diffusion coefficient, sorption isotherm, and water retention curve.

1. Introduction

All heat and moisture transport and storage parameters of building materials are dependent on both temperature and moisture content. This was repeatedly confirmed by many investigators during the last decades. The heat and moisture transport parameters were found generally to increase with temperature but within the limited temperature range characteristic for the climatic conditions of the temperate zone (contrary to the high-temperature conditions) their variations were not very dramatic, typically up to 20–30% [1–4]. The dependence of heat and moisture transport parameters on moisture content was far more important. The thermal conductivity of brick [5], autoclaved aerated concrete (AAC) [3], lime-based renders [6–8], and thermal insulation materials [1,2,9] was reported to increase several times when the values measured in dry state and water saturated state were compared. The measured increase in thermal conductivity of high performance concrete, which can be considered as almost watertight, due to the increasing moisture content was still up to 30–40% [10–12]. The differences between the moisture diffusivity values of various building materials determined for the lowest and highest moisture contents were found to be even substantially higher than in the case of thermal conductivity, typically one or two orders of magnitude [3,7,13,14]. Similarly, the differences in water vapor diffusion coefficients in the ranges of lowest and highest relative humidity were reported as high as one order of magnitude [15,16]. Therefore, neglecting the moisture dependence of heat and moisture transport parameters in any energy-related assessment is certainly not a very good idea, for the thermal insulation materials in particular. The heat loss estimates in such a case can be far from the real values, with all the unpleasant consequences for the analyzed building, as it was analyzed in more detail in [2,17].

While the dependence of the specific heat capacity of building materials on temperature is within the common range of temperatures very low, its dependence on moisture content is always significant because the specific heat capacity of water is four to five times higher, as compared with most building materials in the dry state [3,7,18]. Contrary to the heat transport parameters, an increase in heat storage parameters is, however, positive for a building envelope as it increases its heat accumulation function. If a water sorption isotherm is measured, it is always determined as a function of moisture content and the dependence of adsorbed water on relative humidity is mostly very important [19]. The position and shape of a sorption isotherm also strongly depend on temperature. At higher temperatures, the transport of water molecules is faster, the bonds can be released more easily, and therefore the amount of adsorbed water decreases and capillary condensation occurs at higher relative humidity [20]. Strictly from the point of view of a thermal insulation function of a building envelope a decrease in water accumulation function can be considered

* Corresponding author. Tel.: +420 224355044; fax: +420 224354446.
E-mail address: cernyr@fsv.cvut.cz (R. Černý).

0378-7788/$ – see front matter © 2012 Elsevier B.V. All rights reserved.
http://dx.doi.org/10.1016/j.enbuild.2012.07.002

as positive because a decrease of moisture content results in lower thermal conductivity. However, in some cases the lower moisture accumulation in the thermal insulation layer may lead to worse hygrothermal performance of an envelope and reduced service life [21].

As it follows from the short summary presented above, the measurement of heat and moisture transport and storage parameters of thermal insulation materials in dependence on temperature and moisture is necessary if the energy-related assessments of building envelopes are to be done with a sufficiently high accuracy. However, such measurements are currently not being published very frequently, and even the databases of advanced computer simulation tools are relatively limited and often rely only on the generic data characteristic for a certain class of materials.

In this paper, we would like to contribute to the gradual filling of gaps in the current knowledge on the properties of thermal insulation materials, which is supposed to be coming within the near future, and present the measurements of complete sets of heat and moisture transport and storage parameters of selected thermal insulation materials in a dependence on moisture content.

2. Experimental details

2.1. Materials

Two common thermal insulation materials, namely hydrophobic mineral wool and expanded polystyrene, were selected as reference materials. Two types of hydrophilic mineral wool and a thermal insulation board on AAC basis were the representatives of prospective materials which appeared on the market within the last couple of years. The hydrophilic mineral wool is characterized by fast liquid water transport; it is supposed to be applied for interior thermal insulation systems [18,22,23]. The thermal insulation board on AAC basis is a material with enhanced thermal insulation capability, as compared with common AAC types. It is recommended as thermal insulation layer of walls and roofs, in a combination with heavier AAC products.

The studied hydrophobic mineral wool was Nobasil PTN (produced by Knauf Insulation Trading, s.r.o., we will denote it as MW-HB in what follows), the analyzed expanded polystyrene was Isover EPS 70F (Saint-Gobain Isover CZ, s.r.o., EPS). The thermal insulation material on AAC basis was Ytong Multipor (Xella CZ, s.r.o., YM). The hydrophilic mineral wools were produced specifically for testing purposes by Rockwool, a.s., as advanced versions of the hard and soft parts of the hydrophilic thermal insulation board Inrock. The hard material will be denoted as MW-HLH, the soft material as MW-HLS.

2.2. Measurement methods

2.2.1. Basic physical characteristics

The bulk density of studied thermal insulation materials was determined by measuring the mass and linear dimensions of specimens, the matrix density by the helium pycnometry (Pycnomatic ATC, Porotec). The porosity was calculated using the known values of bulk density and matrix density. The saturation moisture content was determined by the gravimetric method after full immersion of studied specimens in water for 7 days.

2.2.2. Heat transport and storage parameters

The thermal conductivity was measured using the commercial device Isomet 2104 (Applied Precision, Ltd.). The measurement is based on the analysis of the temperature response of the analyzed material to heat flow impulses. The heat flow is induced by electrical heating using a resistor heater having a direct thermal contact with the surface of the sample. The measurement was done in dependence on moisture content from dry state to water saturation.

The specific heat capacity of dry specimens was determined by Isomet 2104 as well. The volumetric heat capacity of wet specimens $\rho_{wet}c_{wet}$ was calculated using the linear theory of mixtures, under the assumption that this heat storage parameter is an additive quantity [20],

$$\rho_{wet}c_{wet} = \rho_{dry}c_{dry} + \rho_w c_w w \tag{1}$$

$$\rho_{wet} = \rho_{dry} + \rho_w w \tag{2}$$

where ρ_{wet} is the bulk density of the wet material, ρ_{dry} the bulk density of the dry material, ρ_w the density of water, and w is the moisture content by volume,

$$w = \frac{V_w}{V} \tag{3}$$

V_w is the volume of water in the pores, V the volume of the whole specimen, c_{wet}, c_{dry} and c_w are the specific heat capacities of the wet material, the dry material and water, respectively.

So, the specific heat capacity vs. moisture content function could be written as

$$c_{wet}(w) = \frac{\rho_{dry}c_{dry} + \rho_w c_w w}{\rho_{dry} + \rho_w w} \tag{4}$$

2.2.3. Moisture transport parameters

The moisture diffusivity was chosen as the main parameter of liquid water transport. It was measured using two different methods. At first, the apparent value of moisture diffusivity was determined on the basis of results of a water absorption experiment. Then, the dependence of moisture diffusivity on moisture content was calculated using an inverse analysis of moisture profiles.

The water absorption experiment was performed using a standard setup [24]. The specimen was water and vapor-proof insulated on four lateral sides and the face side was immersed 1–2 mm in the water. The automatic balance allowed recording the increase of mass. The water absorption coefficient A (in $\mathrm{kg\,m^{-2}\,s^{-1/2}}$) was then calculated as

$$i = A \cdot \sqrt{t} \tag{5}$$

where i is the cumulative water absorption (in $\mathrm{kg\,m^{-2}}$), t the time from the beginning of the experiment. The water absorption coefficient was then employed for the calculation of the apparent moisture diffusivity [25]:

$$\kappa_{app} \approx \left(\frac{A}{w_{sat} - w_0}\right)^2 \tag{6}$$

where w_{sat} is the saturated moisture content (in $\mathrm{kg\,m^{-3}}$) and w_0 the initial moisture content (in $\mathrm{kg\,m^{-3}}$).

In the determination of moisture-dependent moisture diffusivity from moisture profiles, the capacitance method [26] was used for the measurement of moisture content. The moisture profiles were measured using a common capillary suction 1-D experiment in a horizontal position, lateral sides of specimens were water- and vapor-proof insulated. The moisture diffusivity vs. moisture content function was determined by the Matano method [27] as

$$\kappa(w_x) = \frac{1}{2t_0(dw/dx)_{x_0}} \int_{x_0}^{\infty} x \frac{dw}{dx} dx. \tag{7}$$

where w is the moisture content by volume, w_x is the value of moisture content at the position $x = x_0$.

The cup method was used for the determination of water vapor transport properties [28]. The measurement was carried out in steady state under isothermal conditions. It was based on one-dimensional water vapor diffusion, measuring the diffusion water

vapor flux through the specimen and using the values of partial water vapor pressure in the air under and above the specific specimen surfaces. The measurement was done during a time period of two weeks. The steady-state values of mass loss or mass gain determined by linear regression for the last five readings were used for the determination of water vapor diffusion coefficient. In the dry cup method the sealed cup containing silica gel which maintained the relative humidity of about 1.5% was placed in a controlled climatic chamber with 50% relative humidity. In the wet cup method the sealed cup contained saturated water solution of K_2SO_4 with an equilibrium relative humidity close to 98%.

The water vapor diffusion coefficient was calculated from the measured data according to the equation

$$D = \frac{\Delta m \cdot d \cdot R \cdot T}{S \cdot \tau \cdot M \cdot \Delta p_p} \quad (8)$$

where Δm is the amount of water vapor diffused through the sample, d the sample thickness, S the area of specimen surface, τ the period of time corresponding to the transport of mass of water vapor Δm, Δp_p the difference in water vapor pressure in the air under and above specific specimen surface, R the universal gas constant, M the molar mass of water, and T the absolute temperature.

Using the measured water vapor diffusion coefficient, the water vapor diffusion resistance factor, which is the parameter most frequently used in building practice, was determined as

$$\mu = \frac{D_a}{D} \quad (9)$$

where D_a is the diffusion coefficient of water vapor in air.

2.2.4. Moisture storage parameters

The measurement of adsorption isotherms was performed by the desiccators method [28]. The initial state for all the measurements was dry material. The desorption isotherms were determined in a similar way, only the initial state was specimen with maximum hygroscopic moisture content.

The water retention curves could not be determined by the methods commonly used for porous building materials [20]. The analyzed thermal insulation materials did not have sufficient strength so that they would be damaged or even destructed during the experiment. Therefore, an interpolation procedure between the maximum value of hygroscopic moisture content obtained on the adsorption isotherm, w_{hyg}, and the saturation moisture content, w_{sat}, was chosen. As only two points on the $w(p_c)$ curve were known, namely $w(0) = w_{sat}$ and $w(p_{c,hyg}) = w_{hyg}$, where $p_{c,hyg}$ is the capillary pressure corresponding to the maximum value of relative humidity on the adsorption isotherm, φ_{hyg}, a simple interpolation formula given in [29] was used,

$$w = A \cdot \exp(-B \cdot p_c) \quad (10)$$

where the two unknown parameters, A and B, were identified using the two known points of the $w(p_c)$ curve mentioned before:

$$A = w_{sat} \quad (11)$$

$$B = -\frac{1}{p_{c,hyg}} \ln \frac{w_{hyg}}{w_{sat}} \quad (12)$$

Substituting (11) and (12) in (10), the water retention curve was expressed as

$$w = w_{sat} \cdot \exp\left(\ln \frac{w_{hyg}}{w_{sat}} \cdot \frac{p_c}{p_{c,hyg}}\right) \quad (13)$$

2.3. Measurement conditions and material samples

The measurement of all parameters was done in a conditioned laboratory at the temperature of $22 \pm 1\,^{\circ}C$ and 25–30% relative humidity. The following specimens were used in the experiments: basic physical properties – 6 specimens 50 mm × 50 mm × 25 mm, water absorption coefficient – 3 specimens 50 mm × 50 mm × 20 mm, moisture profiles – 3 specimens 20 mm × 40 mm × 300 mm, water vapor transport properties – 3 cylindrical specimens with a diameter of 100 mm and height of 20 mm, sorption isotherms – 3 specimens 40 mm × 40 mm × 10 mm, thermal properties – 3 specimens 70 mm × 70 mm × 50–100 mm.

Table 1
Basic physical characteristics of thermal insulation materials.

Material	Bulk density ($kg\,m^{-3}$)	Matrix density ($kg\,m^{-3}$)	Saturation moisture content ($kg\,m^{-3}$)	Porosity ($\%\,m^3/m^3$)
MW-HLH	170	2380	930	92.9
MW-HLS	70	2260	970	96.9
YM	125	2150	229	94.2
EPS	16.5	1020	65	98.4
MW-HB	100	2960	880	96.6

3. Results and discussion

3.1. Basic physical characteristics

The bulk density, ρ_{dry}, of the studied thermal insulation materials was within the expected range (Table 1). The lowest ρ_{dry} exhibited EPS, the highest the hard hydrophilic mineral wool MW-HLH. All materials had very low ρ_{dry} as compared with other building materials which was due to the high amount of air embodied in their structure.

The bulk density declared by the producer (Tables 5 and 6) was for MW-HB exactly the same as in our experiments, for EPS our measurements fell within the declared range, for YM our ρ_{dry} value was 10 $kg\,m^{-3}$ higher than declared. Inrock is a combined hard-soft board, and the producer did not provide any ρ_{dry} for this material.

The lowest porosity, ψ, showed MW-HLH (Table 1) which reflected its highest bulk density. The highest porosity had EPS with the lowest bulk density. The saturation moisture content determined by immersion, w_{sat}, corresponded with the porosity values only for the hydrophilic materials MW-HLH and MW-HLS. The hydrophobic mineral wool MW-HB had about 10% lower w_{sat} than it would correspond to the measured porosity but this was clearly due to its hydrophobity. For the AAC material YM the difference between w_{sat} and ψ was very high, w_{sat} was about four times lower than it could be anticipated using just the ψ value. This feature, which was already observed before for other AAC materials [3], can be attributed to the trapping of air in dead-end pores at the water-immersion experiment. The highest difference between w_{sat} and ψ exhibited the expanded polystyrene EPS with a partially closed pore system which was not accessible for water but allowed the penetration of small helium molecules in the pycnometry measurements. The w_{sat} value obtained for EPS in this paper was in a good agreement with the data presented in [30] where $w_{sat} = 6\%$ by volume was reported for the expanded polystyrene with a bulk density of 15 $kg\,m^{-3}$. On the other hand, Gnip et al. [31] obtained for the same material produced by several different manufacturers $w_{sat} \approx 1.5$–4% by volume which indicated that the properties of seemingly the same expanded polystyrene can vary within a wide range.

The matrix density, ρ_{mat}, of YM corresponded with other AAC materials [3] which was due to the similarities in their production technology. The hydrophilic mineral wools had ρ_{mat} values close to the lower limit of the density of basalt which is the main raw material used for their production (2400–3100 $kg\,m^{-3}$ in [32]), ρ_{mat} of hydrophobic mineral wool was close to the upper limit (Table 1). The matrix density of expanded polystyrene was close to

Table 2
Thermal properties of thermal insulation materials in dry state.

Material	λ (W/m K)	c (J/kg K)
MW-HLH	0.041	770
MW-HLS	0.037	810
YM	0.047	1070
EPS	0.037	1570
MW-HB	0.036	790

the values characteristic for common polystyrene before expansion (1040 kg m^{-3} according to [33]).

3.2. Heat transport and storage parameters

The lowest thermal conductivity in dry state, λ_{dry}, had MW-HLS, MW-HB and EPS (Table 2) which corresponded with their lowest ρ_{dry}. The λ_{dry} value of MW-HLH was about 10% higher which was a good result, taking into account its significantly greater ρ_{dry}. The highest λ_{dry} exhibited YM, but the achievement of only about 25% higher value of λ_{dry} as compared with low-density mineral wools was a very good result for an AAC material.

The measured λ_{dry} values agreed with the producers' declarations (Tables 5 and 6); the differences were within the error-range of the measurement method. For MW-HB our λ_{dry} was 3% higher, for EPS 5% lower, and for YM 4% higher. λ_{dry} of Inrock was given as one number, so the 7% higher measured value for MW-HLH and 3% lower for MW-HLS was a satisfactory result (the hard part of Inrock has lower thickness than the soft part). Comparing our results with the data obtained for similar materials by other investigators, Yucel et al. [30] reported for the expanded polystyrene with 15 kg m^{-3} bulk density λ_{dry} = 0.038 W/m K, Mıhlayanlar et al. [34] for the same material λ_{dry} = 0.039 W/m K which was in a good agreement with our measurements. Domínguez-Munoz et al. [35] presented an extensive analysis of thermal conductivity of mineral wools with different bulk densities including the uncertainty bands. The measurements of λ_{dry} of all three mineral wools studied in this paper fell within the bands given in [35].

The specific heat capacity in dry state, c_{dry}, was lowest for the mineral wools MW-HLS, MW-HLH and MW-HB (Table 2). This corresponded with the measurements of basalt presented in [36] where c_{dry} was within a range of 600–800 J/kg K. The c_{dry} value of YM was about 10% lower than it was found for AAC materials with higher bulk density [3] which can be considered a reasonable agreement. The measured c_{dry} of EPS conformed with [30] where a value of 1500 J/kg K was reported.

The producers of analyzed thermal insulation materials did not include any satisfactory data for c_{dry} in their material lists (Tables 5 and 6). For MW-HB, EPS and YM no data at all was given, for Inrock only declaratory values according to ČSN 730540 were provided.

The thermal conductivity of all mineral wools increased very fast with increasing moisture content w (Fig. 1). The hydrophobity or hydrophility did not play an important role in that respect. The $\lambda(w)$ functions were very similar and the thermal conductivity at saturation, λ_{sat}, was within a range of 0.7–0.9 W/m K. The reduction of thermal insulation function was significant already for such relatively low moisture contents as 5–20% by volume where λ was typically 0.10–0.14 W/m K. The AAC material YM was losing its thermal insulation capabilities with increasing w even faster than the mineral wools (Fig. 2), λ achieved ≈0.20 W/m K already for $w \approx 20\%$ but its lower saturation moisture content prevented it from an achievement of such high λ_{sat} values as the mineral wools. The expanded polystyrene EPS presented the best performance among the analyzed materials (Fig. 2). Its λ_{sat} was only about 0.051 W/m K which was a very good result.

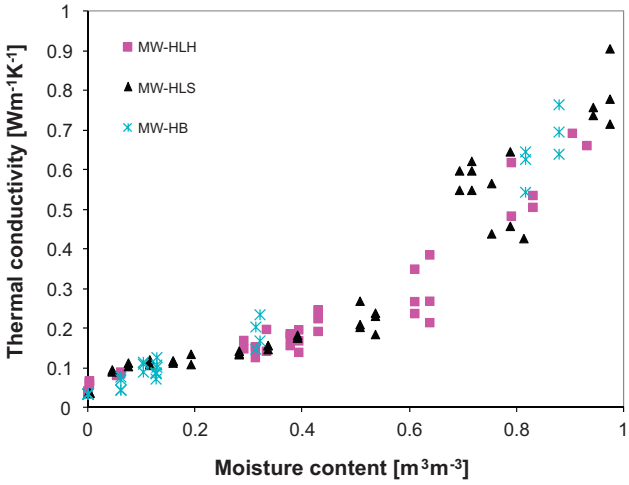

Fig. 1. Thermal conductivity of mineral wools as a function of moisture content.

As for the results presented by other investigators for similar materials, Mar et al. [9] determined $\lambda(w)$ functions for the expanded polystyrene with the bulk density of 20 kg m^{-3} in a wide range of moisture content from dry state to w_{sat} = 0.07 m^3/m^3. They obtained a roughly linear relation with λ_{dry} = 0.037 W/m K and λ_{sat} = 0.052 W/m K which was in an excellent agreement with the measurements presented for EPS in this paper (Fig. 2). The $\lambda(w)$ functions of several different types of mineral wool were reported in [18]. The results were in a good agreement with $\lambda(w)$ functions of mineral wools shown in Fig. 1.

The dependence of the specific heat capacity of the analyzed thermal insulation materials on moisture content was expressed analytically using Eq. (4). Substituting the values of bulk density and specific heat capacity of water in (4), we obtained

$$c_{wet}(w) = \frac{\rho_{dry} c_{dry} + 4.18 \times 10^6 w}{\rho_{dry} + 10^3 w} \tag{14}$$

where the bulk density, ρ_{dry}, can be found in Table 1, and the specific heat capacity in dry state, c_{dry}, in Table 2.

3.3. Moisture transport and storage parameters

The lowest water absorption coefficient A exhibited MW-HB and EPS which was due to their hydrophobity and basically no capillary activity (Table 3). The AAC material YM had the A value

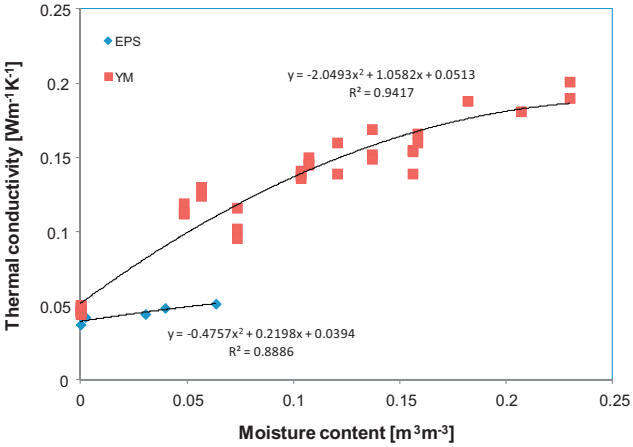

Fig. 2. Thermal conductivity of expanded polystyrene and Ytong Multipor as a function of moisture content.

Table 3
Liquid water transport properties of thermal insulation materials.

Material	A (kg m^{-2} s$^{-1/2}$)	κ_{app} (m^2 s^{-1})
MW-HLH	5.9	4.1×10^{-5}
MW-HLS	2.8	8.5×10^{-6}
YM	0.016	4.9×10^{-9}
EPS	0.0025	1.5×10^{-9}
MW-HB	0.0075	6.1×10^{-11}

several times higher than MW-HB and EPS but still very low as compared with most other building materials. On the other hand, the hydrophilic mineral wools MW-HLH and MW-HLS had extremely high A values (Table 3), which was due to an application of very effective hydrophilic substances on the surface of the fibers. The liquid water transport was thus realized predominantly along the fibers, not in the capillaries which were almost missing in this type of material.

In a comparison of results obtained in this paper with similar studies, the A value of MW-HB corresponded well with the hydrophobic mineral wools analyzed in [18]. The hydrophilic mineral wools MW-HLH and MW-HLS exhibited 5–10 times higher A coefficients than their previous versions INH and INS which were investigated in [18]. This was a very good outcome because the rapidity of liquid moisture transport is a crucial factor in designing effective interior thermal insulation systems [22].

The moisture diffusivity κ of all analyzed materials rapidly increased with increasing moisture content (Fig. 3); the differences between the κ values at lowest and highest moisture contents were up to two orders of magnitude. YM achieved $\kappa(w)$ about one order of magnitude lower than the AAC materials with higher bulk density [3] which was a good result. Its $\kappa(w)$ function corresponded with the apparent moisture diffusivity, κ_{app}, determined in vertical orientation (Table 3). Therefore, the gravity force did not play an important role in liquid water transport in YM.

The hydrophobic mineral wool MW-HB had κ comparable with YM, in absolute numbers (Fig. 3). However, these κ values were several orders of magnitude higher than κ_{app} of MW-HB presented in Table 3. The explanation of the substantial differences in the vertical and horizontal liquid water transport could be found in the interior structure of MW-HB. Contrary to YM where the liquid water was transported due to capillary forces, in MW-HB the transport was realized in the voids between the fibers, no matter their hydrophobity. It should be noted that no external pressure was exerted on the specimens in the experimental setup described above. Water entered the void system of MW-HB through the pore system of a sponge which was in contact with the measured specimen. Similar contacts of mineral wools with capillary active materials appear in the real walls as well.

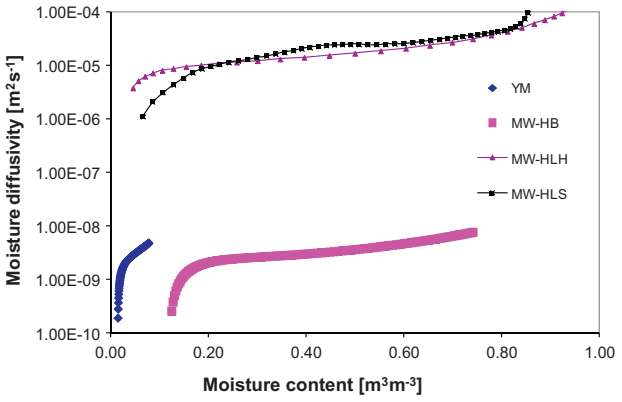

Fig. 3. Moisture diffusivity of thermal insulation materials as a function of moisture content.

Table 4
Water vapor transport properties of thermal insulation materials.

Material	Dry cup		Wet cup	
	D (10^{-6} m^2 s^{-1})	μ	D (10^{-6} m^2 s^{-1})	μ
MW-HLH	8.67	2.7	13.9	1.6
MW-HLS	9.64	2.4	21.9	1.2
YM	2.17	11	12.4	1.9
EPS	0.40	58	0.81	29
MW-HB	8.92	2.6	18.8	1.3

The moisture diffusivities of MW-HLH and MW-HLS were extremely high. The measured κ values roughly corresponded with κ_{app} in Table 3 so that the liquid water transport in the horizontal direction was basically the same as in the vertical direction.

The $\kappa(w)$ curve of EPS was not included in Fig. 3 because no moisture profiles were established during the experiment; in an absence of external pressure EPS was essentially watertight. This finding evokes questions about the apparent moisture diffusivity of EPS (1.5×10^{-9} m^2 s^{-1}) given in Table 3. Apparently, this value is not realistic and should not be used in any computational models of moisture transport. This example indicates the limits of Eq. (6) which is supposed to be used for capillary active materials only. For almost water tight materials such as EPS Eq. (6) leads to a great overestimation of κ_{app} just because of their very low value of saturation moisture content.

Both hydrophilic and hydrophobic mineral wools were highly permeable for water vapor (Table 4), with the water vapor diffusion resistance factor μ only two or three times higher than for the air. YM exhibited substantial differences between μ values obtained in the dry and wet cup arrangements; while for wet cup its μ factor was comparable with the mineral wools, for dry cup it was about four times higher. The apparent reason for these findings was that the water vapor transport coefficients measured in the wet-cup setup for YM partially included also the hydrodynamic transport of capillary condensed water in the pore system, besides the bulk water vapor diffusion. On the other hand, the mineral wools where no capillary pores were presented obviously lacked any capillary condensation.

The expanded polystyrene EPS exhibited much higher μ values than all other studied thermal insulation materials; they roughly corresponded to cement mortar or concrete [20]. The closed pore structure of EPS was apparently an effective barrier to water vapor transport but it was not completely water-vapor tight. This feature may have serious consequences when EPS is used in an improper way in a structure. The water vapor can, though with difficulties, enter the closed pores where it can possibly condense with rather limited possibilities of future removal. Accumulation of condensed water within the seemingly closed pore system presents a potential danger of deterioration of the thermal insulation function of EPS in long-term considerations. This can only be avoided by proper design when no water vapor condensation is allowed in the EPS layer.

The μ data of analyzed thermal insulation materials given by the particular producers were, similarly as with c_{dry}, far from satisfactory (Tables 5 and 6). For MW-HB they were not included at all in the material list, for Inrock they were supposed to be equal exactly to 1, which is a clear nonsense because $\mu = 1$ means that a material has exactly the same water vapor diffusion properties as the air. The measured μ values of EPS were about 50% higher than declared, for YM only one μ value was given by the producer which was 50% higher than in our wet-cup experiment and almost four times lower than in the dry-cup arrangement.

The mineral wools and expanded polystyrene exhibited a rather low capability of adsorption of moisture from the air in their pore systems (Fig. 4). The measured moisture contents were so low that

Table 5
Comparison of measured parameters of thermal insulation materials with producers' declarations.

Parameter	MW-HB		EPS		YM	
	Measured	Declared	Measured	Declared	Measured	Declared
ρ_{dry} (kg m^{-3})	100	100	16.5	13.5–18	125	115
c_{dry} (J/kg K)	790	–	1570	–	1070	–
λ_{dry} (W/m K)	0.037	0.036	0.037	0.039	0.047	0.045
$\mu_{dry\ cup}$	2.6	–	58	40	11	3
$\mu_{wet\ cup}$	1.3	–	29	20	1.9	3

Table 6
Comparison of measured parameters of hydrophilic mineral wools with their previous versions Inrock-hard and Inrock-soft.

Parameter	MW-HLH		MW-HLS	
	Measured	Inrock-hard	Measured	Inrock-soft
ρ_{dry} (kg m^{-3})	170	–	70	–
c_{dry} (J/kg K)	770	840	810	840
λ_{dry} (W/m K)	0.041	0.038	0.037	0.038
$\mu_{dry\ cup}$	2.7	1	2.4	1
$\mu_{wet\ cup}$	1.6	1	1.2	1

they could be considered effectively zero; their difference from zero was within the error range of the measurement method. Similar results for hydrophobic mineral wools and expanded polystyrene were obtained in [37].

The AAC material YM presented certain capability of gaseous moisture adsorption (Fig. 5), and hysteretic effects were observed in the adsorption and desorption phase. However, in a comparison with most other porous building materials ([20,38]) the amount of adsorbed moisture was very low.

The water retention curves of the analyzed thermal insulation materials were expressed in an analytical form using Eq. (13). The capillary pressure corresponding to the maximum hygroscopic moisture content, $p_{c,hyg}$, was determined with the aid of the Kelvin equation in the form [20]

$$p_c = \frac{RT\rho_w}{M} \ln\ \varphi \tag{15}$$

Using the maximum relative humidity, $\varphi_{hyg} = 0.97$, in (15), we obtained $p_{c,hyg} = 4.15 \times 10^6$ Pa, which after substitution in Eq. (13) gave

$$w(p_c) = w_{sat} \cdot \exp\left(\ln \frac{w_{hyg}}{w_{sat}} \cdot \frac{p_c}{4.15 \times 10^6}\right) \tag{16}$$

where the maximum hygroscopic moisture content, w_{hyg}, can be found in Figs. 4 and 5, and the saturation moisture content, w_{sat}, in Table 1.

3.4. Experimental data obtained in this paper in a relation to current EN standards

Current EN standards prescribe only a very limited number of heat and moisture transport and storage parameters for the certification of thermal insulation materials. The most important is, of course, the thermal conductivity λ. According to EN 12667 [39] λ should be measured by the guarded hot plate technique. The conditions for λ measurements are prescribed by EN ISO 10456 [40], so that we have either limit λ values in dry state or declared λ values determined at 23 °C and 50% relative humidity. Both these values can be derived from our results, using the measured $\lambda(w)$ functions and sorption isotherms. Comparing the impulse method (IM) used in our measurements with the guarded hot plate method (GHPM) used in EN 12667, it should be noted that in dry-state conditions the accuracy of GHPM is higher, typically ±2%; for IM in this paper we have ±5%. However, for samples with higher moisture content the situation is changing. While IM can be used with about the same accuracy (the measurement is fast and moisture transfer is negligible during the experiment), the steady-state character of GHPM measurement features systematic errors to the λ determination. The temperature gradient in a specimen induces moisture transport due to the Soret effect which leads in a long-term experiment to the establishment of moisture gradient in the direction of specimen thickness. The measured heat flux includes then not only the Fourier heat flux but also the Dufour effect which is difficult to quantify exactly (see [20] for a detailed thermodynamic analysis).

Among the parameters characterizing the liquid water transport, the short term water absorption (24 h) by partial immersion W_p (EN 1609 [41] in kg m^{-2}), long term water absorption (28 days) by partial immersion W_{lp} (EN 12087 [42] – in kg m^{-2}), and long term water absorption (28 days) by total immersion W_{lt} (EN 12087 – in

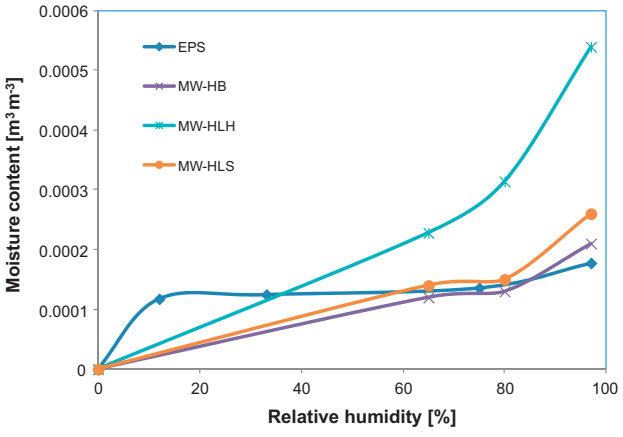

Fig. 4. Sorption isotherms of mineral wools and expanded polystyrene.

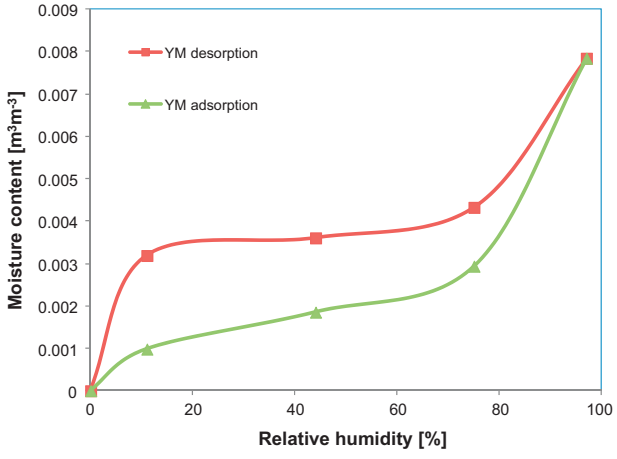

Fig. 5. Adsorption and desorption isotherms of Ytong Multipor.

% m^3/m^3) are required for thermal insulation materials. Our measurement of saturation moisture content was similar to the total immersion experiment in EN 12087. The full immersion of studied specimens in water was done for 7 days but the dimensions of the specimens in our case (50 mm × 50 mm × 25 mm) were smaller than in EN 12087 (200 mm × 200 mm × board thickness) so that the results should be roughly comparable. Contrary to our free water uptake measurement, which was performed in strictly 1-D arrangement, the partial-immersion experiments described in EN 1609 and EN 12087 are performed without any water- and vapor-tight insulation on lateral sides of the specimens, i.e., the water transport is realized in 3D. In this case the results cannot be compared directly; an additional computational analysis would be necessary to achieve that. It should be noted that the standard parameters W_p, W_{lp}, and W_{lt} have a relative value only. They can be used for a comparison of different materials but in any case they cannot serve as input parameters of computational models of coupled heat and moisture transport. For that purpose, the moisture diffusivity as a function of moisture content, or, if it is not available, the apparent moisture diffusivity should be utilized.

The water vapor diffusion parameters of thermal insulation materials are measured according to EN 12086 [43]. The cup-method arrangements used in this paper were almost identical with the A and C modifications of the cup method described in EN 12086. Therefore, our results obtained for the water vapor diffusion resistance factor can be considered as conforming with the EN 12086 standard.

4. Conclusions

The measurement of complete sets of heat and moisture transport and storage parameters of five thermal insulation materials in dependence on moisture content was presented. Two common thermal insulation materials, namely hydrophobic mineral wool and expanded polystyrene, were selected as reference materials. Two types of hydrophilic mineral wool and a thermal insulation board on AAC basis were the representatives of prospective materials which appeared on the market within the last couple of years. The main results can be summarized as follows:

- All studied materials had very low bulk density as compared with other building materials which was due to the high amount of air embodied in their structure.
- The saturation moisture content determined by immersion, w_{sat}, corresponded with the porosity, ψ, values only for the hydrophilic mineral wools. The hydrophobic mineral wool had about 10% lower w_{sat} than it would correspond to ψ; this was due to the hydrophobity of fibers.
- For the AAC-based material the difference between w_{sat} and ψ was very high, w_{sat} was about four times lower than it could be anticipated using just the ψ value. This can be attributed to the trapping of air in dead-end pores at the water-immersion experiment.
- The highest difference between w_{sat} and ψ exhibited expanded polystyrene with a partially closed pore system which was not accessible for water but allowed the penetration of small helium molecules in the pycnometry measurements.
- The thermal conductivity of all mineral wools increased very fast with increasing moisture content w; the thermal conductivity at saturation, λ_{sat}, was within a range of 0.7–0.9 W/m K. The reduction of thermal insulation function was significant already for relatively low moisture contents of 5–20% by volume where λ was typically 0.10–0.14 W/m K.
- The AAC material YM was losing its thermal insulation capabilities with increasing w even faster than the mineral wools, λ was ≈0.20 W/m K already for $w \approx 20\%$ but its lower saturation moisture content prevented it from an achievement of such high λ_{sat} values as the mineral wools.
- The expanded polystyrene EPS presented the best heat-insulating properties among the analyzed materials; its λ_{sat} was only about 0.051 W/m K.
- The moisture diffusivity, κ, of all analyzed materials rapidly increased with increasing moisture content; the differences between the κ values at lowest and highest moisture contents were up to two orders of magnitude.
- The AAC based material achieved $\kappa(w)$ about one order of magnitude lower than the AAC materials with higher bulk density.
- The hydrophobic mineral wool exhibited substantial differences in the vertical and horizontal liquid water transport. While in the vertical orientation such transport was almost eliminated due to the absence of capillary pores, in the horizontal orientation the transport was realized in the voids between the fibers, no matter their hydrophobity.
- The moisture diffusivity of hydrophilic mineral wools was extremely high. The liquid water transport was realized here predominantly along the fibers covered by hydrophilic substances which attracted the water in liquid state.
- Expanded polystyrene was in an absence of external pressure essentially watertight. For this material, the commonly performed estimates of the apparent moisture diffusivity, κ_{app}, using the data of water absorption experiment should be avoided. They can lead to a great overestimation of κ_{app} just because of the very low value of saturation moisture content of EPS.
- Both hydrophilic and hydrophobic mineral wools had very low water vapor diffusion resistance factor μ so that they were highly permeable for water vapor.
- The AAC material exhibited substantial differences between μ values obtained in the dry and wet cup arrangements; while for wet cup its μ factor was comparable with the mineral wools, for dry cup it was about four times higher.
- Expanded polystyrene exhibited much higher μ values than all other studied thermal insulation materials; they roughly corresponded to cement mortar or concrete.
- The mineral wools and expanded polystyrene exhibited a rather low capability of adsorption of moisture from the air in their pore systems. The measured moisture contents were so low that they could be considered effectively zero.
- The AAC material presented certain capability of gaseous moisture adsorption, and hysteretic effects were observed in the adsorption and desorption phase. However, in a comparison with most other porous building materials the amount of adsorbed moisture was very low.

Acknowledgment

This research has been supported by the Czech Science Foundation, under Project No. P105/12/G059.

References

[1] F. Ochs, W. Heidemann, H. Mueller-Steinhagen, Effective thermal conductivity of moistened insulation materials as a function of temperature, International Journal of Heat and Mass Transfer 51 (2008) 539–552.
[2] A. Karamanos, S. Hadiarakou, A.M. Papadopoulos, The impact of temperature and moisture on the thermal performance of stone wool, Energy and Buildings 40 (2008) 1402–1411.
[3] M. Jerman, M. Keppert, J. Výborný, R. Černý, Moisture and heat transport and storage characteristics of two commercial autoclaved aerated concretes, Cement, Wapno, Beton 16/78 (2011) 18–29.
[4] Z. Pavlík, R. Černý, Determination of moisture diffusivity as a function of both moisture and temperature, International Journal of Thermophysics (2011), http://dx.doi.org/10.1007/s10765-011-1006-y.
[5] Z. Pavlík, L. Fiala, E. Vejmelková, R. Černý, Application of effective media theory for determination of thermal properties of hollow bricks as a

function of moisture content, International Journal of Thermophysics (2012), http://dx.doi.org/10.1007/s10765-012-1183-3.
[6] Z. Pavlík, E. Vejmelková, L. Fiala, R. Černý, Effect of moisture on thermal conductivity of lime-based composites, International Journal of Thermophysics 30 (2009) 1999–2014.
[7] E. Vejmelková, M. Keppert, Z. Keršner, P. Rovnaníková, R. Černý, Mechanical, fracture-mechanical, hydric, thermal, and durability properties of lime-metakaolin plasters for renovation of historical buildings, Construction and Building Materials 31 (2012) 22–28.
[8] E. Vejmelková, M. Keppert, P. Rovnaníková, Z. Keršner, R. Černý, Application of burnt clay shale as pozzolan addition to lime mortar, Cement and Concrete Composites 34 (2012) 486–492.
[9] J.D. Mar, E. Litovsky, J. Kleiman, Modeling and database development of conductive and apparent thermal conductivity of moist insulation materials, Journal of Building Physics 32 (2008) 9–31.
[10] E. Vejmelková, M. Pavlíková, M. Keppert, Z. Keršner, P. Rovnaníková, M. Ondráček, M. Sedlmajer, R. Černý, Performance concrete with Czech metakaolin: experimental analysis of strength, toughness and durability characteristics, Construction and Building Materials 24 (2010) 1404–1411.
[11] E. Vejmelková, M. Pavlíková, Z. Keršner, P. Rovnaníková, M. Ondráček, M. Sedlmajer, R. Černý, High performance concrete containing lower slag amount: a complex view of mechanical and durability properties, Construction and Building Materials 23 (2009) 2237–2245.
[12] E. Vejmelková, M. Pavlíková, M. Keppert, Z. Keršner, P. Rovnaníková, M. Ondráček, M. Sedlmajer, R. Černý, Fly-ash influence on the properties of high performance concrete, Cement, Wapno, Beton 13/75 (2009) 189–204.
[13] J. Carmeliet, H. Hens, S. Roels, O. Adan, H. Brocken, R. Černý, Z. Pavlík, C. Hall, K. Kumaran, L. Pel, Determination of the liquid water diffusivity from transient moisture transfer experiments, Journal of Thermal Envelope and Building Science 27 (2004) 277–305.
[14] P. Tesárek, J. Drchalová, J. Kolísko, P. Rovnaníková, R. Černý, Flue gas desulfurization gypsum: study of basic mechanical, hydric and thermal properties, Construction and Building Materials 21 (2007) 1500–1509.
[15] L. Kuishan, Z. Xu, G. Jun, Experimental investigation of hygrothermal parameters of building materials under isothermal conditions, Journal of Building Physics 32 (2009) 355–370.
[16] Z. Pavlík, J. Žumár, M. Pavlíková, R. Černý, A Boltzmann transformation method for investigation of water vapor transport in building materials, Journal of Building Physics 35 (2012) 213–223.
[17] F. Björk, T. Enochsson, Properties of thermal insulation materials during extreme environment changes, Construction and Building Materials 23 (2009) 2189–2195.
[18] M. Jiřičková, R. Černý, Effect of hydrophilic admixtures on moisture and heat transport and storage parameters of mineral wool, Construction and Building Materials 20 (2006) 425–434.
[19] Z. Pavlík, J. Žumár, I. Medveď, R. Černý, Water vapor adsorption in porous building materials: experimental measurement and theoretical analysis, Transport in Porous Media 91 (2012) 939–954.
[20] R. Černý, P. Rovnaníková, Transport Processes in Concrete, Spon Press, London, 2002.
[21] V. Kočí, J. Maděra, R. Černý, Exterior thermal insulation systems for AAC building envelopes: computational analysis aimed at increasing service life, Energy and Buildings 47 (2012) 84–90.
[22] Z. Pavlík, R. Černý, Experimental assessment of hygrothermal performance of an interior thermal insulation system using a laboratory technique simulating on-site conditions, Energy and Buildings 40 (2008) 673–678.
[23] J. Toman, A. Vimmrová, R. Černý, Long-term on-site assessment of hygrothermal performance of interior thermal insulation system without water vapour barrier, Energy and Buildings 41 (2009) 51–55.
[24] E. Vejmelková, M. Pavlíková, M. Jerman, R. Černý, Free water intake as means of material characterization, Journal of Building Physics 33 (2009) 29–44.
[25] M.K. Kumaran, Moisture diffusivity of building materials from water absorption measurements, Journal of Thermal Envelope and Building Science 22 (1999) 349–355.
[26] P. Semerák, R. Černý, A capacitance method for measuring moisture content of building materials, Stavební obzor 6 (1997) 102–103 (in Czech).
[27] C. Matano, On the relation between the diffusion coefficient and concentration of solid metals, Japanese Journal of Physics 8 (1933) 109–115.
[28] S. Roels, J. Carmeliet, H. Hens, O. Adan, H. Brocken, R. Černý, Z. Pavlík, C. Hall, K. Kumaran, L. Pel, R. Plagge, Interlaboratory comparison of hygric properties of porous building materials, Journal of Thermal Envelope and Building Science 27 (2004) 307–325.
[29] A.R. Dexter, E.A. Czyż, G. Richard, A. Reszkowska, A user-friendly water retention function that takes account of the textural and structural pore spaces in soil, Geoderma 143 (2008) 243–253.
[30] K.T. Yucel, C. Basyigit, C. Ozel, Thermal insulation properties of expanded polystyrene as construction and insulating materials, in: 15th Symposium on Thermophysical Properties, NIST/ASME, Boulder, Colorado, June 22–27, 2003, pp. 54–66.
[31] I.Y. Gnip, V. Kersulis, S. Vejelis, S. Vaitkus, Water absorption of expanded polystyrene boards, Polymer Testing 25 (2006) 635–641.
[32] D.R. Lide (Ed.), CRC Handbook of Chemistry and Physics, 79th ed., CRC Press, Boca Raton, 1998.
[33] J. Joshi, R. Lehman, T. Nosker, Selected physical characteristics of polystyrene/high density polyethylene composites prepared from virgin and recycled materials, Journal of Applied Polymer Science 99 (2006) 2044–2051.
[34] E. Mıhlayanlar, S. Dilmac, A. Guner, Analysis of the effect of production process parameters and density of expanded polystyrene insulation boards on mechanical properties and thermal conductivity, Materials and Design 29 (2008) 344–352.
[35] F. Domínguez-Munoz, B. Anderson, J.M. Cejudo-López, A. Carrillo-Andrés, Uncertainty in the thermal conductivity of insulation materials, Energy and Buildings 42 (2010) 2159–2168.
[36] M.S. Mostafa, N. Afify, A. Gaber, E.F. Abu Zaid, Investigation of thermal properties of some basalt samples in Egypt, Journal of Thermal Analysis and Calorimetry 75 (2004) 179–188.
[37] I.Y. Gnip, S.A. Veyalis, V.I. Kershulis, Isotherms of water vapor sorption by light inorganic and polymer heat-insulating materials, Journal of Engineering Physics and Thermophysics 79 (2006) 40–47.
[38] K.K. Hansen, Sorption Isotherms, Technical Report 163/86, The Technical University of Denmark, Lyngby, 1986.
[39] ČSN EN 12667, Thermal Performance of Building Materials and Products—Determination of Thermal Resistance by Means of Guarded Hot Plate and Heat Flow Meter Methods—Products of High and Medium Thermal Resistance, Czech Standards Institute, Prague, 2001.
[40] ČSN EN ISO 10456, Building Materials and Products—Hygrothermal Properties—Tabulated Design Values and Procedures for Determining Declared and Design Thermal Values (ISO 10456:2007), Czech Office for Standards, Metrology and Testing, Prague, 2010.
[41] ČSN EN 1609, Thermal Insulating Products for Building Applications—Determination of Short Term Water Absorption by Partial Immersion, Czech Standards Institute, Prague, 2007.
[42] ČSN EN 12087, Thermal Insulating Products for Building Applications—Determination of Long Term Water Absorption by Immersion, Czech Standards Institute, Prague, 2007.
[43] ČSN EN 12086, Thermal Insulating Products for Building Applications—Determination of Water Vapour Transmission Properties, Czech Standards Institute, Prague, 1998.

Selected paper 2 – Construction and Building Materials

Jerman, M., Keppert, M., Výborný, J., Černý, R., ***Hygric, thermal and durability properties of autoclaved aerated concrete*** – 2013

As problems started to occur around 2010 in the form of cracks in the exterior and interior plaster on aerated concrete structures, a detailed examination of the aerated concrete was undertaken. One of the results is this submitted article. The thermal and moisture properties of selected aerated concrete are studied in detail. Furthermore, the pore distribution curve is determined, as it has a great influence on the final behavior of the material as a whole. The influence of freezing cycles on the lifetime of aerated concrete is also evaluated. These results are again applicable for scientific purposes and practical optimization of production processes. From its publication to 2023, this paper has received 159 citations in WoS.

Contribution to practical use: In addition to designers, the results of this article can also be used by aerated concrete manufacturers to optimize their production processes. Along with thermal and moisture properties, the influence of pore size on frost resistance and moisture conductivity is evaluated. Based on these results, the manufacturing process of aerated concrete can be optimized.

Construction and Building Materials 41 (2013) 352–359

Contents lists available at SciVerse ScienceDirect

Construction and Building Materials

journal homepage: www.elsevier.com/locate/conbuildmat

Hygric, thermal and durability properties of autoclaved aerated concrete

Miloš Jerman, Martin Keppert, Jaroslav Výborný, Robert Černý *

Department of Materials Engineering and Chemistry, Faculty of Civil Engineering, Czech Technical University in Prague, Thákurova 7, 166 29 Prague 6, Czech Republic

HIGHLIGHTS

- Three AAC with different bulk density and compressive strength are studied.
- Complete sets of hygric and thermal properties are measured.
- Basic physical characteristics and durability properties are determined.
- Thermal conductivity is six times higher at water saturation than in dry state.
- Moisture diffusivity remarkably increases with moisture content.

GRAPHICAL ABSTRACT

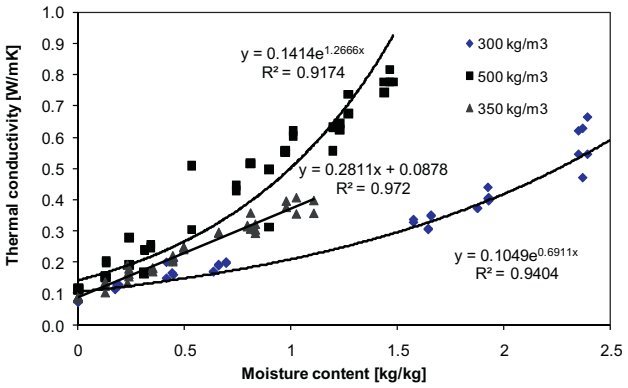

ARTICLE INFO

Article history:
Received 12 January 2011
Received in revised form 17 December 2012
Accepted 19 December 2012
Available online 12 January 2013

Keywords:
Autoclaved aerated concrete
Hygric properties
Thermal properties
Durability properties

ABSTRACT

The hygric and thermal properties of autoclaved aerated concrete (AAC) given in the manufacturers' lists include mostly just the thermal conductivity in dry state and generic data for the specific heat capacity and water vapor diffusion resistance factor. Durability characteristics are not listed at all. This greatly limits any service life assessment studies of AAC-based building envelope systems. In this paper, complete sets of hygric and thermal properties of three commercially produced AAC with different bulk density and compressive strength are measured, together with the basic physical characteristics and durability properties. Experimental results show that the thermal conductivity can be as much as six times higher in capillary water saturation state than in dry conditions. Thermal conductivity is also found to increase up to 50% when temperature is increased from 2 °C to 40 °C. The dependence of moisture diffusivity on moisture content is remarkable; the differences as high as one order of magnitude are observed if its values obtained for low and high moisture contents are compared. The freeze/thaw resistance of capillary saturated samples is found satisfactory up to 25 cycles and increases with compressive strength. For the moisture content lower than 10% by volume AAC in the range of compressive strength of 1.8–4 MPa can successfully resist to 50 cycles.

1. Introduction

Autoclaved aerated concrete (AAC) is a structural material which is commonly used around Europe, particularly as it combines ease of construction with excellent combination of mechanical and thermal properties. As it can also be considered environmentally friendly material, it may have considerable potential for future applications. However, the empirical principles often employed in the construction design during the past few decades have led to substantial failures, such as cracking of both external and internal finishes, detachment of renders from the AAC blocks, sometimes with the AAC itself, cracks around windows or doors, frost failure of external render.

* Corresponding author.
E-mail address: cernyr@fsv.cvut.cz (R. Černý).

0950-0618/$ - see front matter © 2013 Elsevier Ltd. All rights reserved.
http://dx.doi.org/10.1016/j.conbuildmat.2012.12.036

Although some of the failures caused by the improper design were at least mitigated step by step, on the basis of the negative experience, the empirical design still prevailed until recently and in the service life assessments of AAC-based building envelope systems a complex view was mostly missing. Complex analyzes of hygrothermal performance of the AAC-based building envelopes based on sound scientific knowledge and complemented with durability considerations are not performed up to now. However, the design of this type of envelopes is not obvious; they should be considered as a system consisting of AAC, internal and external finishes and possibly also thermal insulation layer. In the design process, the details are to be solved using suitable methods as well.

Computational simulation of heat and moisture transport processes is a powerful tool making possible to find weak points of building envelopes in advance, during the design process already. The results of simulations can also serve as a basis for service life assessment studies. However, the quality of any computer simulation study depends on the quality of input data. These include two types of parameters which have to be known in advance. The first are initial and boundary conditions. Initial conditions can be determined using on site analysis. Boundary conditions can be applied in the form of meteorological data for temperatures, relative humidities, rainfall and solar radiation. The second type of input parameters is the moisture and heat transport and storage parameters of the materials of the wall which appear in the balance equations. For the problem of coupled moisture and heat transport, these parameters include moisture diffusivity and water vapor diffusion resistance factor as water transport parameters, sorption isotherm and water retention curve as water storage parameters, specific heat capacity as heat storage parameter and thermal conductivity as heat transport parameter.

The moisture and heat transport and storage parameters can be determined by common laboratory methods. However, even for the most common AAC products they are not known in sufficient complexity.

The catalogue lists of AAC manufacturers are mostly confined to water vapor transport parameters and heat transport and storage parameters, both given in the form of a single value. This is far from satisfactory. The thermal conductivity of porous building materials is known to depend on both moisture content and temperature in a significant way. The moisture transport occurs also in the liquid form. Moisture accumulation can be very important in the winter period, in particular.

Complete sets of hygric and thermal properties were, however, not published as results of research studies for very common types of AAC either, at least not in the form that they could be directly used as input parameters of computer codes. Considering the high application frequency of AAC in building practice, it seems to be surprising how rarely AAC becomes subject of scientific papers (only about 150 publications in the WoS database during the last 30 years). Thermal conductivity is probably the most frequently studied AAC-related topic [1–6], together with the mechanical properties [5,7–13]. Performance assessments of particular AAC materials and structures in specific conditions have also been published [14–18]. On the other hand, the number of publications on hygric parameters, gas permeability and hygric and thermal movements is extremely low. The papers by Wagner et al. [19] on gas permeability, Gottfredsen et al. [20] on hygric expansion, Janz [21], Goual et al. [22] and Ioannou et al. [23] on water sorptivity and Tada and Watanabe [24] and Goual et al. [22] for sorption isotherms belong to the very few exceptions in that respect. Computational simulation of hygrothermal performance of AAC-based structures was presented in several papers [25–27] but the results of calculations were used more or less just for model validation purpose.

In this paper, complete sets of hygric and thermal properties of three commercially produced AAC with different bulk density and compressive strength are measured, together with the basic physical properties and durability properties. The obtained data will make it possible to substantially improve the quality of service life assessment studies of AAC-based building envelopes commonly used in the practice.

2. Experimental

2.1. Materials

Three different autoclaved aerated concretes manufactured by Xella CZ, Ltd., were studied, P1.8-350, P2-350 and P4-500. In the marks of the particular products, the first number means compressive strength in MPa, the second number the bulk density in kg m^{-3}. According to the manufacturer's list [28] their supposed application is for non-bearing- and load-bearing walls, fireproof walls and retention walls and linings in the interior. The data for hygric and thermal properties given by the manufacturer [28] include only the thermal conductivity in dry state, the specific heat capacity (one value according to ČSN EN 1745) and the water vapor diffusion resistance factor (two values according to ČSN EN 1745).

2.2. Methods

All the experiments were realized in the air-conditioned laboratory at constant temperature 25C ± 1 °C and relative humidity 30 ± 5%.

2.2.1. Basic characteristics

The bulk density ρ_b (kg m^{-3}), open porosity ψ (% m^3 m^{-3}), saturation moisture content $w_{sat,vac}$ (kg m^{-3}), and matrix density ρ_{mat} (kg m^{-3}) were determined using the water vacuum saturation method [29]. The experiments were done on six cubic samples of side 50 mm. The capillary saturation moisture content $w_{sat,cap}$ (kg m^{-3}) was measured on six cubic samples of side 100 mm which were submerged under water for 48 h. The matrix density and open porosity was determined by the helium pycnometry as well, for the purpose of comparison. The measurements were performed by Pycnomatic ATC equipment (Porotec, Germany).

The compressive strength was measured according to ČSN EN 679. Characterization of the pore structure was done by mercury intrusion porosimetry (MIP). The experiments were carried out using the instruments Pascal 140 and 440 (Thermo Scientific).

2.2.2. Hygric properties

The water absorption coefficient A (kg m^{-2} $s^{-1/2}$) was measured using an experimental setup with automatic data acquisition [30]. In order to test the isotropy of analyzed materials, the measurements were done for two sets of three cubic samples of side 50 mm which were cut from the original AAC blocks in two directions; A was along the block (within the plane of the wall) and B across the block (across the wall). The apparent moisture diffusivity κ_{app} (m^2 s^{-1}) was calculated using the data for water absorption coefficient and vacuum saturation moisture content according to the basic formula given in [31].

The moisture diffusivity κ (m^2 s^{-1}) as a function of moisture content w (m^3 m^{-3}) was determined by an inverse analysis of moisture profiles measured by a capacitance method [32]. The measurement was done in horizontal position on three rectangular prismatic specimens with the dimensions of 20 mm × 40 mm × 300 mm. The experimental moisture profiles were approximated by the linear filtration method with Gaussian weights [33] and the moisture diffusivity calculated in dependence on moisture content using the Boltzmann–Matano method [34].

The dry cup and wet-cup methods were employed in the measurement of water vapor transport properties [29]. The experiments were done for two sets of three cylindrical samples with the diameter of 100 mm and height of 20 mm which were cut from the original AAC blocks in two directions A, B in the same way as in the measurement of water absorption coefficient. The water vapor diffusion permeability δ (s), water vapor diffusion coefficient D (m^2 s^{-1}) and water vapor diffusion resistance factor μ (–) were the investigated parameters.

Water adsorption isotherms were measured using the desiccators' method [29]. Three specimens with the dimensions of 40 mm × 40 mm × 10 mm were used. Water retention curves were determined using the results of porosimetric measurements according to the method described in [35].

2.2.3. Thermal properties

The thermal conductivity λ (W m^{-1} K^{-1}) and specific heat capacity c (J kg^{-1} K^{-1}) were measured using the commercial device Isomet 2104 (Applied Precision, Ltd.). Isomet 2104 is equipped with various types of optional probes, needle probes are for porous, fibrous or soft materials, and surface probes are suitable for hard materials. The measurement is based on the analysis of the temperature response of the analyzed material to heat flow impulses. The heat flow is induced by electrical heating using a resistor heater having a direct thermal contact with the surface of the sample. The measurements of thermal conductivity at room temperature were done in dependence on moisture content by mass u (kg kg^{-1}). Thermal conductivity

of dry specimens was also measured as a function of temperature from 2 °C to 40 °C. The specific heat capacity was measured in the dry state only. Its dependence on moisture content was determined using the linear theory of mixtures (the specific heat capacity as a heat storage parameter is an additive quantity) according to the equation.

$$c_{wet}(u) = \frac{c_{dry} + c_w u}{1 + u} \quad (1)$$

where u is the moisture content by mass, c_{dry} the specific heat capacity in dry state, c_w the specific heat capacity of water. Three cubic samples of side 100 mm were used for each moisture content and temperature.

2.2.4. Durability properties

The basic freeze resistance tests were done according to ČSN EN 15304. 12 cubic samples (6 for testing and 6 for reference) of side 100 mm were dried at first, then submerged in water for 48 h and left for another 24 h in the laboratory in polyethylene bags for moisture content equilibration. The freeze resistance test consisted in exposing always three samples to 25 and 50 freeze/thaw cycles; freezing was realized for 8 h at −15 °C, thawing for 8 h at 20 °C. After the test, the mass of water saturated samples was determined, samples were dried and their mass was measured again. Freeze resistance was evaluated on the basis of the total amount of scaling residue (mass loss) and compressive strength.

The standard test described above is only partially suitable for making computational service life estimates of building envelopes as the materials involved are only rarely in fully water saturated state [36,37]. Therefore, extended tests of freeze resistance were done as well where the samples in the beginning of the experiment were in the dry state and in the state with the equilibrated moisture content of 10% by volume. In this case, the samples remained in polyethylene bags during the whole time of their exposure to freeze/thaw cycles to ensure constant moisture content. Otherwise, the conditions of the test were the same as in ČSN EN 15304.

3. Results and discussion

3.1. Basic characteristics

The bulk densities measured by water vacuum saturation method (Table 1) agreed with the marks of the particular AAC materials within 4%. This was acceptable, taking into account the supposed nonhomogeneity of AAC. The open porosities determined by water vacuum saturation method (Table 1) and helium pycnometry (Table 2) differed up to 3% which was a reasonable agreement. They also decreased with increasing bulk density as expected. However, the matrix densities measured by water vacuum saturation method and helium pycnometry (Tables 1 and 2) exhibited differences in the range of 10–20%. The explanation can be found in the different character of both methods. While water in the vacuum saturation method penetrates into evacuated samples, helium in the pycnometric method intrudes into the samples under a pressure of 0.21 MPa. In water vacuum saturation method rectangular samples having a volume of 125 cm^3 are used, in helium pycnometry powder samples of about 20–30 cm^3 are analyzed. On the other hand, the results obtained by these two methods for concrete in previous measurements [38] agreed very well, within 2%. The observed differences in matrix density in the case of AAC may be attributed to a possible imperfect evacuation of its complex pore structure at the water vacuum saturation measurement. For fine-grained materials with complex pore structure the helium pycnometry should give more precise values of matrix density than the water vacuum saturation method despite the smaller size of the specimens because the small helium molecules can enter even the smallest pores of the crushed samples.

The measured compressive strengths (Table 2) were 10–15% higher than the marks specified by the manufacturer. This was quite a satisfactory result.

The capillary saturation moisture content (Table 2) of all studied AAC was more than two times lower than the vacuum saturation moisture content (Table 1). Such differences in saturation moisture content under vacuum and in the conditions of capillary water uptake were observed already before for other materials [29,39]. They were usually caused by trapping of air in dead-end pores at capillary water uptake which was also the supposed reason in the case of AAC analyzed in this paper.

The porosity determined by MIP (Table 3) was three to six times lower than the total open porosity measured by the water vacuum saturation method (Table 1). As MIP can only identify pores under 100 μm, the difference can be attributed to the pores of higher radii. This opinion is supported by the SEM analysis in [23] which revealed for similar AAC of the same manufacturer an unusual micro/macro-structure, which comprised a fine pored matrix within which were dispersed large aeration pores formed by foaming the wet slurry.

The pore size distribution of P1.8-300 and P2-350 was similar (Fig. 1). Two main peaks at about 20 nm and 200 nm could be observed, the first one being more distinct for P1.8-300, the second for P2-350. The material P4-500 had two to three times lower amount of pores in the whole range of 3–100 μm. The maxima were in a similar range of radii as in the case of other two AAC although they were not so pronounced.

Table 1
Basic characteristics measured by water vacuum saturation method.

Material	Saturation moisture content (kg m^{-3})	Matrix density (kg m^{-3})	Open porosity (% m^3 m^{-3})	Bulk density (kg m^{-3})
P1.8-300	873	2451	87.4	304
P2-350	818	2048	81.9	363
P4-500	802	2527	80.2	500

Table 3
Global characteristics of the pore space measured by mercury intrusion porosimetry.

Material	Total pore volume (cm^3 g^{-1})	Porosity (pores under 100 μm) (% m^3 m^{-3})
P1.8-300	0.8229	24.7
P2-350	0.7575	22.7
P4-500	0.2825	14.1

3.2. Hygric properties

The water absorption coefficient and apparent moisture diffusivity (Tables 4a and 4b) increased with increasing bulk density (and decreasing porosity) which was an unexpected behavior. The explanation may be found in the highest volume of large pores above 100 μm in P4-500 which can be estimated as the difference

Table 2
Basic characteristics measured by other methods.

Material	Capillary saturation moisture content (kg m^{-3})	Compressive strength (MPa)	Matrix density (helium pycnometry) (kg m^{-3})	Open porosity (helium pycnometry) (% m^3 m^{-3})
P1.8-300	356	2.05	2034	85.1
P2-350	385	2.24	2228	83.7
P4-500	389	4.6	2229	77.6

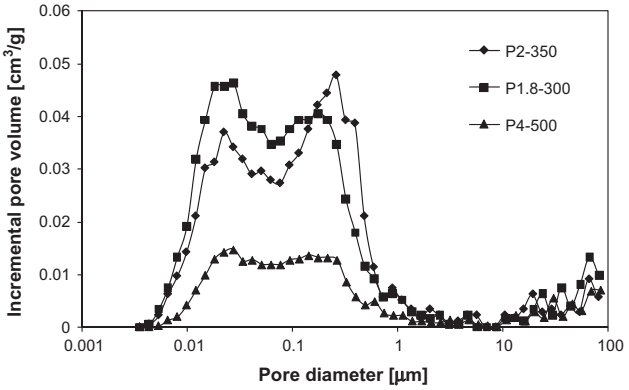

Fig. 1. Pore size distribution.

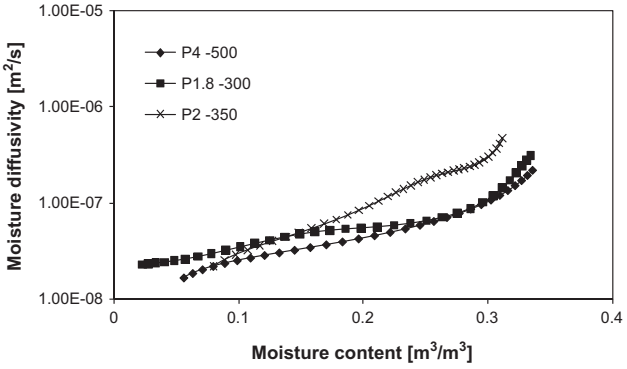

Fig. 2. Moisture diffusivity as a function of moisture content.

Table 4a
Liquid water transport parameters – direction A.

Material	Water absorption coefficient ($kg\ m^{-2}\ s^{-1/2}$)	Apparent moisture diffusivity (calculated using $w_{sat,vac}$) ($m^2\ s^{-1}$)	Apparent moisture diffusivity (calculated using $w_{sat,cap}$) ($m^2\ s^{-1}$)
P1.8-300	0.028	1.03×10^{-9}	6.19×10^{-9}
P2-350	0.032	1.53×10^{-9}	6.91×10^{-9}
P4-500	0.044	3.01×10^{-9}	1.28×10^{-8}

Table 4b
Liquid water transport parameters – direction B.

Material	Water absorption coefficient ($kg\ m^{-2}\ s^{-1/2}$)	Apparent moisture diffusivity (calculated using $w_{sat,vac}$) ($m^2\ s^{-1}$)	Apparent moisture diffusivity (calculated using $w_{sat,cap}$) ($m^2\ s^{-1}$)
P1.8-300	0.030	1.18×10^{-9}	7.10×10^{-9}
P2-350	0.031	1.44×10^{-9}	6.48×10^{-9}
P4-500	0.044	3.01×10^{-9}	1.28×10^{-8}

between capillary moisture content and pore volume determined by MIP (Tables 2 and 3).

The differences of water absorption coefficients in two principal directions (across and along the block) were for all three AAC within the error range of the measuring method. Therefore, the analyzed materials could be considered isotropic from the point of view of liquid water transport.

The moisture diffusivity κ of all AAC materials increased fast with increasing moisture content w (Fig. 2), the differences in κ for the lowest and highest moisture contents were approximately one order of magnitude. The $\kappa(w)$ function of P4-500 was lowest over the whole moisture range studied. This was in a qualitative agreement with the pore size distribution measurements (Fig. 1); P4-500 had in the range of 10 nm–1 μm substantially lower pore volume than other two materials. For moisture contents higher than $\approx 0.15\ m^3/m^3$ the moisture diffusivity of P2-350 was up to three times higher as compared to other two AAC. This corresponded with the highest pore volume in the range of 200–600 nm observed for P2-350 (Fig. 1).

It should be noted that the moisture dependent moisture diffusivity in Fig. 2 was as much as one to two orders of magnitude higher than the apparent moisture diffusivity in Tables 4a and 4b. This difference was too great to be attributed solely to the overall higher quality of the method involving inverse analysis of moisture profiles (it is capable of providing the $\kappa(w)$ function contrary to the sorptivity method which works with an assumption of constant κ). The effect of gravity was a factor that could also play an important role. The sorptivity experiment was performed in vertical position while the measurement of moisture profiles was done in horizontal position. In the unusual micro/macro-structure of AAC, which was observed in [23] and confirmed by the measurement of basic physical parameters in this paper, the fine pores of the matrix made good prerequisites for capillary transport but the aeration pores which are known even not to be interconnected during the capillary transport exhibited only weak capillary suction. In the vertical orientation of the sorptivity experiment the gravity force slowed down the water transport in aeration pores which decreased the calculated apparent moisture diffusivity. Yet another factor was the value of saturation moisture content used for the calculation of apparent moisture diffusivity κ_{app}. In this paper the water vacuum saturation moisture content $w_{sat,vac}$ was utilized as it was common in previous studies [31]. However, the observed high differences in saturation moisture content under vacuum and in the conditions of capillary water uptake (Tables 1 and 2) may advice against this choice; the sorptivity experiment uses a free water uptake setup. If the capillary saturation moisture content $w_{sat,cap}$ (Table 2) was used for the calculation of κ_{app}, its values were four to six times higher than using $w_{sat,vac}$ (Tables 4a and 4b).

The fastest water vapor transport was observed for P1.8-300 in both wet-cup and dry-cup arrangements (Tables 5a and 5b) which was in accordance with its highest porosity (Table 1). However, the water vapor diffusion permeability of P4-500 was higher than P2-350 despite its lower open porosity. Similarly as in the case of liquid water transport this could be explained by the higher volume of pores with the radii above 100 μm in P4-500 (Tables 1 and 3). In this type of pores the water vapor transport was faster than in smaller pores due to the relatively lower importance of the friction on pore walls. Any pronounced anisotropy in water vapor transport was not observed for all three studied AAC. The differences in water vapor diffusion permeabilities in two directions A, B were either within or on the edge of the error range of the measuring method.

The water vapor diffusion permeabilities δ measured using the wet-cup method were systematically higher than the corresponding δ values acquired in the dry cup method. The apparent reason for this finding was that the water vapor transport parameters measured in the wet-cup setup partially include also hydrodynamic transport of capillary condensed water in the pore system, besides the bulk water vapor diffusion.

The water vapor adsorption capability of P1.8-300 was highest in the range of low relative humidity but for higher relative humidity the highest moisture content was observed for P2-350 (Fig. 3). This was in accordance with the pore size distribution measurements (Fig. 1). P1.8-300 had the highest amount of pores in the

Table 5a
Water vapor transport parameters in the dry-cup arrangement (5–50%).

Material	Direction A			Direction B		
	Water vapor diffusion permeability (s)	Water vapor diffusion coefficient ($m^2\ s^{-1}$)	Water vapor diffusion resistance factor (–)	Water vapor diffusion permeability (s)	Water vapor diffusion coefficient ($m^2\ s^{-1}$)	Water vapor diffusion resistance factor (–)
P1.8-300	2.4×10^{-11}	3.3×10^{-6}	7.2	2.4×10^{-11}	3.4×10^{-6}	7.1
P2-350	1.12×10^{-11}	1.52×10^{-6}	15.3	1.41×10^{-11}	1.93×10^{-6}	12.0
P4-500	1.7×10^{-11}	2.3×10^{-6}	10.2	1.9×10^{-11}	2.6×10^{-6}	9.7

Table 5b
Water vapor transport parameters in the wet-cup arrangement (97–50%).

Material	Direction A			Direction B		
	Water vapor diffusion permeability (s)	Water vapor diffusion coefficient ($m^2\ s^{-1}$)	Water vapor diffusion resistance factor (–)	Water vapor diffusion permeability (s)	Water vapor diffusion coefficient ($m^2\ s^{-1}$)	Water vapor diffusion resistance factor (–)
P1.8-300	5.92×10^{-11}	8.14×10^{-6}	2.9	9.75×10^{-11}	1.34×10^{-5}	2.2
P2-350	5.64×10^{-11}	7.69×10^{-6}	3.0	5.12×10^{-11}	6.98×10^{-6}	3.3
P4-500	5.91×10^{-11}	8.13×10^{-6}	2.9	5.58×10^{-11}	7.68×10^{-6}	3.1

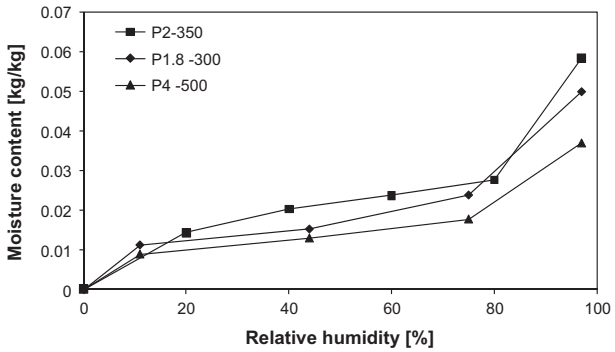

Fig. 3. Adsorption isotherms.

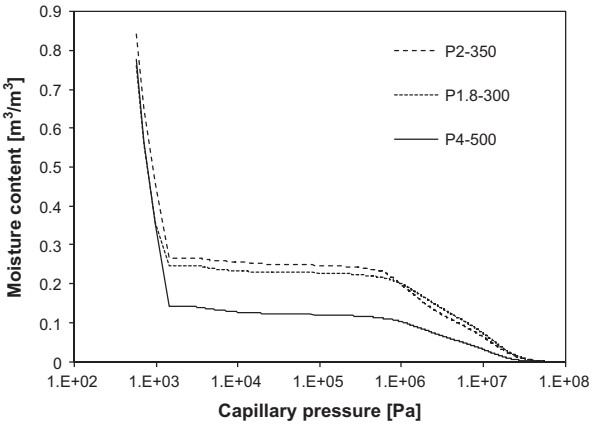

Fig. 4. Water retention curves.

range of smallest pores, thus also the highest specific pore surface area which was responsible for the highest water vapor adsorption. The moisture content of P4-500 decreased with capillary pressure very quickly (Fig. 4) which reflected its highest pore volume above 100 μm (Tables 1 and 3). The highest moisture content for lower capillary pressures exhibited P2-350.

Comparison of hygric properties of AAC determined in this paper with the results presented by other investigators could be done in a limited extent only because for some parameters the available data was very sparse if any.

The water absorption coefficient A was the most often studied hygric parameter. However, the obtained results differed even for seemingly very similar types of AAC. For instance, for AAC with 450 kg/m^3 (Ytong-DK) $A = 0.045\ kg\ m^{-2}\ s^{-1/2}$ was obtained [23] (which was roughly the same as P4-500 in this paper) while for Ytong-CZ with the same bulk density of 450 kg/m^3 $A = 0.168\ kg\ m^{-2}\ s^{-1/2}$ was found [30]. This indicated remarkable differences in AAC production process even in the factories of the same manufacturer located in different countries. The manufacturing details were, however, obviously not accessible to anybody outside the company so that it was not possible to assess the differences in an analytic way.

For the moisture diffusivity of AAC given as a function of moisture content $\kappa(u)$ only two references were found in the WoS database [21,40]. In [21] the author determined $\kappa(u)$ of AAC with the bulk density of 500 kg/m^3 in a series of absorption tests and obtained $\kappa \approx 2 \times 10^{-8}\ m^2\ s^{-1}$ for lowest moisture contents and $\kappa \approx 1 \times 10^{-6}\ m^2\ s^{-1}$ for highest moisture contents, i.e., values almost one order of magnitude higher compared to P4-500. The $\kappa(u)$ function measured in [40] for AAC with the bulk density of 450 kg/m^3 ranged from $2.3 \times 10^{-9}\ m^2\ s^{-1}$ to $1.2 \times 10^{-7}\ m^2\ s^{-1}$, i.e., for lower moisture contents it was about four times lower compared to P4-500 but for higher moisture contents very similar. It should be noted that $\kappa(u)$ functions may be available in some other databases as well because many researchers dealt with that parameter in the past. However, such databases are often difficult to access. Therefore, we confined ourselves to a comparison within the standard WoS database only.

The water vapor adsorption isotherm of AAC with 480 kg/m^3 presented in [24] was similar in shape to P4-500 in this paper but the amount of adsorbed water was 20–50% higher in the analyzed range of relative humidity.

Table 6
Thermal conductivity as a function of temperature ($W\ m^{-1}\ K^{-1}$).

Material	2 °C	10 °C	15 °C	25 °C	30 °C	40 °C
P1.8-300	0.0625	0.0700	0.0737	0.0802	0.0815	0.0938
P2-350	0.0802	0.0814	0.0837	0.0843	0.0856	0.0864
P4-500	0.0941	0.1060	0.1088	0.1218	0.1288	0.1438

Table 7
Comparison of measured parameters with manufacturer's declarations.

Parameter	P1.8-300		P2-350		P4-500	
	Measured	Declared	Measured	Declared	Measured	Declared
ρ (kg m^{-3})	304	300	363	350	500	500
c_{dry} (J kg^{-1} K^{-1})	1080	1000	1160	1000	1050	1000
λ_{dry} (W m^{-1} K^{-1})	0.0802	0.080	0.0843	0.085	0.1218	0.120
$\mu_{dry\ cup}$ (–)	7.1	10	13.6	10	10.0	10
$\mu_{wet\text{-}cup}$ (–)	2.5	5	3.3	5	3.0	5
f_c (MPa)	2.05	1.8	2.24	2.0	4.6	4.0

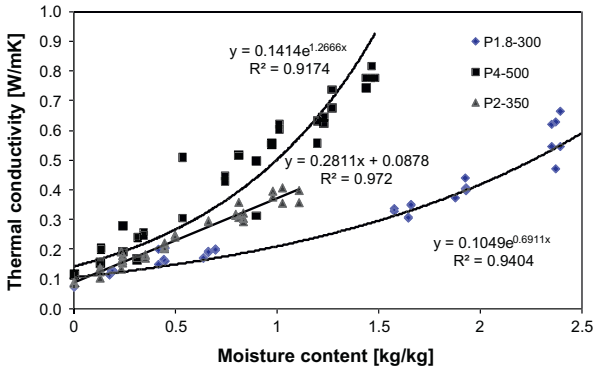

Fig. 5. Thermal conductivity as a function of moisture content.

The data for water vapor diffusion resistance factor μ given by the manufacturer (Table 7) differed from the measured values in the range of 30–50%. However, it should be noted that the manufacturer used only general data given in ČSN EN 1745 and their μ values were the same for products with large differences (300–500 kg/m^3) in bulk density, thus not very reliable.

3.3. Thermal properties

The thermal conductivity λ of analyzed AAC was for higher moisture contents up to six times higher than in the dry state (Fig. 5). This was very significant finding, in particular from the point of view of practical applicability of λ values included in various standards and material lists of manufacturers which are mostly in the dry state only. The highest λ in the whole range of moisture content from dry state to capillary water saturation exhibited P4-500, the lowest λ had P1.8-300 which was in accordance with the bulk density and pore size distribution (Table 1 and Fig. 1).

The dependence of thermal conductivity on temperature (Table 6) was far less important than its dependence on moisture content. In the temperature range of 2–30 °C the lowest λ exhibited P1.8-300, the highest λ had P4-500 which corresponded to their bulk density (Table 1). At 40 °C, sudden increase of λ was observed for P1.8-300 and P4-500. This could be caused by the increased role of radiation in larger pores above 100 μm.

The values of the specific heat capacity in dry state, c_{dry}, differed for the particular types of AAC only within 10% (Table 7) which was roughly within the error range of the measuring method so that the differences could be considered not very significant. The dependence of the specific heat capacity on moisture content by mass can be calculated using Eq. (1) and the measured c_{dry} values in Table 7.

The thermal conductivity in dry state λ_{dry} was widely studied by other investigators. For instance, in [4] λ_{dry} = 0.141 W/m K was found for AAC with the bulk density of 500 kg/m^3. This was 15% higher than λ_{dry} of P4-500 in this paper. In [5] for AAC with 500 kg/m^3 λ_{dry} = 0.12 W/m K was obtained which was in a very good agreement with λ_{dry} of P4-500. The values of λ_{dry} declared by the manufacturer (Table 7) agreed with the measurements in this paper within 1–2% which was excellent.

The measured specific heat capacity in dry state was for the three studied AAC up to 20% higher than the data given by the manufacturer (Table 7). However, similarly as in the case of water vapor diffusion resistance factor also this data was only general values taken from ČSN EN 1745.

3.4. Durability properties

In the standard freeze/thaw resistance tests with capillary water saturated samples the best performance from the point of view of both mass loss and loss of compressive strength after 25 and 50 cycles exhibited P4-500 (Tables 8a and 8b) which correlated with its highest compressive strength. The loss of mass of only 1.5% and loss of compressive strength of 16.6% after 50 freeze/thaw cycles was quite satisfactory. The values obtained for P1.8-300 and P2-350 were several times higher than for P4-500. The observed loss of compressive strength which was as high as 46% meant that both P1.8-300 and P2-350 effectively lost their load bearing function after 50 cycles. On the other hand, the loss of compressive strength after 25 cycles was for all AAC in the range of 5–12% which could still be considered acceptable. It should also be noted that an exposure of AAC in a structure to 50 freeze/thaw cycles in water saturated state is during their service life very unlikely.

The extended freeze/thaw resistance tests showed that in dry state all three AAC had an excellent resistance to freeze/thaw cycles; the loss of both mass and compressive strength was negligible (Tables 8a and 8b). If the initial moisture content in the samples was 10% by volume, which was more likely to appear in a real structure than full water saturation, the results for P4-500 and P2-350 were similar. The mass loss of 4–5% and loss of compressive

Table 8a
Freeze resistance – 25 freeze/thaw cycles.

Material	Dry samples		Samples with 10% moisture content		Capillary water saturated samples	
	Mass loss (%)	Loss of compressive strength (%)	Mass loss (%)	Loss of compressive strength (%)	Mass loss (%)	Loss of compressive strength (%)
P1.8-300	0	0	1.7	7.5	8.0	12.1
P2-350	0	0	0.53	4.5	10.1	8.1
P4-500	0	0	0.24	5.1	0.7	5.2

Table 8b
Freeze resistance – 50 freeze/thaw cycles.

Material	Dry samples		Samples with 10% moisture content		Capillary water saturated samples	
	Mass loss (%)	Loss of compressive strength (%)	Mass loss (%)	Loss of compressive strength (%)	Mass loss (%)	Loss of compressive strength (%)
P1.8-300	0.50	0.10	1.3	16.3	14.5	46.0
P2-350	0.36	0.03	1.4	6.3	23.5	45.7
P4-500	0.43	0.00	1.5	8.0	1.5	16.6

strength of 6–8% after 50 cycles was acceptable. P1.8-300 achieved worse results than the other two AAC but 16% loss of compressive strength after 50 cycles was still relatively good, taking into account the compressive strength value in dry state (Table 2).

The obtained results were in a qualitative agreement with the findings presented in [41] where cellular concretes with bulk density in the range of 500–600 kg/m^3 and compressive strength between 1 MPa and 2 MPa provided good freeze/thaw resistance if the initial moisture content was less than 16%.

4. Conclusions

Three autoclaved aerated concretes of the same manufacturer, with the bulk density of 300–500 kg/m^3 and compressive strength of 1.8–4 MPa, were studied. The main results achieved at the investigation of their basic physical characteristics, hygric, thermal and durability properties can be summarized as follows:

- The analyzed AAC exhibited high liquid water transport capability which was comparable for instance with ceramic brick. The dependence of moisture diffusivity on moisture content was remarkable. For high moisture content it was as much as one order of magnitude greater than for the lowest moisture content.
- The water vapor was transported very quickly in the investigated AAC. The water vapor permeability coefficient was for high relative humidity up to five times higher than for low relative humidity.
- All three AAC products were found isotropic from the point of view of water and water vapor transport.
- The moisture storage capability of analyzed AAC was relatively high which made possible their utilization as moisture buffering layers in building envelopes.
- Any palpable correlation of water- and water vapor transport and storage properties with the bulk density in the range of 300–500 kg/m^3 was not manifested in the experimental results. The apparent reason was using specific additives and technology adjustments by the manufacturer which, however, could not be exactly identified due to the lack of necessary details on the production process.
- The thermal conductivity in dry state was in a good correlation with the bulk density in the range of 300–500 kg/m^3. This indicated that the manufacturers probably achieved their current limits in the homogenization of the pore structure of their products.
- The thermal conductivity increased with moisture content up to six times compared with the dry state. This was very significant finding, in particular from the point of view of practical applicability of thermal conductivity values included in various standards and material lists of manufacturers which are mostly in the dry state only.
- The dependence of thermal conductivity on temperature was less pronounced than on moisture content. In the temperature range of 2–40 °C its increase was up to 50% only. However, for hygrothermal calculations this difference may also be very important.
- The freeze/thaw resistance increased with compressive strength of AAC. In the standard test with capillary saturated samples the loss of mass and compressive strength after 25 cycles was acceptable for all studied AAC but for 50 cycles only the material with the compressive strength of 4 MPa performed satisfactorily. In the extended tests with samples which were initially dry or contained 10% of water the freeze/thaw resistance was tolerable for all materials, i.e., in the range of compressive strength of 1.8–4 MPa.

Acknowledgement

This research has been supported by the Czech Science Foundation, under Project No. P105/12/G059.

References

[1] Laurent JP. An estimation model for the dry thermal-conductivity of autoclaved aerated concrete. Mater Struct 1991;24:221–6.
[2] Laurent JP, Guerrechaley C. Influence of water-content and temperature on the thermal-conductivity of autoclaved aerated concrete. Mater Struct 1995;28:464–72.
[3] Boutin C. Thermal conductivity of autoclaved aerated concrete: modelling by the self-consistent method. Mater Struct 1996;29:609–15.
[4] Kubicar L, Bohac V, Vretenar V, Barta S, Neuer G, Brandt R. Thermophysical properties of heterogeneous structures measured by pulse transient method. Int J Thermophys 2005;26:1949–62.
[5] Albayrak M, Yorukoglu A, Karahan S, Atlihan S, Aruntas HY, Girgin I. Influence of zeolite additive on properties of autoclaved aerated concrete. Build Environ 2007;42:3161–5.
[6] Zapotoczna-Sytek G, Zmywaczyk J, Koniorczyk P, Lubińska K, Górska B. Investigations of 'thickness effect curve' in sand autoclaved aerated concrete (SAAC 500). Cem Wapno Beton 2009;14:301–7.
[7] Trunk B, Schober G, Helbling AK, Wittmann FH. Fracture mechanics parameters of autoclaved aerated concrete. Cem Concr Res 1999;29:855–9.
[8] Narayanan N, Ramamurthy K. Prediction relations for compressive strength of aerated concrete. ACI Mater J 2000;97:367–73.
[9] Benazzouk A, Douzane O, Mezreb K, Queneudec M. Physico-mechanical properties of aerated cement composites containing shredded rubber waste. Cem Concr Compos 2006;28:650–7.
[10] Cabrillac R, Florio B, Beaucour AL, Dumontet H, Ortola S. Experimental study of the mechanical anisotropy of aerated concretes and of the adjustment parameters of the introduced porosity. Constr Build Mater 2006;20:286–95.
[11] Kurama H, Topcu IB, Karakurt C. Properties of the autoclaved aerated concrete produced from coal bottom ash. J Mater Process Technol 2009;209:767–73.
[12] Laukaitis A, Keriene J, Mikulskis D, Sinica M, Sezemanas G. Influence of fibrous additives on properties of aerated autoclaved concrete forming mixtures and strength characteristics of products. Constr Build Mater 2009;23:3034–42.
[13] Karakurt C, Kurama H, Topçu IB. Utilization of natural zeolite in aerated concrete production. Cem Concr Compos 2010;32:1–8.
[14] Al-Mudhaf HA, Attiogbe EK. Performance of autoclaved aerated-concrete masonry walls in Kuwait. Mater Struct 1996;29:448–52.
[15] Kus H, Nygren K. Microenvironmental characterization of rendered autoclaved aerated concrete. Build Res Inf 2002;30:25–34.
[16] Kus H, Nygren K, Norberg P. In-use performance assessment of rendered autoclaved aerated concrete walls by long-term moisture monitoring. Build Environ 2004;39:677–87.
[17] Kaska O, Yumrutas R. Comparison of experimental and theoretical results for the transient heat flow through multilayer walls and flat roofs. Energy 2008;33:1816–23.
[18] Mousa MA, Uddin N. Experimental and analytical study of carbon fiber-reinforced polymer (FRP)/autoclaved aerated concrete (AAC) sandwich panels. Eng Struct 2009;31:2337–44.
[19] Wagner F, Schober G, Mortel H. Measurement of the gas-permeability of autoclaved aerated concrete in conjunction with its physical-properties. Cem Concr Res 1995;25:1621–6.

[20] Gottfredsen FR, Knutsson HH, Nielsen A. Determination of length changes due to moisture variations in autoclaved aerated concrete. Mater Struct 1997;30:148–53.
[21] Janz M. Moisture diffusivities evaluated at high moisture levels from a series of water absorption tests. Mater Struct 2002;35:141–8.
[22] Goual MS, Bali A, de Barquin F, Dheilly RM, Quéneudec M. Isothermal moisture properties of clayey cellular concretes elaborated from clayey waste, cement and aluminium powder. Cem Concr Res 2006;36:1768–76.
[23] Ioannou I, Hamilton A, Hall C. Capillary absorption of water and n-decane by autoclaved aerated concrete. Cem Concr Res 2008;38:766–71.
[24] Tada S, Watanabe K. Dynamic determination of sorption isotherm of cement based materials. Cem Concr Res 2005;35:2271–7.
[25] Becker R. Validation of a mathematical and numerical model for dynamic 1-D moisture content evolution in layered building elements. Mater Struct 2002;35:382–8.
[26] Holm AH, Kuenzel HM. Practical application of an uncertainty approach for hygrothermal building simulations – drying of an AAC flat roof. Build Environ 2002;37:883–9.
[27] Salagnac P, Glouannec P, Lecharpentier D. Numerical modeling of heat and mass transfer in porous medium during combined hot air, infrared and microwaves drying. Int J Heat Mass Transfer 2004;47:4479–89.
[28] http://www.xella.cz/html/czk/cz/ytong-presne-tvarnice.php.
[29] Roels S, Carmeliet J, Hens H, Adan O, Brocken H, Černý R, et al. Interlaboratory comparison of hygric properties of porous building materials. J Therm Envelope Build Sci 2004;27:307–25.
[30] Vejmelková E, Pavlíková M, Jerman M, Černý R. Free water intake as means of material characterization. J Build Phys 2009;33:29–44.
[31] Kumaran MK. Moisture diffusivity of building materials from water absorption measurements. J Therm Envelope Build Sci 1999;22:349–55.
[32] Semerák P, Černý R. A Capacitance method for measuring moisture content of building materials. Stavební obzor 1997;6:102–3.
[33] Hamming RW. The numerical methods for scientists and engineers. New York: McGraw-Hill; 1962.
[34] Matano C. On the relation between the diffusion coefficient and concentration of solid metals. Jpn J Phys 1933;8:109–15.
[35] Černý R, editor. Complex system of methods for directed design and assessment of functional properties of building materials: assessment and synthesis of analytical data and construction of the system. Prague: Czech Technical University in Prague; 2010.
[36] Kočí V, Maděra J, Černý R, Rovnaníková P. Application of a combined computational-experimental approach for service life estimate of exterior plasters of historical buildings. In: Brebbia C, editor. Structural studies, repairs and maintenance of heritage architecture XI. Southampton: WIT Press; 2009. p. 303–14.
[37] Maděra J, Kočí J, Vejmelková E, Černý R, Rovnaníková P, Ondráček M, et al. Influence of material characteristics of concrete and thermal insulation on the service life of exterior renders. In: Brebbia C, Carlomagno GM, editors. Computational methods and experimental measurements XIV. Southampton: WIT Press; 2009. p. 13–23.
[38] Vejmelková E, Pavlíková M, Keršner Z, Rovnaníková P, Ondráček M, Sedlmajer M, et al. High performance concrete containing lower slag amount: a complex view of mechanical and durability properties. Constr Build Mater 2009;23:2237–45.
[39] Roels S, Carmeliet J, Hens H, Adan O, Brocken H, Černý R, et al. A comparison of different techniques to quantify moisture content profiles in porous building materials. J Therm Envelope Build Sci 2004;27:261–76.
[40] Qiu X, Haghighat F, Kumaran MK. Moisture transport phenomena across interfaces in multi-layered building materials. J Therm Envelope Build Sci 2003;26:213–36.
[41] Tikalsky PJ, Pospisil J, MacDonald W. A method for assessment of the freeze–thaw resistance of preformed foam cellular concrete. Cem Concr Res 2004;34:889–93.

Selected paper 3 – Cement and Concrete Composites:

Jerman, M., Scheinherrová, L., Medveď, I., Krejsová, J., Doleželová, M., Bezdička, P., Černý, R., ***Effect of cyclic wetting and drying on microstructure, composition and length changes of lime-based plasters*** – 2019

For two materials to form a structure, they must be compatible with each other. In addition to chemical compatibility, physical properties must also be considered. If the two bonded materials have different moisture content coefficients, the change in moisture content would cause mutual stresses and subsequent cracking of the structure. In this paper, the longitudinal moisture expansion coefficient is measured beyond current standards from zero moisture to a fully water-saturated state. The test bodies are subjected to a total of five wetting and drying cycles under isothermal conditions. Length changes are monitored during each cycle. In addition, the microstructure of the material is studied, and chemical changes and changes in the pore distribution curve are monitored.

Contribution to practical use: The greatest contribution of the paper is the finding that the greatest length changes take place at humidities close to zero, i.e., in the region outside the standard range. Neglecting this fact can lead, in some cases, to shrinkage cracks and defects in facades.

A further benefit is the finding that the largest length changes take place immediately after the first cycle, with further length changes during cyclic wetting and drying being smaller, which can be crucial for the material's practical use. Based on the results of the coefficient of longitudinal moisture expansion of the plasters studied, manufacturers can make an educated guess as to whether a given plaster is compatible with their construction materials.

Cement and Concrete Composites 104 (2019) 103411

Contents lists available at ScienceDirect

Cement and Concrete Composites

journal homepage: www.elsevier.com/locate/cemconcomp

Effect of cyclic wetting and drying on microstructure, composition and length changes of lime-based plasters

Miloš Jerman[a], Lenka Scheinherrová[a], Igor Medveď[a], Jitka Krejsová[a], Magdaléna Doleželová[a], Petr Bezdička[b], Robert Černý[a,*]

[a] Department of Materials Engineering and Chemistry, Czech Technical University in Prague, Thákurova 7, 166 29, Prague 6, Czech Republic
[b] Institute of Inorganic Chemistry of the Czech Academy of Sciences, Husinec – Řež 1001, 250 68, Řež, Czech Republic

ARTICLE INFO

Keywords:
Lime plasters
Wetting
Drying
Microstructure
Composition
Length changes

ABSTRACT

Plasters as surface layers of building structures are often exposed to cyclic wetting and drying during their service life. In this paper, the impact of cyclic wetting and drying on microstructure, composition, and length changes of lime-based plasters is investigated using mercury intrusion porosimetry, optical microscopy, qualitative and quantitative X-ray diffraction analysis, simultaneous thermal analysis, and contact dilatometry. Lime-cement- and lime-metakaolin plasters as typical representatives of this group are saturated by water at first and then subjected to five consecutive drying-wetting cycles. Hydration processes, together with carbonation and possible partial dissolution of portlandite and calcite after immersion of samples in water, are identified as the most important reactions affecting the microstructure and composition of the lime-cement plaster, while for the lime-metakaolin plaster the pozzolanic reaction resulting in monocarbonate production, together with possible portlandite and calcite dissolution, are probably the most significant factors. The measurements of hygric strain show that the wetting-drying process is near-reversible since the beginning of the second cycle, whereas capillary pressure is the dominant shrinkage/swelling mechanism.

1. Introduction

According to the standards, most parameters of lime- and cement-based materials are determined for 28-days old samples. However, these parameters may be changed over time, which can be caused either by microstructural changes induced by hydration, carbonation and pozzolanic reactions, or by external factors.

Hydration processes and pozzolanic reactions in concrete and mortars can be considered as beneficial over a long time horizon. The increase of compressive strength of ternary cement-based composites over time has been observed by many researchers [1–4]. The strength development of new cementitious materials without Portland cement, such as carbide lime and fly ash, has been recently discussed as well [5]. The application of burnt clay shale [6] or metakaolin [7] as pozzolan additions to lime mortars can present another positive example of the improvement of compressive strength over time. In most cases, the increase of compressive strength was related to a reduction of porosity, which was for cement-based materials described long time ago by Powers [8].

The variation of external conditions can contribute to changes in properties of lime- and cement-based materials in a less straightforward way. El-Turki et al. [9] observed that the cyclic regime of wetting and drying encouraged hydration and consequently caused an increase in strength of lime mortars during the initial 28 days. However, the magnitude of this effect depended on many factors, such as the mix design, number of cycles, and the age of mortar. On the other hand, Wu et al. [10] reported an increase of porosity of concrete after cyclic wetting and drying. Besides the relative humidity changes, they also studied the effect of temperature during drying. More intensively dried samples (50 °C and 105 °C) showed higher gaseous transport properties than gently step-wise dried samples (21 °C). The external factors, such as humidity, temperature, and carbon dioxide concentration can affect significantly also the rate of carbonation [9,11]. The process of carbonation is complex; it requires carbon dioxide to be dissolved in water before the reaction can be developed [12]. Adequate relative humidity conditions in the range of 40%–80% must be maintained [13,14]; ideally with moderate temperatures [12]. Therefore, when cyclic drying and wetting occurs, it can lead to acceleration of carbonation [15], resulting in microstructural changes of lime- and cement-based materials. Carbonation under cyclic drying and wetting conditions can

* Corresponding author.
E-mail address: cernyr@fsv.cvut.cz (R. Černý).

https://doi.org/10.1016/j.cemconcomp.2019.103411
Received 30 July 2018; Received in revised form 10 May 2019; Accepted 3 September 2019
Available online 04 September 2019
0958-9465/

be also accelerated by chloride penetration [16].

Hygric and thermal expansion/shrinkage characteristics of lime- and cement-based composites making possible to determine their length changes in building structures were studied frequently over the last several decades [10,17–22]. However, the investigations in the conditions of cyclic wetting and drying were very rare. The measurement of length changes of autoclaved aerated concrete reported in [23] can be mentioned as one of the very few exceptions in that respect. A more considerable attention has been paid to the compatibility of adjacent layers in multi-layered building structures. Güney and Caner [24] measured thermal and hygric expansion characteristics of mortars and bricks. They found homogeneity of the construction and coherent behavior of materials constituting a structure in ambient conditions crucial for the structural stability and long term durability. The importance of the effect of volume changes resulting from wetting and drying processes and temperature variations was demonstrated also by computational analyses of different concrete structures [25,26]. Cracking of plasters and their detachment from the underlying load bearing materials was observed, which was caused by asymmetric moisture loss during drying and development of tensile stresses.

In this study, the impact of cyclic wetting and drying on microstructure, composition, and length changes of lime-cement- and lime-metakaolin plasters is investigated. The main contribution of the paper to the current state of knowledge is the determination of hygric strain and linear hygric expansion/shrinkage coefficient of lime-based plasters in dependence on the moisture content in both hygroscopic and overhygroscopic range and on the number of previous wetting-drying cycles. For lime-based plasters, which are commonly exposed to varying climatic conditions, a detailed knowledge of cyclic changes of hygric strain is essential for a proper understanding of their long-term behavior in building structures. The availability of hygromechanical parameters of plasters in dependence on moisture content and wetting and drying cycles can affect positively the assessment of possible cumulative damage. In particular, their application as input data of computational damage models can increase the accuracy of service life prediction analyses, as compared with the use of commonly available hygric expansion/shrinkage data.

2. Experimental

2.1. Materials and mix design

The lime-cement plaster (LC) was a commercial product available on the Czech market as a dry mixture of lime, white cement, and aggregates specified by the producer as plaster sand. The recommended water/dry substances ratio of 0.24 was used. The lime-metakaolin plaster (LM) was mixed according to [7] where it was, among the analyzed non-commercial lime–metakaolin plasters, identified as the best in terms of mechanical, fracture-mechanical, hydric, thermal, and durability properties. It had the following composition: 2.08 kg of lime, 7.5 kg of quartz, and 0.42 kg of metakaolin, the water/dry substances ratio was 0.223.

The chemical composition of LC dry mixture, lime, and metakaolin was determined by the high resolution X-ray fluorescence method. A Thermo ARL 9400 XP device was used, data evaluation was done by the standard-less software UniQuant 4. The results are summarized in Table 1.

The mineralogical composition of the raw powders was determined using the XRD method. It was found that lime contained mainly portlandite (95.3 wt%) and calcite (4.7 wt%), metakaolin consisted of 76.1 wt% of amorphous phase, 10.9 wt% of kaolinite, 4.0 wt% of mullite, 2.7 wt% of cristobalite, 2.5 wt% of quartz, 2.0 wt% of illite, and 1.8 wt% of anatase. The commercial LC dry mixture contained 13.8 wt % of C_3S, 2.9 wt% of C_4AF, 2.5 wt% of C_2S, and 2.0 wt% of C_3A, indicating that the amount of the white cement was 21.2 wt% of the dry mixture. The lime content was lower, as only 6.6 wt% of portlandite was found. Quartz and muscovite were the main aggregate components. The mix contained also 19.6 wt% of calcite which was partially involved in lime but its major part was apparently used in the form of fine aggregates. Anorthite, albite, chlorite, and traces of basanite were detected as minor compounds.

Table 1
Chemical composition of raw materials (in wt.%).

Material	LC dry mixture	Lime	Metakaolin
SiO_2	13.30	-	58.70
Al_2O_3	3.40	-	38.50
Fe_2O_3	0.60	-	0.72
CaO	78.40	97.40	0.20
MgO	1.50	0.60	0.38
K_2O	0.40	-	0.85
Na_2O	0.30	-	0.50
SO_3	1.70	0.13	-

2.2. Curing and conditioning

The samples were prepared in 40 × 40 × 160 mm molds. After two days they were demolded and stored for another 26 days in a climatic chamber with the relative humidity of 80%.

After reaching 28 days of age, the cyclic wetting and drying process was started by full immersion of samples in water for 48–72 h. Then, they were put in airtight bags and placed into a climatic chamber set to 25 °C for another 48–72 h to achieve thermal equilibrium. At this point, where the studied samples reached the overhygroscopic range of moisture, some initial measurements were done, in accordance with the applied methods (e.g., length changes, initial mass). This procedure of saturation and consecutive placing of samples into the climatic chamber was repeated several times in order to obtain a sufficient number of length measurements for the overhygroscopic range.

In the next step, the conditioning in the hygroscopic range was started. The samples were put into a climatic chamber with constant relative humidity of 80% and temperature of 25 °C. They were left in the chamber until they achieved the constant mass; in other words, until they were in hygric equilibrium with the chamber environment. After finishing all corresponding measurements at this stage, the samples were put back in the climatic chamber.

The relative humidity was gradually decreased, representing stepwise drying at 25 °C from 80% to 50%, 30%, and 5% (for the achievement of the last relative humidity value, an application of silica gel was necessary). Similarly, to the previous stage, the samples were always left in the climatic chamber until hygric equilibrium with the chamber environment was reached. The moisture equilibration process took three to four weeks for every relative humidity value.

In total, the whole wetting and drying procedure was repeated five times. Finally, the specimens were dried at 105 °C in an oven and then cooled at 25 °C in a desiccator containing silica gel. The conditioning regime is summarized in Fig. 1.

2.3. Methods

2.3.1. Microstructure

Microstructural changes of studied plasters were analyzed using mercury intrusion porosimetry (MIP) and optical microscopy (OM). Pore size distribution curves were measured by Pascal 140 and 440 (Thermo Scientific) devices, having the ability to determine the amount of pores with a radius greater than 0.003 μm and lesser than 100 μm. The surface tension of mercury was assumed 480 mN/m, with a contact angle 130°. All measurements were done on homogenous samples having a mass of ~1 g. Optical microscope images of sample surfaces were obtained using a Carl Zeiss Axio Zoom.V16 device. Samples did not need to be specially prepared before observing (dried, polished,

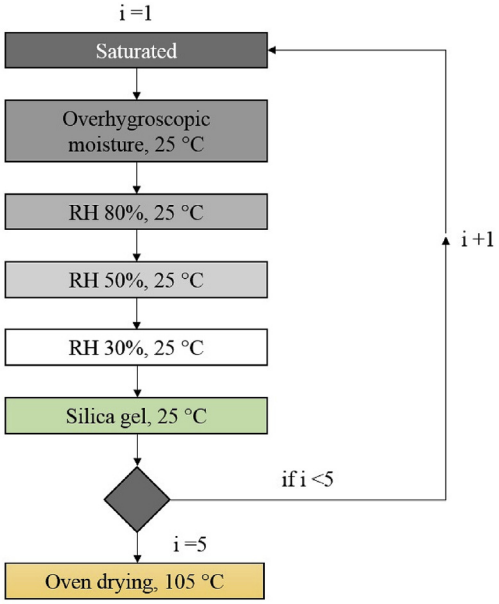

Fig. 1. Scheme of wetting and drying cycles.

etc.). The microscope allowed individual shots composition of examined samples which resulted in a high depth of field and a good resolution of the final image.

2.3.2. Composition

The changes in composition of the analyzed materials were determined by qualitative and quantitative X-ray diffraction (XRD) analysis, differential scanning calorimetry (DSC), and thermogravimetry (TG).

X-ray diffraction patterns were collected using a PANalytical X'Pert PRO diffractometer equipped with a conventional X-ray tube (Cu K_α radiation, 40 kV, 30 mA, line focus) and a linear position sensitive detector PIXCel with an anti-scatter shield. X-ray patterns were measured in the range from 5 to 90° 2 Θ with step of 0.013° and 600 s counting per step, which produced a scan of about 4 h 20 min. A conventional Bragg-Brentano geometry with 0.04 rad Soller slit, 0.25° divergence slit, and 15 mm mask in the incident beam, 0.5 anti-scatter slit, 0.04 rad Soller slit and Ni beta-filter in the diffracted beam was used. XRD patterns were not pre-treated before interpretation as no background correction was needed.

The qualitative XRD analysis was performed with the HighScorePlus software package (PANalytical, The Netherlands, version 4.7.0) and JCPDS PDF-4 database [27]. For the quantitative analysis of XRD patterns, the Profex/BGMN software package was used with structural models based on ICSD database [28,29]. This software tool permits to estimate the mass fractions of crystalline phases by means of Rietveld refinement procedure. The degree of crystallinity was calculated also by the Diffrac-Plus Topas program.

DSC and TG analyses were performed simultaneously using a Labsys Evo (Setaram) instrument. Before the analyses, all studied materials were dried to the constant mass. Specimens for the analysis were taken from the central region of the materials and were ground by hand in a porcelain mill. A 50 ± 1 mg powder sample of each studied material was then placed into an alumina crucible with a volume of 100 mm^3. All experiments were done in the temperature range from 25 to 1000 °C with a heating rate of 5 °C/min in an argon atmosphere (40 mL/min). As blank curves, the data from the second measurement of the same material under identical conditions was used. Therefore, any reversible processes that took place in the studied material, such as α to β transformation of quartz, could not be registered by the simultaneous analysis.

2.3.3. Length changes

The linear hygric expansion coefficient was determined in accordance with the general requirements of the European standard ČSN EN 13009 [30]. Three 40 × 40 × 160 mm specimens were used in the experiments. The length changes were determined using a contact dilatometer provided with an electronic dial indicator (± 1 μm accuracy) and a standard. The specimens had square gauge plugs glued on both face sides to facilitate the measurement.

At first, the reference lengths of the samples, L_S, which corresponded to the state of capillary water saturation (see Section 2.2), and the reference length of the standard, L_{ref}, were measured by a slide gauge with an accuracy of ± 10 μm. The initial readings on dial indicators for both the measured samples and the standard, $L_{S,0}$ and $L_{ref,0}$, respectively, and the initial mass, m_{sat}, of the samples were recorded as well.

Then, after the achievement of every particular state of hygric equilibrium (see Section 2.2 for details), always the mass of the samples, m_i, was determined, and another readings on the dial indicators corresponding to the length changes of the samples and the standard, $L_{S,i}$ and $L_{ref,i}$, respectively, were taken. Each sample was measured three times, and the average of the measured values was used for calculations of the hygric strain, $\varepsilon_{w,i}$ [m/m], as follows:

$$\varepsilon_{w,i} = \frac{(L_{S,0} - L_{S,i}) - (L_{ref,0} - L_{ref,i})}{L_S}. \quad (1)$$

After finishing the measurement for the lowest chosen value of relative humidity in the chamber and the following "chemical" drying process (using silica gel), the mass of the samples, m_n, and the length readings $L_{S,n}$ and $L_{ref,n}$ at the end of the first cycle were determined.

The experiments in the subsequent four cycles were done in exactly the same way as in the first cycle, starting with the capillary water saturated state and finishing with the "chemical" dry state.

Finally, after carrying out oven drying of the samples at 105 °C and their consequent cooling at 25 °C in a desiccator containing silica gel (see Section 2.2), the mass of the samples in the "thermal" dry state, m_d, and the respective length readings, $L_{S,d}$ and $L_{ref,d}$, were recorded.

The moisture content by mass, u_i, [kg/kg] corresponding to each $\varepsilon_{w,i}$ value calculated using Eq. (1) was determined according to the formula

$$u_i = \frac{m_i - m_d}{m_d - m_{plug}} \quad (2)$$

where m_{plug} is the mass of the gauge plugs, and then recalculated to the moisture content by volume w_i [m^3/m^3] as

$$w_i = u_i \frac{\rho_d}{\rho_w} \quad (3)$$

where ρ_d is the bulk density of the material and ρ_w the density of water. In this way, a function $\varepsilon_w(w)$ defined by the set of points [w_i, $\varepsilon_{w,i}$] was determined for every wetting-drying cycle. The corresponding linear hygric expansion coefficient as a function of moisture content, $\alpha_w(w)$ [$(m^3/m^3)^{-1}$], which already presents a parameter directly applicable in the hygromechanical computer simulation tools, was calculated as

$$\alpha_w(w) = \frac{d\varepsilon_w(w)}{dw}. \quad (4)$$

It should be noted that the linear hygric expansion coefficient was considered as a function of moisture content only. The other possible factors, such as the effect of carbonation, were not analyzed separately; they were included, in fact, into the $\alpha_w(w)$ function.

3. Results

3.1. Microstructure

Fig. 2 shows that for the LC plaster the application of wetting-drying

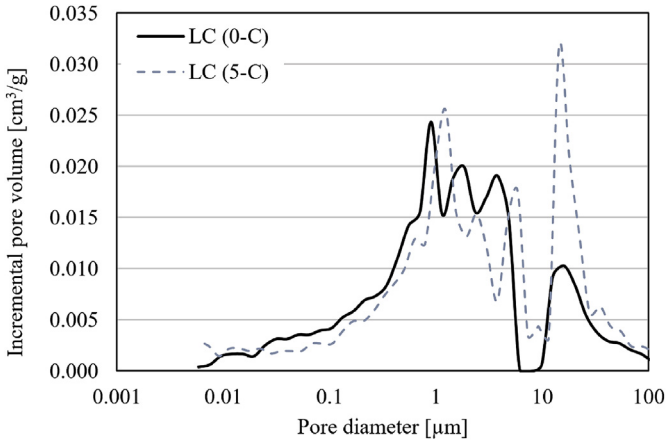

Fig. 2. Pore size distribution of lime-cement plaster LC in the reference state and after five cycles.

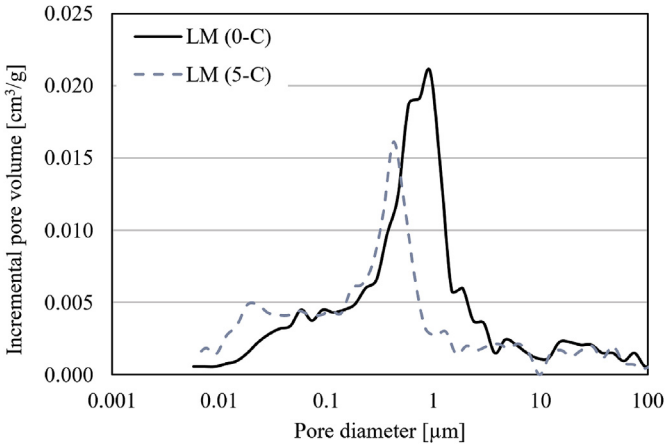

Fig. 4. Pore size distribution of lime-metakaolin plaster LM in the reference state and after five cycles.

cycles led to the development of larger pores. While for the reference samples the main peaks were observed in the area between 0.9 and 3.8 μm, for the samples after the last cycle the main peak was moved to 14 μm. The most important difference between unexposed material and material exposed to five cycles was observed in the range of 10–100 μm. The total porosity of LC samples in the reference state, as determined by MIP, was 44%, after five cycles it increased to 52%. The obtained results were in a good agreement with [10], where also an increase of porosity of concrete after cyclic drying and wetting was observed.

The OM images of LC (Fig. 3) confirmed a higher volume of coarser pores. Fig. 3d shows, that these coarser pores were partially filled with calcium carbonate (calcite, $CaCO_3$). Contrary to the MIP measurements, OM detected open pores with a diameter of 100 μm and higher on the surface of studied samples. Apparently, the quantitative disagreement between these two methods was caused by the limitations of the Pascal 140 device (detectable diameter of pores was 116–3.8 μm [31]), which could not detect larger pores close to 100 μm with a sufficient accuracy. The "ink-bottle effect" [32], which leads to an overestimation of smaller pores and an underestimation of larger pores could also play a role in that respect.

Contrary to the LC plaster, the LM plaster exhibited finer pore size distribution curves after being exposed to cyclic wetting and drying (Fig. 4). The maximal peak was found at 0.9 μm for reference samples but it was moved to 0.4 μm after cycling. The amount of pores within the 0.01–0.1 μm range increased significantly after cycling. The total porosity in the initial state found by MIP was 34% and decreased to 31% after the last cycle.

The OM images confirmed a finer pore structure of LM samples after five wetting-drying cycles, as compared with the reference state (Fig. 5), but they showed also an appearance of cracks several μm wide and several tens of μm long after cycling. The length of some of the microcracks reached ~400 μm; these could not be detected by MIP.

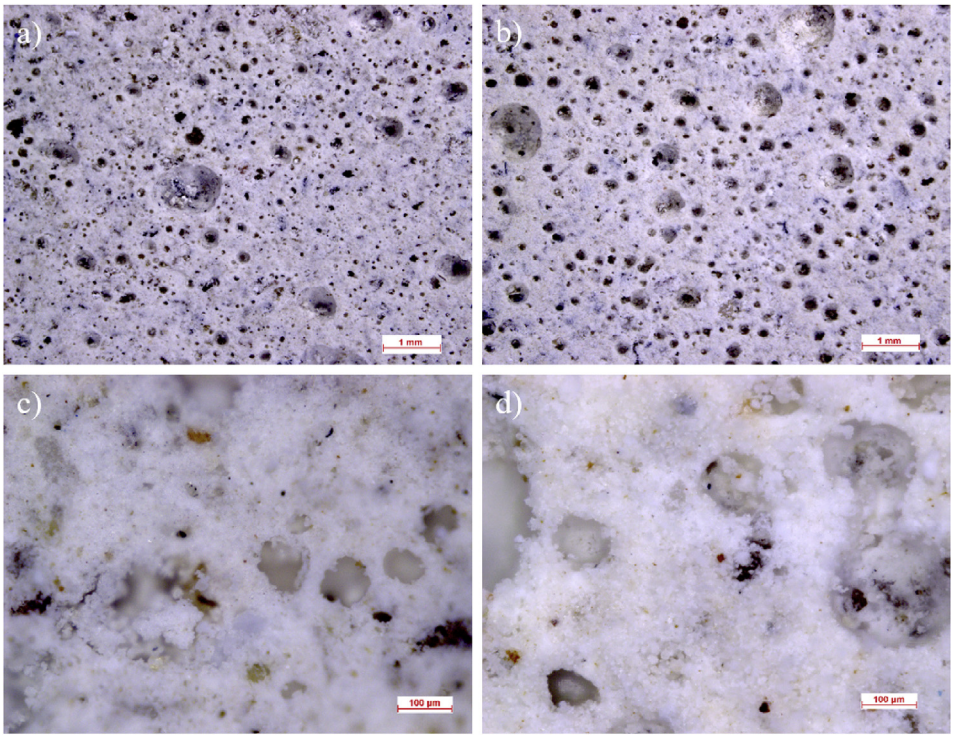

Fig. 3. Optical microscope images of the LC plaster: a) and c) reference state, b) and d) after five cycles.

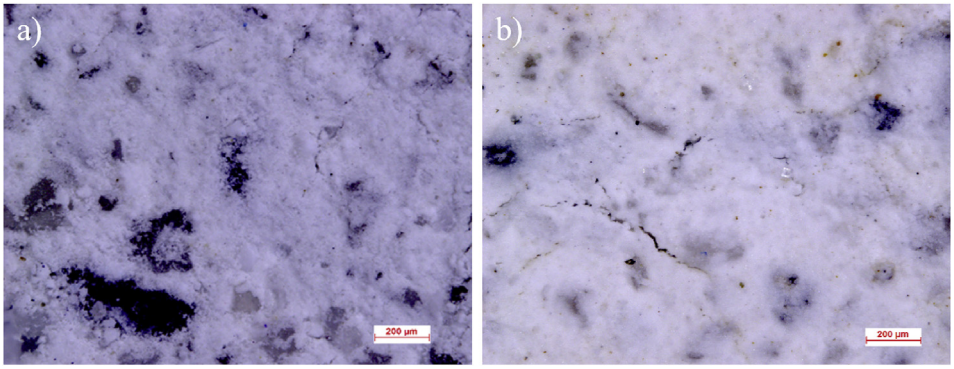

Fig. 5. Optical microscope images of the LM plaster: a) reference state, b) after five cycles.

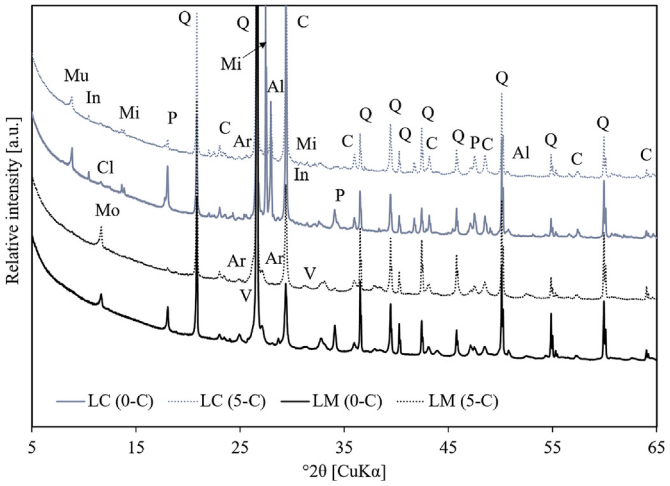

Fig. 6. XRD patterns for LC and LM in the reference state (0-C) and after five cycles (5-C); Al – albite ($NaAlSi_3O_8$), Ar – aragonite ($CaCO_3$), C – calcite ($CaCO_3$), Cl – clinochlore ($Mg_3(Mg_2Al)(Si_3Al)O_{10}(OH)_2O_3$), In – indialite ($Mg_2(Al_4Si_5O_{18})$), Mi – microcline ($KAlSi_3O_8$), Mo – monocarbonate ($Ca_4Al_2(CO_3)(OH)_{12}(H_2O)_5$), Mu – muscovite ($KAl_2(Si_3Al)O_{10}(OH)_2$), P – portlandite ($Ca(OH)_2$), Q – quartz ($SiO_2$), V – vaterite ($CaCO_3$).

3.2. Composition

The XRD analysis of the LC plaster in the reference state is summarized in Fig. 6. No residual amounts of clinker minerals were found which indicated that cement hydration was completed after 28 days already. Quartz was the main component of the aggregates. The presence of albite, muscovite, indialite, chlorite, and microcline indicated the choice of mixed aggregates by the producer, probably for economic reasons. The most important difference between the reference samples and samples exposed to five wetting-drying cycles was the decrease of portlandite amount from 4.8% to 1.1% and the increase of the amount of calcite. The amount of calcite in the LC plasters could be only estimated by means of XRD due to the overlapping peaks and high amount of amorphous content, especially in its reference state (12.9%) which could contain besides C-S-H gels also amorphous $CaCO_3$, not detectable by XRD [33]. Therefore, a more accurate information about the $CaCO_3$ content in the LC plaster is provided by TGA reported below. The amount of calcite in the LC plasters increased after five cycles by 6.3% when compared to the reference state.

The LM plasters contained quartz as the only aggregate component, portlandite as the main component of the lime binder, and calcite, vaterite and aragonite as carbonation products (Fig. 6). Monocarbonate, ($Ca_4Al_2(CO_3)(OH)_{12}(H_2O)_5$), was found as the only crystalline product of the pozzolanic reaction between calcium hydroxide and metakaolin, which was in accordance with the results obtained by Gameiro et al. [34] for lower metakaolin dosage in lime-based blended binders. The amount of portlandite decreased from 4.1% to 0.9% after five cycles, the amount of monocarbonate increased from 4.0% to 5.2%, and the total content of calcium carbonate was changed only slightly (from 28.8% to 28.1%).

The results of DSC and TG analyses in the form of heat flow (in W/g) and relative mass change curves (in %) obtained for the reference materials (without cycling) and samples exposed to one and five wetting and drying cycles are summarized in Figs. 7 and 8. For achieving a better resolution and identification of consecutive mass losses, the derivative of relative mass change curve (DTG, in mg/min) is also provided.

For the LC plaster the decomposition of C-S-H gels and the release of physically bound water from pores took place in the temperature range from 29 to 230 °C (Fig. 7a), which was in a good accordance with [35]. The accompanying mass loss (Fig. 7b) in this temperature interval was higher for samples exposed to wetting-drying cycles, implying that some late hydration processes might take place during cycling,

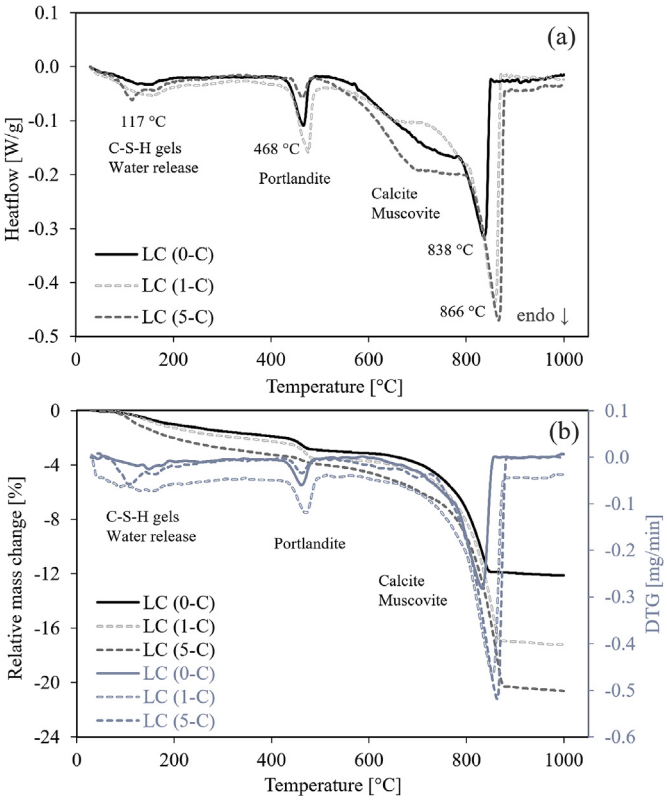

Fig. 7. a) Heat flow, b) relative mass change and DTG curves of the LC plaster.

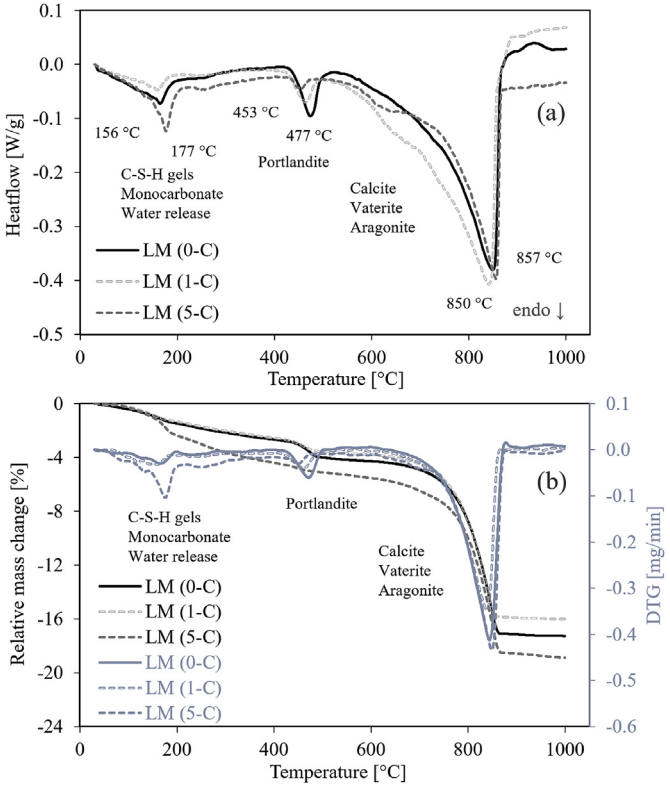

Fig. 8. a) Heat flow, b) relative mass change and DTG curves of the LM plaster.

enhanced by the water environment. It should though be pointed out that the low mass loss detected in this temperature interval indicated that the drying processes caused a partial collapse of C-S-H gels [10] and possibly also some other hydration products, which contained water in their structure and decomposed in the same temperature interval.

The decomposition of portlandite was observed in the temperature range from 425 to 497 °C (Fig. 7a and b). The associated mass loss was 1.1% for LC (0-C), 1.3% for LC (1-C) and 0.7% for LC (5-C) samples. The portlandite content was calculated using the known value of mass change during the decomposition of pure portlandite [36]. The samples without the cyclic treatment contained 4.5% of portlandite, samples after the first cycle 5.4%, while for samples after five cycles its amount was only 2.8%. The difference between the unexposed sample and the first cycle was on the edge of the measurement uncertainty. In a comparison with the XRD data, the portlandite content determined by the TG method was higher because in thermal analysis no overlapping peaks were in this temperature interval, which was not the case of XRD where many other peaks could be overlapping.

The last observed reaction referred to the decomposition of $CaCO_3$ and muscovite. These overlapping decomposition reactions took place in the temperature range from 506 to 878 °C (Fig. 7a and b). In [37], muscovite powder was studied using thermal analysis. The most significant mass loss (about 4.5%) was observed between 770 and 1000 °C, corresponding to the dehydroxylation [38] and decomposition of muscovite, respectively. However, according to these measurements, the amount of muscovite detected by thermogravimetry was probably lower than 0.4%. Thus, the main mass loss in this temperature interval corresponded to the decomposition of $CaCO_3$. The $CaCO_3$ content was, similarly to portlandite, calculated using the known value of mass change during the decomposition of pure $CaCO_3$ [36]. The reference sample contained 20.3% of $CaCO_3$. Compared to the XRD of the raw LC powder, its amount increased only by 0.7% within the 28-days curing period. After the first cycle, the amount of $CaCO_3$ increased to 30.3% and for samples exposed to five cycles it reached 37.1%.

The heat flow curves measured for the LM plaster showed, similarly to the LC plaster, three significant endothermic peaks (Fig. 8a). In this case, the first peak corresponded not only to the decomposition of C-S-H gels and water release from the samples but also to the decomposition of monocarbonate, a product of pozzolanic reaction. The peak temperature was 156 °C for LM (0-C) and 177 °C for LM (5-C). The accompanied mass loss (Fig. 8b) was for LM (5-C) higher than for the reference sample, 1.6% by mass of the whole sample. The next relevant peak in the temperature range of 400–530 °C referred to the decomposition of portlandite. Its content was 4.7% for LM (0-C), 4.1% for LM (1-C), and 1% for LM (5-C) samples which was in a very good agreement with the XRD results. The peak in the temperature interval from 530 °C to 880 °C was due to the decomposition of $CaCO_3$ polymorphs (calcite, aragonite and vaterite) [34,39]; the total $CaCO_3$ content was 28.4% for LM (0-C), 27.7% for LM (1-C), and 30.8% for LM (5-C). The difference in $CaCO_3$ content between the unexposed LM and after the first cycle was very low. Nevertheless, the $CaCO_3$ content for LM (5-C), as obtained from the TGA, was 2.7% higher in a comparison with the XRD measurements. It was probably caused by the presence of amorphous $CaCO_3$, which is not detectable by XRD [33], or by the uncertainty of measurements.

3.3. Length changes

The $\varepsilon_w(w)$ functions of LC and LM plasters (Figs. 9 and 10, $\varepsilon_w = 0$ corresponds to the water saturated state before the first drying) had two common characteristic features. The first was their very different shape in the hygroscopic and overhygroscopic ranges (the maximum hygroscopic moisture content corresponding to 97% relative humidity was 0.076 m^3/m^3 for LC and 0.107 m^3/m^3 for LM), which was observed for all five wetting-drying cycles; the second was the difference between the first cycle and the subsequent ones.

In the first cycle, the relative length change in the overhygroscopic range was $\sim 4{\cdot}10^{-5}$ m/m for LC and $\sim 1.1{\cdot}10^{-4}$ m/m for LM, while the total ε_w values (determined on samples exposed to 5% relative humidity) were $\sim 1{\cdot}10^{-3}$ m/m for LC and $\sim 1.3{\cdot}10^{-3}$ m/m for LM.

At the beginning of the second cycle, a permanent relative deformation was observed, $(4–5){\cdot}10^{-4}$ m/m for LC and $(6–7){\cdot}10^{-4}$ m/m for LM. The total hygric strain (determined under assumption that $\varepsilon_w = 0$ corresponds to the water saturated state before the first drying) in the "chemical" dry state was $\sim 1.2{\cdot}10^{-3}$ m/m for LC and $\sim 1.5{\cdot}10^{-3}$ m/m for LM, which was somewhat higher than in the first cycle. However, the maximum hygric strain during the second cycle (obtained by subtracting the permanent relative deformation from the total hygric strain reached at the desiccator containing silica gel at 25 °C) was lower than during the first cycle, $\sim 0.8{\cdot}10^{-3}$ m/m for LC and $\sim 0.9{\cdot}10^{-3}$ m/m for LM.

During the subsequent three wetting-drying cycles, further

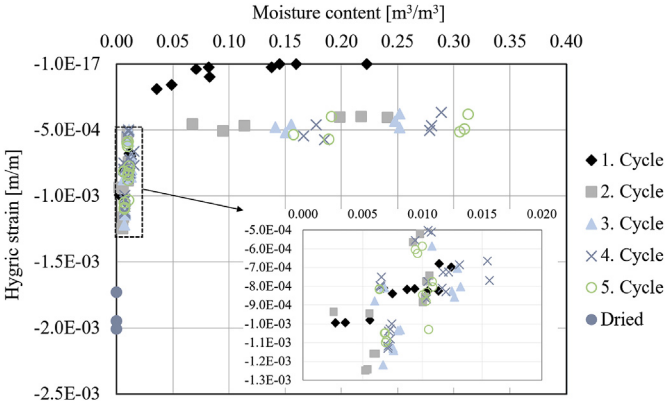

Fig. 9. Hygric strain of the LC plaster.

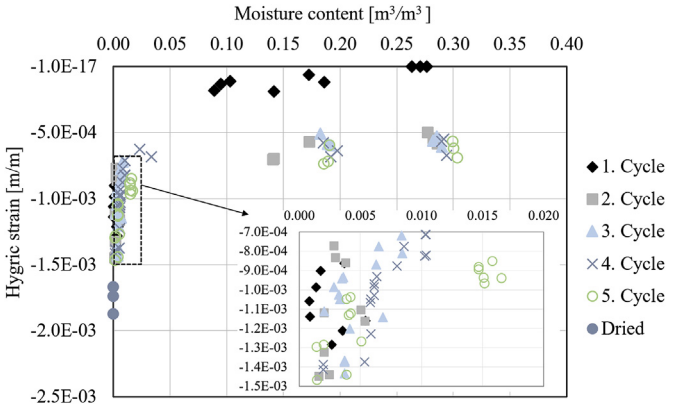

Fig. 10. Hygric strain of the LM plaster.

significant changes of $\varepsilon_w(w)$ functions were not observed for both LC and LM, as compared to the second cycle. Therefore, the drying-wetting process could be considered as near-reversible since the beginning of the second cycle. The highest strain in total was measured at the end of the fifth cycle, when the samples were dried at 105 °C.

The regression analysis of the measured $\varepsilon_w(w)$ relations showed that the hyperbolic function

$$\varepsilon_w(w) = B - \frac{A}{(w + w_0)} \tag{5}$$

with the A, B constants given in Table 2 appeared as the most suitable mathematical representation of the experimental data. The parameter w_0 was determined from the dried state at 105 °C, dried state at 25 °C and 5% RH and from the hygric strain reached for both states. Without this limiting coefficient the approximation would provide an infinite value for $w = 0$.

This led, according to Eq. (4), to the following relation for α_w:

$$\alpha_w(w) = \frac{A}{(w + w_0)^2} \tag{6}$$

Fig. 11 shows an example of the approximation of $\varepsilon_w(w)$ data measured for the LM plaster using Eq. (5) which confirms the good fit indicated by the high R^2 values in Table 2.

Figs. 12 and 13 present the α_w(w) functions of LC and LM plasters, calculated using Eq. (6). The linear hygric expansion coefficient of both plasters decreased with the increasing moisture content very fast. The differences in α_w between the dry state and water saturated state were up to five orders of magnitude. The permanent relative deformations observed on the $\varepsilon_w(w)$ functions (Figs. 9 and 10) at the beginning of the second cycle were reflected by the decrease of the linear hygric expansion coefficient over the whole range of moisture content in the second cycle, as compared with the first cycle; for LC the α_w values decreased approximately two times, for LM even four times. The differences in α_w(w) functions corresponding to the second cycle and the subsequent ones were much lower.

Table 2
Results of the regression analysis of the measured $\varepsilon_w(w)$ relations of the plasters.

Material	Cycle	A·10⁶	B·10⁴	w_0·10³	R^2
LC	1	12.68	0.60	6.659	0.980
	2	5.49	−3.97	3.500	0.970
	3	6.00	−4.17	3.756	0.975
	4	4.48	−4.50	2.861	0.974
	5	3.53	−4.66	0.449	0.973
LM	1	22.49	0.46	16.734	0.960
	2	2.39	−5.95	2.105	0.972
	3	3.82	−5.45	3.288	0.976
	4	4.40	−5.56	3.546	0.988
	5	4.54	−6.52	4.500	0.992

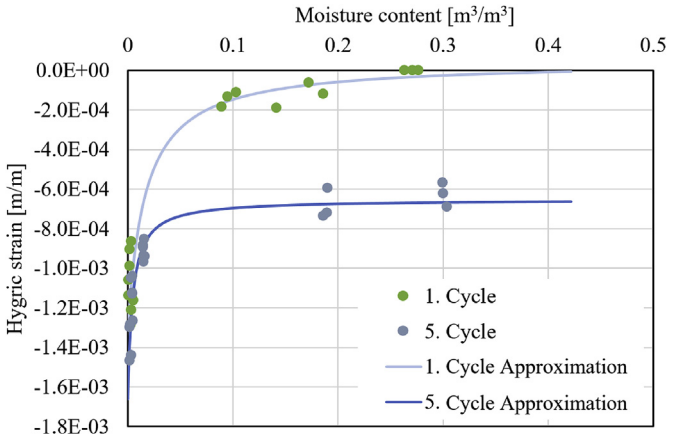

Fig. 11. Hygric strain of the LM plaster – measured values and their approximation.

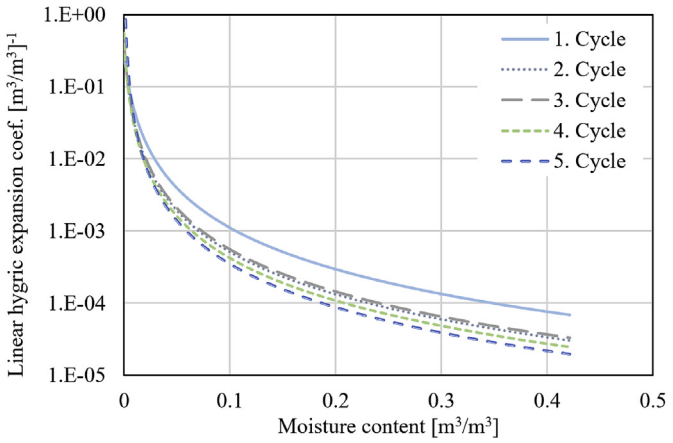

Fig. 12. Linear hygric expansion coefficient of the LC plaster.

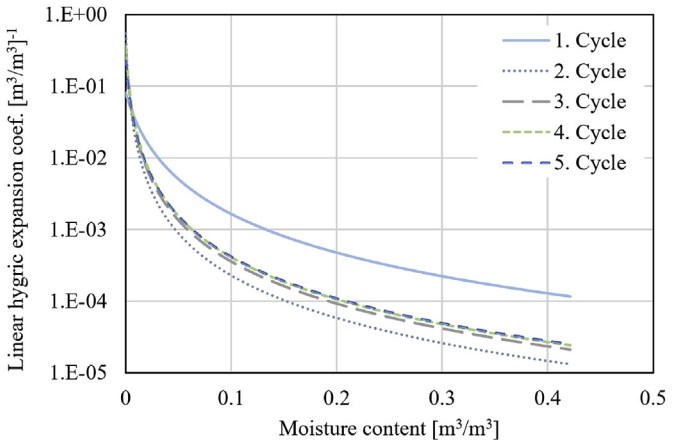

Fig. 13. Linear hygric expansion coefficient of the LM plaster.

4. Discussion

The studied lime-cement and lime-metakaolin plasters responded differently to the applied wetting and drying cycles. The differences were found in both chemical and physical properties.

4.1. Microstructure and composition

The lime-cement plaster contained economically cheap fillers, such as quartz and muscovite. The raw powder contained also about 20 wt% of calcite which was partially involved in lime but its major part was apparently used in the form of fine aggregates. The initial amount of calcite in the LC plaster was about 15 wt% higher than in the lime-metakaolin plaster, prepared with the utilization of only one type of aggregates (quartz). Whereas the main hydration products between lime and cement in the LC plaster were C-S-H gels, portlandite and calcite, in the case of the lime-metakaolin plaster the pozzolanic reactions between lime and metakaolin led besides the formation of these products also to the creation of monocarbonate. Its content slightly increased after the application of five wetting and drying cycles (about 1.2 wt%). The portlandite and $CaCO_3$ contents in the studied plasters were determined by means of thermal analysis, together with the XRD method. In terms of the determination of portlandite content these two methods provided very similar results. However, the analysis of the content of calcite was more challenging when using XRD, especially due to the overlapping peaks and the presence of amorphous matter, which cannot be qualified using this method [33]. Therefore, thermal analysis provided more reliable results.

For the LC plasters it was determined that the amount of portlandite slightly increased, comparing 28 days old samples and samples exposed to the first cycle (about 1 wt%). This difference was on the edge of the measurement uncertainty. Portlandite in the lime-metakaolin plaster had been gradually consumed during the whole analyzed period. After five cycles, it decreased to about 3 wt% in the LC plaster, whereas only 1 wt% remained in the LM plaster. In terms of $CaCO_3$, its content significantly increased between the reference state and after the first cycle for the LC plaster (10 wt%). When compared to its initial state (raw powder), the difference in the $CaCO_3$ content after the first cycle was lower than 1%, which could refer to slow initial progress of carbonation processes, contrary to the results observed for the lime-metakaolin plaster. In the case of the LM plaster, the initial amount of about 5 wt% of $CaCO_3$ in the dry mixture significantly increased (about 23 wt%) after 28 days. However, its amount slightly decreased after the first cycle (less than 1 wt%) to finally reach about 30 wt%. Therefore, it can be seen that even though the $CaCO_3$ content was significantly lower in the dry mixture of LM, its final values after five cycles were comparable with those obtained for the LC plaster.

The determined changes in amounts of portlandite and $CaCO_3$ in the studied plasters after the application of wetting-drying cycles could be caused by:

- Pozzolanic reactions which could lead to the gradual decrease of portlandite in the LM plaster, where lime reacted with metakaolin (pozzolan active material). Portlandite, which was initially formed, was quickly consumed during pozzolanic reactions.
- Hydration processes ongoing between lime and cement in the LC plaster. A possible increase of portlandite between the reference state and the first cycling could be caused by continuing hydration processes which were supported by a relatively high relative humidity during the first weeks.
- Carbonation processes, during which portlandite was gradually transformed into $CaCO_3$, which could be related to the high increase of $CaCO_3$ after the first cycle in LM. The lower amount of portlandite available for further transformation into $CaCO_3$ could explain the lower increase of $CaCO_3$ within the subsequent cycles in the case of LM.
- Partial dissolution of portlandite and $CaCO_3$ due to the application of wetting-drying cycles. Especially the immersion of samples in water during the first stage of cycling (saturation) could lead to their dissolution, supported by the presence of larger pores [40–42].
- Combination of the pozzolanic/hydration reactions, carbonation and partial dissolution of portlandite and $CaCO_3$.

The changes in composition were reflected on the results of MIP and OM. In the case of the LC plaster, the application of wetting-drying cycles led to the development of larger pores, which was in contradiction to the results obtained for the LM plaster. Both MIP and OM confirmed that the LC plaster exhibited a coarser microstructure after cycling. Microcracks were though not found by OM on the surface after wetting-drying cycles (samples after the fifth cycle were not dried at 105 °C before the OM analysis), as it would be expected [10]. A possible explanation could lie in the lower resolution of OM or in the presence of cracks deeper under the surface. The observed increase of pore size could be caused by several phenomena, such as the cracking on microstructural level due to wetting-drying processes and volumetric shrinkage due to carbonation. Whereas the wetting-drying processes lead to the creation of larger pores, especially on the surface of the samples, the carbonation causes an increase in solid volume (about 11–12%) as a result of portlandite conversion to calcite [43–45]. Therefore, these reactions have the opposite effects. Dissolution of calcite and portlandite during the first stage (immersion in water) of each cycle is another important factor which could have caused the increase of pore size. When portlandite and calcite dissolve, it leads to the development of new or larger pores [40–42].

The LM plaster exhibited a finer microstructure after cycling, which was probably a consequence of the formation of C-S-H and C-A-H compounds due to the pozzolanic reaction. The presence of these amorphous and poorly crystalline phases was indicated by the XRD measurements, showing an ~11% increase of amorphous content for LM (5-C), as compared with the unexposed LM material. The finer pore structure of LM samples after five wetting-drying cycles was confirmed by the OM images. Nevertheless, these images also showed an appearance of cracks several μm wide and several tens of μm long after cycling, which could be caused by the competition of the carbonation process producing compounds with higher density than portlandite [46] with the pozzolanic reaction resulting in lower-density products [46,47], and also by the applied wetting-drying cycles (volumetric changes) [10]. As already reported above, the dissolution mechanisms of calcite and portlandite during the first stage (immersion in water) of each cycle also could cause cracking leading to an increase of pore size [40–42]. Nevertheless, at this point, it is nearly impossible to clarify which of these phenomena had the highest impact on the determined microstructural changes.

In a comparison with the lime-cement plaster, the lime-metakaolin plaster exhibited a denser microstructure after cycling, which was mainly a result of pozzolanic reaction between lime and metakaolin. However, the exposed surface of LM contained more microcracks than LC. In the summary, the lime-metakaolin plaster was more prone to volumetric shrinkage and microcracking during the applied wetting-drying procedures than the lime-cement-plaster.

4.2. Carbonation depth

It was assumed that the progress of carbonation processes in the plasters exposed to wetting-drying cycles was probably slower than if the samples were kept in the air environment during the whole studied period. It is given by the diffusion rate of carbon dioxide which is in water far lower than in air [48]. On the other hand, the rate of carbonation in the air environment highly depends on the external relative humidity, with the optimum conditions at ~50% RH [49–51]. Therefore, the carbonation process could vary during the subsequent phases of the drying procedure, accelerating after reaching the hygroscopic moisture content and then slowing down again for lower RH values.

At the interpretation of the effects of carbonation on lime- and cement-based composites, the carbonation depth is a frequently used parameter, which is often determined by the colorimetric method (phenolphthalein test) [52,53]. In this paper, we estimated the carbonation depth using mathematical formulas developed before by other investigators. According to the mathematical model proposed by Balen

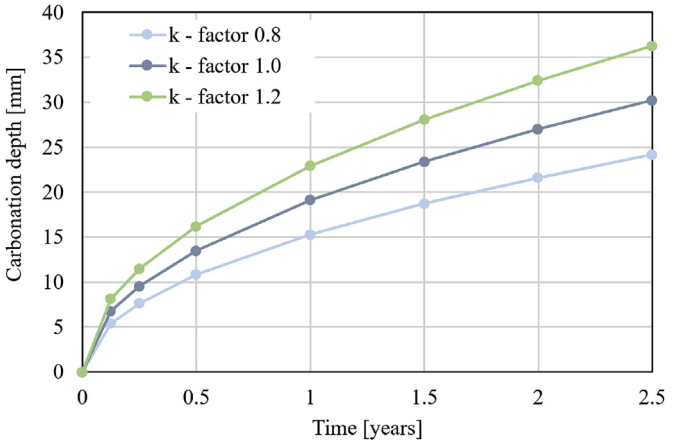

Fig. 14. Carbonation depth in lime-based plasters calculated as a function of time for different *k* factors identified in [52,53,55].

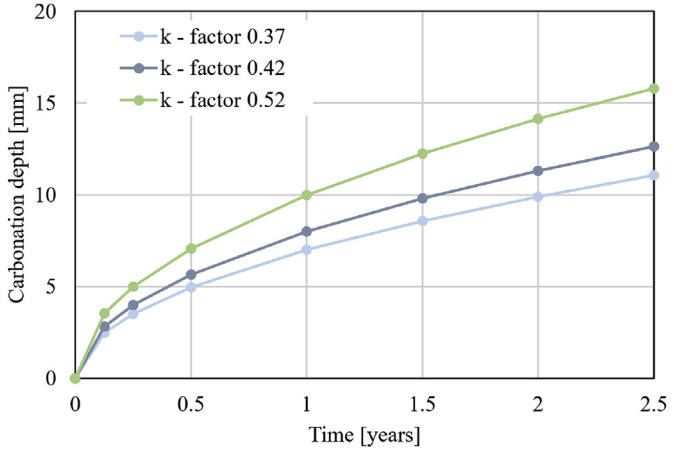

Fig. 15. Carbonation depth in cement-based composites containing limestone calculated as a function of time for different *k* factors identified in [56].

and Gemert [13], the progress of lime/cement plaster carbonation can be expressed as

$$x = k\sqrt{t} \tag{7}$$

where x is the carbonation depth; k is a factor and t is the time. The k factor is usually determined experimentally and it is related to the property of the material [13]. It was shown that the k factor increases with increasing water to binder ratio [54]. In [52,53,55], the k factor was assumed to be ranging between 0.8 and 1.2 mm/(day)$^{1/2}$ for lime-based plasters with bioclastic, oolitic and sand aggregates exposed to natural unforced carbonation at 60% RH and 20 °C.

Fig. 14 shows the carbonation depth calculated using Eq. (7) for the time horizon corresponding to the experimental work presented in this paper for different k factors (0.8, 1.0 and 1.2 mm/(day)$^{1/2}$). The results obtained with the k factor value of 0.8 can be assumed as the lowest limit for the progress of carbonation in the LM materials. In this study, every cycle took approximately half a year. Taking into account the data in Fig. 14, it can be assumed that the LM prisms having dimensions of 40 × 40 × 160 mm were probably fully carbonated already after the second cycle.

In the case of the LC plaster, the most visible difference in carbonation rate was observed on the thermogravimetric curves between the unexposed plaster and the plaster after the first cycle. Generally, when Portland cement is used, the penetration rate of CO_2 can reach about 1 mm/(year)$^{1/2}$ with w/c of 0.4 and it moves to 8 mm/(year)$^{1/2}$ with w/c of 0.7 [56]. In blended cements, moderate levels of limestone (up to 15 wt%) keep the CO_2 penetration rate at similar values to ordinary concrete. The penetration rate increases with higher ground limestone additions, as it can be seen in Fig. 15 for concrete with water to cement ratio of 0.7. The k factor of 0.37 is related to the concrete prepared from Portland cement of CEM I 52.5 R. The k factor of 0.42 represents Portland cement partially replaced by 15 wt% of ground limestone, and finally, the k factor of 0.52 is a result of 25 wt% replacement of cement with ground limestone [56]. As the LC plasters studied in this paper contained a significant amount of calcite, it can be assumed that their carbonation rate could be comparable to concretes analyzed in [56]. Assuming the k factor of 0.52, the carbonation depth could reach 16 mm after the fifth cycle.

4.3. Length changes

Apparently, drying shrinkage caused by internal water evaporation due to low relative humidity of the environment in the climatic chamber [57] was probably the dominant mechanism already during the first cycle, which was started after 28 days of curing. As no residual amounts of clinker minerals were found in LC by the XRD analysis at the beginning of the first cycle (Fig. 6), self-desiccation was probably very low and could be neglected. This finding was in accordance with the experimental work of Carette et al. [58] for cement-based composites after the 28 days curing period. On the other hand, carbonation shrinkage could present another important factor during the first cycle. Using the relation recommended by Despotou et al. [53] for old lime-based plasters, the calculated carbonation depth after the first cycle could be 10–15 mm for both LC and LM, which could represent a potential cause of the observed shrinkage.

The permanent relative deformation observed at the beginning of the second cycle could be attributed to the carbonation shrinkage along with effects of pozzolanic reactions which are irreversible processes.

Surprisingly, during the following three wetting-drying cycles no further significant changes were observed for both plasters. Apparently, the capillary pressure (or the pore liquid pressure) was the dominant shrinkage mechanism in this phase, which was in accordance with the theoretical considerations of Rahman and Grasley [59].

A comparison with the results obtained by other investigators could be done in a limited extent only as the experimental data on hygric expansion/shrinkage of lime plasters are very sparse in common databases. Güney and Caner [24] studied hygric expansion characteristics of mortars and bricks in the dome structures of Turkish Baths from 14th and 15th century. They increased the relative humidity from 30% to 80% with a rate of 10% per 4 h at a constant temperature of 30 °C. The total relative displacement of both brick and mortar was within the range of (1–2) $\cdot 10^{-4}$ m/m, which was two to three times lower than in the measurements of hygric shrinkage of lime-based plasters in this paper. The difference could be attributed to different experimental conditions; in our study the samples were left in the climatic chamber until they reached the hygric equilibrium with the chamber which was probably not the case of samples analyzed in [24]. Arizzi and Cultrone [60] tested the shrinkage of aerial lime-based mortars in order to assess their quality as repair rendering materials. The dimensional variations of the samples during the first 7 days after mixing were between 1.3 and 1.4% of their total length. However, also in this case the experimental conditions were very different from this paper; the length changes were dominated by autogenous shrinkage.

5. Conclusions

The effect of five consecutive wetting-drying cycles on microstructure, composition and length changes of lime-cement (LC) and lime-metakaolin (LM) plasters was studied in the paper. The main results can be summarized as follows:

- The microstructure of the LC plaster became coarser after being

exposed to the wetting-drying cycles and the amount of pores in the range of 10–100 μm increased. Contrary to LC, the LM plaster showed a finer microstructure after the cycling procedure and its pore volume increased in the 0.01–0.1 μm range as a consequence of an ~10% increase of amorphous content identified by XRD.

- The XRD, DSC, and TG analyses showed that besides C-S-H gels, portlandite and calcite were the most important compounds observed in LC. No residual amounts of clinker minerals were found which indicated that cement hydration was completed already after 28 days. The most important difference between the reference samples and samples exposed to five wetting-drying cycles was the decrease of portlandite amount, which was probably caused by a combination of several factors, such as carbonation and partial dissolution of portlandite due to the immersion of samples in water at the beginning of each cycle. These effects had an impact on the corresponding increase of the amount of calcite, which was most intensive during the first cycle.
- The LM plaster contained portlandite as the main component of the lime binder, and calcite, vaterite and aragonite as carbonation products. The amount of $CaCO_3$ polymorphs significantly increased after 28-days curing period when compared to the raw mixture (about 23 wt%) which was a more significant increase than in LC. However, the further increase of $CaCO_3$ content during the first cycle was much lower in LM. Monocarbonate, $C_3A{\cdot}CaCO_3{\cdot}11H_2O$, was found as the only crystalline product of the pozzolanic reaction between calcium hydroxide and metakaolin. The influence of wetting-drying cycles was manifested by the decrease of portlandite content and increase of monocarbonate content, while the total content of calcium carbonate was changed only slightly. Therefore, the pozzolanic reaction together with possible portlandite/calcite dissolution were the main factors affecting the composition of the LM plaster during the wetting and drying period.
- The measurements of hygric strain as a function of moisture content, $\varepsilon_w(w)$, showed that for both LC and LM plasters drying shrinkage was the dominant mechanism already during the first cycle, which was started after 28 days of curing. Self-desiccation was very low but carbonation shrinkage could present an important factor during the first cycle.
- At the beginning of the second cycle, a permanent relative deformation was observed, $(4–5){\cdot}10^{-4}$ m/m for LC and $(6–7){\cdot}10^{-4}$ m/m for LM. It was attributed to the carbonation shrinkage which is an irreversible process.
- The wetting-drying process could be considered as near-reversible since the beginning of the second cycle. Apparently, the capillary pressure (or the pore liquid pressure) was the dominant shrinkage mechanism in this phase.
- The regression analysis of the measured $\varepsilon_w(w)$ relations showed the hyperbolic function $\varepsilon_w(w) = B - A/(w+w_o)$ as the most suitable mathematical representation of experimental data during all five wetting-drying cycles. Accordingly, the linear hygric expansion coefficient, as a parameter directly applicable in the computational models, was expressed as $\alpha_w(w) = A/(w+w_o)^2$.

Acknowledgement

The research was supported by the Czech Science Foundation, under project No 17-01365S.

Appendix A. Supplementary data

Supplementary data to this article can be found online at https://doi.org/10.1016/j.cemconcomp.2019.103411.

References

[1] F. Han, Z. Zhang, Hydration, mechanical properties and durability of high-strength concrete under different curing conditions, J. Therm. Anal. Calorim. 132 (2018) 1–12.
[2] X.-Y. Wang, Analysis of hydration and strength optimization of cement-fly ash-limestone ternary blended concrete, Cement Concr. Compos. 166 (2018) 130–140.
[3] X.-Y. Wang, Y. Luan, Modeling of hydration, strength development, and optimum combinations of cement-slag-limestone ternary concrete, Int. J. Concr. Struct. Mater. 12 (2018) 12.
[4] P.O. Awoyera, J.O. Akinmusuru, A.R. Dawson, J.M. Ndambuki, N.H. Thom, Microstructural characteristics, porosity and strength development in ceramic-laterized concrete, Cement Concr. Compos. 86 (2018) 224–237.
[5] S. Dueramae, W. Tangchirapat, C. Jaturapitakkul, Strength and heat generation of concrete using carbide lime and fly ash as a new cementitious material without Portland cement, Adv. Powder Technol. 29 (2018) 672–681.
[6] E. Vejmelková, M. Keppert, P. Rovnaníková, Z. Keršner, R. Černý, Application of burnt clay shale as pozzolan addition to lime mortar, Cement Concr. Compos. 34 (2012) 486–492.
[7] E. Vejmelková, M. Keppert, Z. Keršner, P. Rovnaníková, R. Černý, Mechanical, fracture-mechanical, hydric, thermal, and durability properties of lime–metakaolin plasters for renovation of historical buildings, Constr. Build. Mater. 31 (2012) 22–28.
[8] T.C. Powers, Structure and physical properties of hardened Portland cement paste, J. Am. Ceram. Soc. 41 (1958) 1–6.
[9] A. El-Turki, R.J. Ball, S. Holmes, W.J. Allen, G.C. Allen, Environmental cycling and laboratory testing to evaluate the significance of moisture control for lime mortars, Constr. Build. Mater. 24 (2010) 1392–1397.
[10] Z. Wu, H.S. Wong, N.R. Buenfeld, Transport properties of concrete after drying-wetting regimes to elucidate the effects of moisture content, hysteresis and microcracking, Cement Concr. Res. 98 (2017) 136–154.
[11] A. El-Turki, R.J. Ball, G. Allen, The influence of relative humidity on structural and chemical changes during carbonation of hydraulic lime, Cement Concr. Res. 37 (2007) 1233–1240.
[12] R. Veiga, Air lime mortars: what else do we need to know to apply them in conservation and rehabilitation interventions? A review, Constr. Build. Mater. 157 (2017) 132–140.
[13] K. Van Balen, D. Van Gemert, Modelling lime mortar carbonation, Mater. Struct. 27 (1994) 393–398.
[14] M.A.N. Oliveira, A Multi–Physics Approach Applied to Masonry Structures with Non–hydraulic Lime Mortars, PhD Thesis University of Minho, 2016.
[15] B. Lagerblad, Carbon Dioxide Uptake during Concrete Life-State of the Art, CBI Report 2:2005, Swedish Cement and Concrete Research Institute (CBI), Stockholm, 2005.
[16] H. Chang, S. Mu, P. Feng, Influence of carbonation on “maximum phenomenon” in surface layer of specimens subjected to cyclic drying-wetting condition, Cement Concr. Res. 103 (2018) 95–109.
[17] R. Černý, A. Kunca, V. Tydlitát, J. Drchalová, P. Rovnaníková, Effect of pozzolanic admixtures on mechanical, thermal and hygric properties of lime plasters, Constr. Build. Mater. 20 (2006) 849–857.
[18] R. Černý, J. Maděra, J. Poděbradská, J. Toman, J. Drchalová, T. Klečka, K. Jurek, P. Rovnaníková, The effect of compressive stress on thermal and hygric properties of Portland cement mortar in wide temperature and moisture ranges, Cement Concr. Res. 30 (2000) 1267–1276.
[19] Q. Zeng, K. Li, T. Fen-Chong, P. Dangla, Effect of porosity on thermal expansion coefficient of cement pastes and mortars, Constr. Build. Mater. 28 (2012) 468–475.
[20] J. Toman, R. Černý, Thermal and hygric expansion of high performance concrete, Acta Polytech. 41 (2001).
[21] B. Mazhoud, F. Collet, S. Pretot, J. Chamoin, Hygric and thermal properties of hemp-lime plasters, Build. Environ. 96 (2016) 206–216.
[22] E. Vejmelková, D. Koňáková, M. Čáchová, M. Keppert, R. Černý, Effect of hydrophobization on the properties of lime–metakaolin plasters, Constr. Build. Mater. 37 (2012) 556–561.
[23] M. Jerman, I. Medveď, R. Černý, Length changes of autoclaved aerated concrete exposed to cyclic wetting and drying, Cem. Wapno Beton 20/82 (2015) 139–149.
[24] B.A. Güney, E. Caner, Thermal and hygric expansion characteristics of mortars and bricks used in the dome structures of Turkish Baths from 14th and 15th centuries, Constr. Build. Mater. 95 (2015) 757–761.
[25] T. Koudelka, J. Kruis, J. Maděra, Coupled shrinkage and damage analysis of autoclaved aerated concrete, Appl. Math. Comput. 267 (2015) 427–435.
[26] Y. Gao, J. Zhang, Y. Luosun, Shrinkage stress in concrete under dry–wet cycles: an example with concrete column, Mech. Time-Dependent Mater. 18 (2014) 229–252.
[27] JCPDS PDF-4 Database, International Centre for Diffraction Data, Newtown Square, PA, USA release, 2018.
[28] N. Doebelin, R. Kleeberg, Profex: a graphical user interface for the Rietveld refinement program BGMN, J. Appl. Crystallogr. 48 (2015) 1573–1580.
[29] ICSD Database, FIZ Karlsruhe, Germany, 2017 release.
[30] ČSN EN 13009, Hygrothermal Performance of Building matenals and Products - Determination of Hygric Expansion Coefficient, Czech Standards Institute, Prague, 2000 2001.
[31] Thermo Scientific Pascal Series Mercury Porosimeters - Product Sheet, ThermoFisher Scientific, 2019.
[32] S. Diamond, Mercury porosimetry: an inappropriate method for the measurement of pore size distributions in cement-based materials, Cement Concr. Res. 30 (2000) 1517–1525.
[33] K. Scrivener, R. Snellings, B. Lothenbach, A Practical Guide to Microstructural Analysis of Cementitious Materials, CRC Press, 2016.
[34] A. Gameiro, A.S. Silva, R. Veiga, A. Velosa, Hydration products of lime–metakaolin pastes at ambient temperature with ageing, Thermochim. Acta 535 (2012) 36–41.

[35] W. Sha, E.A. O'Neill, Z. Guo, Differential scanning calorimetry study of ordinary Portland cement, Cement Concr. Res. 29 (1999) 1487–1489.
[36] J. Dweck, P.M. Buchler, A.C.V. Coelho, F.K. Cartledge, Hydration of a Portland cement blended with calcium carbonate, Thermochim. Acta 346 (2000) 105–113.
[37] J. Feifei, J. Su, S. Song, Can natural muscovite be expanded? Colloid. Surf. Physicochem. Eng. Asp. 471 (2015) 19–25.
[38] S. Guggenheim, Y.H. Chang, A.F. Koster van Groos, Muscovite dehydroxylation: high-temperature studies, Am. Mineral. 72 (1987) 537–550.
[39] M. Maciejewski, H.-R. Oswald, A. Reller, Thermal transformations of vaterite and calcite, Thermochim. Acta 234 (Supplement C) (1994) 315–328.
[40] T. Van Gerven, G. Cornelis, E. Vandoren, C. Vandecasteele, Effects of carbonation and leaching on porosity in cement-bound waste, Waste Manag. 27 (2007) 977–985.
[41] E.J. Garboczi, D.P. Bentz, Multi-scale picture of concrete and its transport properties: introduction for non-cement researchers, National Institute of Standards and Technology (NIST), Gaithersburg, Maryland, 1996 NISTIR 5900.
[42] L. Luquot, P. Gouze, P., Experimental determination of porosity and permeability changes induced by injection of CO2 into carbonate rocks, Chem. Geol. 265 (2009) 148–159.
[43] C. Gervais, A.C. Garrabrants, F. Sanchez, R. Barna, P. Moszkowicz, D.S. Kosson, The effects of carbonation and drying during intermittent leaching on the release of inorganic constituents from a cement-based matrix, Cement Concr. Res. 34 (2004) 119–131.
[44] M. Yousuf, A. Mollah, T.R. Hess, Y.N. Tsai, D.L. Cocke, An FTIR and XPS investigations of the effects of carbonation on the solidification/stabilization of cement based systems-Portland type V with zinc, Cement Concr. Res. 23 (1993) 773–784.
[45] F.M. Lea, The Chemistry of Cement and Concrete, 3d edition, Chem. Publ. Co., 1967.
[46] M. Balonis, F.P. Glasser, The density of cement phases, Cement Concr. Res. 39 (2009) 733–739.
[47] P.D. Tennis, H.M. Jennings, A model for two types of calcium silicate hydrate in the microstructure of Portland cement pastes, Cement Concr. Res. 30 (2000) 855–863.
[48] K. Van Balen, Carbonation reaction of lime, kinetics at ambient temperature, Cement Concr. Res. 35 (2005) 647–657.
[49] N.I. Fattuhi, Concrete carbonation as influenced by curing regime, Cem.Concr. Res. 18 (1988) 426–430.
[50] Y. Wang, S. Nanukuttan, Y. Bai, P.A.M. Basheer, Influence of combined carbonation and chloride ingress regimes on rate of ingress and redistribution of chlorides in concretes, Constr. Build. Mater. 140 (2017) 173–183.
[51] S. Goni, A. Guerrero, Accelerated carbonation of Friedel's salt in calcium aluminate cement paste, Cement Concr. Res. 33 (2003) 21–26.
[52] R.M.H. Lawrence, A Study of Carbonation in Non-hydraulic Lime Mortars, Doctoral dissertation University of Bath, 2006.
[53] E. Despotou, A. Shtiza, T. Schlegel, F. Verhelst, Literature study on the rate and mechanism of carbonation of lime in mortars/Literaturstudie über Mechanismus und Grad der Karbonatisierung von Kalkhydrat im Mörtel, Mauerwerk 20 (2016) 124–137.
[54] M. Arandigoyen, J.I. Alvarez, J.I., Carbonation process in lime pastes with different water/binder ratio, Mater. Construcción 56 (2006) 5–18.
[55] R.M.H. Lawrence, T.J. Mays, P. Walker, D. D'ayala, Determination of carbonation profiles in non-hydraulic lime mortars using thermogravimetric analysis, Thermochim. Acta 444 (2006) 179–189.
[56] M. Collepardi, S. Collepardi, J.O. Olagot, F. Simonelli, The influence of slag and fly ash on the carbonation of concrete, Proc. Of 8th CANMET/ACI Int. Conf. on Fly Ash, Silica Fume, Slag, and Natural Pozzolans in Concrete, 2004, pp. 23–29.
[57] L. Wu, N. Farzadnia, C. Shi, Z. Zhang, H. Wang, Autogenous shrinkage of high performance concrete: a review, Constr. Build. Mater. 149 (2017) 62–75.
[58] J. Carette, S. Joseph, O. Cizer, S. Staquet, Decoupling the autogenous swelling from the self-desiccation deformation in early age concrete with mineral additions: micromacroobservations and unified modelling, Cement Concr. Compos. 85 (2018) 122–132.
[59] S.F. Rahman, Z.C. Grasley, The significance of pore liquid pressure and disjoining pressure on the desiccation shrinkage of cementitious materials, Int. J. Adv. Eng. Sci. Appl. Math. 9 (2017) 87–96.
[60] A. Arizzi, G. Cultrone, The water transfer properties and drying shrinkage of aerial lime-based mortars: an assessment of their quality as repair rendering materials, Environ. Earth Sci. 71 (2014) 1699–1710.

Selected paper 4 – Building and Environment:

Jerman, M., Palomar, I., Kočí, V., Černý, R., Thermal and hygric properties of biomaterials suitable for interior thermal insulation systems in historical and traditional buildings – 2019

In this paper, natural growing materials that can relatively easily undergo biocorrosion under adverse conditions are studied. For this reason, it is always necessary to consider very carefully their incorporation into the design. However, complete data are needed for this assessment, which are lacking. In this article, complete data are presented as a function of humidity and as a function of temperature. The paper has had 39 citations in a relatively short time.

The materials for the article were selected based on market research. The materials investigated are offered by manufacturers or suppliers for internal thermal insulation. Internal wall insulation is very risky. Fiberboards have already been used for internal insulation in an apartment building in Plzeň, a First Republic villa in Zbraslav, and during the reconstruction of historic buildings in Switzerland. Flax insulation is used in the Netherlands. Hemp insulation and sheep's wool are recommended by manufacturers and suppliers for wooden buildings or as inter-roof and above-roof thermal insulation. The author of this article neither confirms nor refutes the functionality of the chosen insulation system. The paper aimed to accurately and unbiasedly determine the material characteristics of natural materials, which are essential for assessing the functionality of the system as a whole and are very often missing. The material characteristics serve as input values for the computer simulations. Detailed computer analyses are then used to confirm or refute the functionality of the system.

Contribution to practical use: The paper provides the data needed to assess the thermal moisture behavior of the thermal insulation system as a whole.

Building and Environment 154 (2019) 81–88

Contents lists available at ScienceDirect

Building and Environment

journal homepage: www.elsevier.com/locate/buildenv

Thermal and hygric properties of biomaterials suitable for interior thermal insulation systems in historical and traditional buildings

Miloš Jerman, Irene Palomar, Václav Kočí, Robert Černý*

Department of Materials Engineering and Chemistry, Faculty of Civil Engineering, Czech Technical University in Prague, Thákurova 7, 166 29, Prague 6, Czech Republic

ARTICLE INFO

Keywords:
Hygric properties
Thermal properties
Interior thermal insulation
Biomaterials
Historical buildings
Experimental analysis

ABSTRACT

Historical and traditional buildings account for 10–40% of the building stock in various countries and regions. Retrofitting of their building envelopes aimed at the improvement of thermal performance is often feasible using interior thermal insulation systems only. The effectiveness of systems without vapor barrier depends on the application of modern insulation materials with enhanced water transport properties contributing to fast liquid moisture redistribution and mitigating the risks related to water vapor condensation. In this paper, thermal and hygric properties of several biomaterials potentially applicable as thermal insulation boards on the interior side of historical building envelopes are investigated. The obtained experimental data include all transport and storage parameters necessary for appropriate hygrothermal- and energy-related assessment of buildings provided with interior thermal insulation systems using advanced computer simulation tools. Wood fiberboard, flax fibers, hemp fibers, jute fibers, and sheep wool are found to have, at the same time, low thermal conductivity ($\sim 0.05\ W\,m^{-1}\,K^{-1}$) and high moisture diffusivity ($1.1 \times 10^{-6} - 1.2 \times 10^{-5}\ m^2\,s^{-1}$) which can classify them as good candidates for the use in interior thermal insulation systems without water vapor barrier. They exhibit convenient water vapor diffusion parameters and hygroscopic properties as well, which favors their use on the interior side. The natural origin presents another benefit. In a comparison with conventional materials (calcium silicate, hydrophilic mineral wool) having similar thermal and hygric properties, they bring more harmony to the process of retrofitting historical building envelopes.

1. Introduction

Thermal insulations have become an essential part of most building envelopes during the past decades since current requirements on thermal protection of buildings practically cannot be met without them [1,2]. In case of facade walls, the exterior thermal insulation systems are preferred mainly due to their easier application, protection of the walls against weather conditions, and more effective elimination of thermal bridges. On the other hand, some issues arise concerning their cost, low adaptability to original facades and hygrothermal performance in cold climates [3]. Furthermore, the application of exterior thermal insulation systems is excluded in case of historical and traditional buildings, or generally buildings under preservationists' surveillance as they irreversibly change the facades' appearance. Since these buildings may account for 10–40% of the building stock [4], depending on the region and age threshold that classifies them as historical, the number of applications when only interior thermal insulation systems can be considered might be higher than it seems at the first glance.

Being not exposed to weather conditions directly, the interior thermal insulations have longer durability which makes them more cost effective from a long-term point of view. Additionally, the absence of environmental effects enables a more diverse material solution. On the other hand, interior thermal insulation systems exhibit higher water vapor condensation risk [5,6] which is necessary to be prevented as it might induce frost damage, biodegradation, or other damage patterns. According to Vereecken and Roels [7], creation of vapor tight system is one of the possibilities how to do that. This opinion is in agreement with some other researchers who reported various types of solutions in their studies, e.g. in form of OSB boards [8], plasters [9], impregnations [10], or paintings [11]. According to another group of researchers, proper hygrothermal performance of interior thermal insulation systems can though be achieved without any vapor barrier, using materials with enhanced water transport properties. Besides the thermal insulating function, the role of thermal insulation consists then also in fast moisture redistribution to prevent creation of condensation zones or at least minimize the duration of their appearance.

The condition of enhanced water transport properties is met particularly by the use of capillary active or hydrophilic materials. The

* Corresponding author.
E-mail address: cernyr@fsv.cvut.cz (R. Černý).

https://doi.org/10.1016/j.buildenv.2019.03.020
Received 10 January 2019; Received in revised form 11 March 2019; Accepted 12 March 2019
Available online 15 March 2019
0360-1323/

Nomenclature

A (kg·m^{-2}·s$^{-0.5}$) water absorption coefficient
c (J·kg^{-1}·K^{-1}) specific heat capacity
C_t (kg·m^{-2}) cumulative inflow per unit area
$\delta_a = 1.993 \times 10^{-10}$ kg m^{-1} s^{-1}·Pa^{-1} water vapor permeability of air at 25 °C
δ_m (s) water vapor diffusion permeability
$\delta_{m,corr}$ (s) corrected water vapor diffusion permeability using the air layer resistance
Δm (kg) mass increase
Δp_v (Pa) partial pressure difference
d (m) sample thickness
d_a (m) thickness of the air layer
D (m^2·s^{-1}) water vapor diffusion coefficient
$D_a = 2.82 \times 10^{-5}$ m^2 s^{-1} water vapor diffusion coefficient in air at 25 °C
κ_{app} (m^2·s^{-1}) apparent moisture diffusivity
λ (W·m^{-1}·K^{-1}) thermal conductivity
μ (−) water vapor diffusion resistance factor
m_0 (kg) mass of a dry sample
$m_{w(i)}$ (kg) steady state mass of a sample (at i-value of relative humidity)
$M = 0.01802$ kg mol^{-1} molar mass of water
ρ (kg·m^{-3}) matrix density
ρ_v (kg·m^{-3}) bulk density
$R = 8.314$ Pa m^3 mol^{-1}·K^{-1} gas constant
S (m^2) surface area of a specimen
t (s) time
T (K) temperature
ψ (%) open porosity
w_{cap} (kg·m^{-3}) capillary moisture content
$w_{m(i)}$ (kg·kg^{-1}) gravimetric moisture content (calculated at i-value of relative humidity)
w_{max} (% m^3·m^{-3}) maximal moisture content

capillary activity of insulation materials is gained due to specific pore space arrangement which provides the ability of a liquid to flow without assistance or even in opposition to external forces. A positive contribution of capillary active materials on hygric performance of walls with interior thermal insulation has been reported, e.g., by Zhao et al. [12], Zhou et al. [13], or Hamid and Wallenten [14]. Calcium silicate, a typical representative in that respect, has become an objective of many research studies. As Vereecken and Roels [15], Feng and Janssen [16], or Janetti et al. [17] concluded, this material is typical for high moisture diffusivity and low water vapor diffusion resistance factor. Such parameters guarantee enhanced moisture transport properties and fast moisture redistribution. Besides the capillary action, intensified surface transport within the porous space of insulating materials can help to achieve it as well. Hydrophilic mineral wool can be stated as a typical example, evincing this kind of transport phenomenon. Jerman and Černý [18] reported that it had similar water transport properties to capillary active materials which predisposed it to be used as interior thermal insulation. Calcium silicate and hydrophilic mineral wool represent relatively new, modern insulating materials. However, in the light of retrofitting of historical building envelopes, it would be convenient to consider more natural alternatives, i.e. insulating materials that could be produced and applied in the distant past when the historical buildings were built. This assumption predisposes them to be more compatible with the materials of historical walls.

Thermal insulation capabilities of biomaterials were indicated, e.g., by Troppová et al. [19] who assessed thermal behavior of wood-based fiberboard under different temperature and moisture content scenarios and confirmed its promising thermal insulating properties. The suitability of flax and hemp fibers for thermal insulation systems was reported in experimental studies published by Kymalainen and Sjoberg [20], or Latif et al. [21]. Korjenic et al. [22] investigated flax, hemp, and jute fibers to develop new insulation materials, fulfilling the building physical, mechanical and ecological requirements. Zach et al. [23] analyzed a thermal insulation made of sheep wool and found out

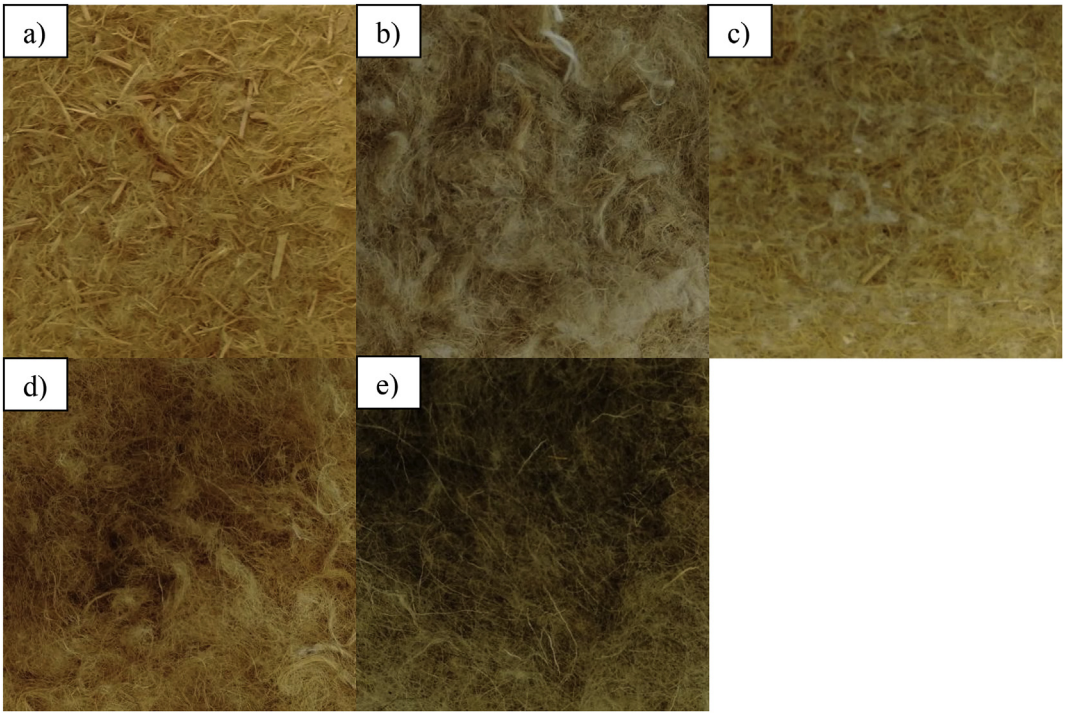

Fig. 1. Biomaterials for thermal insulations: a) WFB, b) FF, c) HF, d) JF, e) SW.

that it showed similar characteristics to conventional mineral wool.

In this paper, thermal and hygric properties of five different biomaterials are analyzed from the point of view of their possible application for interior thermal insulation systems. It is assumed that, due to the hydrophilic nature of their compounds, these materials may exhibit enhanced water transport properties. Their high porosity makes good prerequisites for the achievement of low thermal conductivity. The low embodied energy [24] brings an added value in the form of environmental benefits. Contrary to other experimental studies on biomaterials, the measured sets of heat and moisture transport and storage parameters are complete, allowing their immediate use in computer simulation tools. The application of computational modeling brings substantial advantages to the building design process. As it can provide preliminary hygrothermal- and energy-related assessments without a necessity of constructions to be built, it represents the first step towards a wider application of biomaterials in the building sector. Energy savings estimation [25] or verification of proper hygrothermal function [26,27] belong to characteristic examples of practical implications of the data presented.

2. Materials and methods

Wood fiberboard (further denoted as WFB), flax fibers (FF), hemp fibers (HF), jute fibers (JF), and sheep wool (SW) were selected for the experimental study in this paper. Their pictures are shown in Fig. 1.

As they belong to typical representatives of natural fibrous materials, all of them can be potentially used for thermal insulation. A detailed experimental investigation is, however, necessary prior to their practical applications. The experimental methods used in this paper cover determination of basic physical properties, as well as heat and moisture transport and storage parameters. A detailed description of the methods used is given in following subsections.

2.1. Basic physical properties

Bulk density, ρ_v (kg·m^{-3}), matrix density, ρ (kg·m^{-3}), open porosity, ψ (%), and maximal moisture content, w_{max} (% m^3·m^{-3}), were the investigated basic physical properties. Bulk density was calculated in accordance with EN 1602 [28]. Five test samples, of which dimensions complied with EN 822 [29], EN 823 [30], and EN 12085 [31] (300 mm × 300 mm × 80 mm), were measured and weighed to calculate the bulk density according to the common gravimetric formula. Matrix density was determined using the water saturation principle and open porosity was calculated as

$$\psi = \left(1 - \frac{\rho_v}{\rho}\right)\cdot 100\% \tag{1}$$

Maximal moisture content, describing the maximal amount of water that is a material able to keep, was measured by the gravimetric method.

2.2. Moisture transport and storage properties

The water vapor transport parameters were determined using both wet-cup and dry-cup methods following the principles given in EN ISO 12572 [32]. Having dimensions of 100 mm × 100 mm and thickness of 30–70 mm, three samples of each material were stored in laboratory conditions (22 ± 2 °C and 50 ± 5% of RH) until tested.

The specimens were placed on metal cup containing water or silica gel and the samples' lateral sides were sealed to achieve one-dimensional moisture flux (see Fig. 2a). The cups with specimens were then placed into a climatic chamber that maintained constant temperature of 25 °C and constant relative humidity of 55% during the testing procedure (dry cup: 140 h, wet cup: 160 h) while distilled water and silica gel in the cups provided 100% and 10% relative humidity conditions, respectively (see Fig. 2b). Such an arrangement induced one dimensional moisture flux through the sample. Establishing a relative humidity of 100% in the cup using distilled water, the underside of high water vapor transport resistant specimens might be susceptible to water condensation which may raise the measurement beyond the hygroscopic range. However, in case of low water vapor transport resistant specimens, which are the investigated materials supposed to be, the high flow rate through the specimens prevents from this risk [32]. The mass increase of the assembly was recorded every 12 h until the steady state was reached. Finally, the water vapor diffusion permeability, δ_m (s), water vapor diffusion coefficient, D (m^2·s^{-1}), and water vapor diffusion resistance factor, μ (−), were calculated according to equations (2)–(4)

$$\delta_m = \frac{\Delta m \cdot d}{t \cdot S \cdot \Delta p_v}, \tag{2}$$

$$D = \frac{\delta_m \cdot R \cdot T}{M} \tag{3}$$

$$\mu = \frac{D_a}{D}, \tag{4}$$

In Eqs. (2)–(4) Δm (kg) is the mass increase, d (m) is the sample thickness, t (s) is time, S (m^2) is the surface area of the specimen, Δp_v (Pa) is the partial pressure difference, $D_a = 2.82 \times 10^{-5}$ m^2 s^{-1} is the water vapor diffusion coefficient in air at 25 °C [33], $R = 8.314$ Pa m^3 mol^{-1}·K^{-1} is the gas constant, T (K) stands for temperature and $M = 0.01802$ kg mol^{-1} is molar mass of water. equations (2)–(4) do not involve resistance of air layers in the test cup and/or above the test cup. They are therefore applicable only for specimens that are not very permeable, i.e. the air layer resistance is much smaller than the material resistance. Since the specimens investigated are expected to be very permeable, the resistance of the air layer in the cup

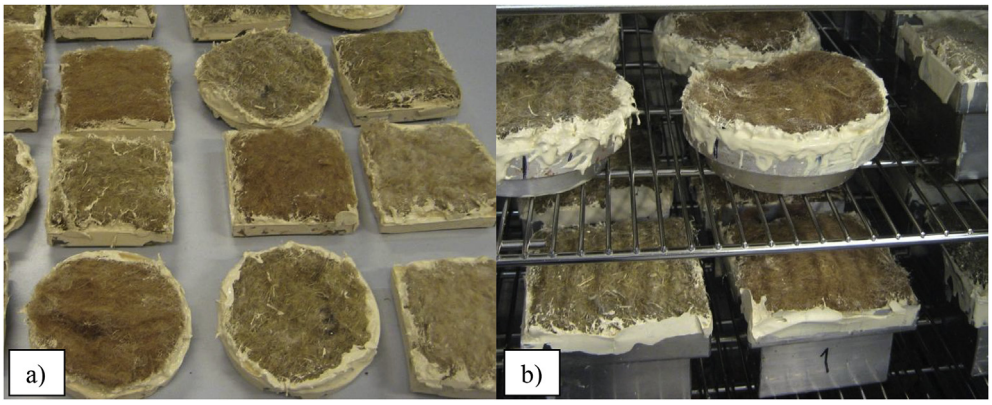

Fig. 2. Determination of water vapor transport parameters: a) specimen preparation, b) measurement in the climatic chamber.

must be involved and the corrected water vapor diffusion permeability, $\delta_{m,corr}$ (s), is then expressed as

$$\delta_{m,corr} = \frac{d}{\frac{t \cdot S \cdot \Delta p_v}{\Delta m} - \frac{d_a}{\delta_a}}, \quad (5)$$

where d_a (m) is the thickness of the air layer and $\delta_a = 1.993 \times 10^{-10}$ kg m^{-1} s^{-1}·Pa^{-1} is the water vapor permeability of air at 25 °C. The resistance of the layer above the cup could be neglected because the air in the test chamber was stirred, so that the velocity above each specimens was kept at least to 2 m s^{-1} which meets the requirements prescribed in EN ISO 12572 [32].

The determination of the liquid water transport parameters was carried out according to EN ISO 15148 [34]. Five samples with intake area of 95–190 cm^2 and thickness of 60–140 mm were sealed on the lateral sides in order to achieve one-dimensional water flux and stored in laboratory conditions (22 ± 2 °C and 50 ± 5% of RH) until tested. The bottom face of the samples was then partially immersed in water (5 ± 2 mm) and the samples were continuously weighed by an automatic balance for 36 h [35]. The water absorption coefficient, A (kg·m^{-2}·s$^{-0.5}$), was determined as

$$A = \frac{C_t}{\sqrt{t}}, \quad (6)$$

where C_t (kg·m^{-2}) is the cumulative inflow (mass difference) per unit area calculated as

$$C_t = \frac{\Delta m}{S} \quad (7)$$

The capillary moisture content, w_{cap} (kg·m^{-3}), was expressed as moisture content at the end of water intake stage, where the capillary forces are acting. The apparent value of moisture diffusivity, κ_{app} (m^2·s^{-1}), was calculated as

$$\kappa_{app} = \left(\frac{A}{w_{cap}}\right)^2 \quad (8)$$

The moisture storage properties are described by water vapor adsorption isotherms that were measured using the desiccator method. Following the procedure described by Roels et al. [36], dried samples were placed into desiccators with different salt solutions to reach various steady relative humidity conditions. The mass of samples was recorded and the experimental procedure was finished when steady state values of mass were achieved. Then, the gravimetric moisture content, $w_{m,i}$ (kg·kg^{-1}), was calculated for particular values of relative humidity, i, in the desiccators,

$$w_{m,i} = \frac{m_{w,i} - m_0}{m_0} \quad (9)$$

where $m_{w,i}$ (kg) is the steady state mass of the sample at i-value of relative humidity and m_0 (kg) is the mass of the dry sample.

2.3. Heat transport and storage properties

Heat transport and storage properties, namely thermal conductivity, λ (W·m^{-1}·K^{-1}), and specific heat capacity, c (J·kg^{-1}·K^{-1}), were measured using a commercially available Isomet 2104 device made by Applied Precision, Ltd. The measurement is based on the evaluation of temperature response of an analyzed material to heat flow pulses. The heat flow is induced by an electrical resistor heater having direct thermal contact with the sample. Due to the soft nature of all the samples investigated, a needle probe was used. The values of thermal conductivity were determined as a function of temperature and moisture content.

3. Results and discussion

The results of experimental measurements are summarized in following subsections. The data presented was completed by results of uncertainty analysis performed according to ISO/IEC 98-3, which is known as GUM [37]. In case the replicate observation had not been applied, the uncertainty was evaluated by means of standard uncertainty of type B which is based on manufacturer's information, calibration certificates of measuring instruments, or expert's estimates. Otherwise, the standard uncertainty of type A was included, being based on statistical evaluation of sets of measured data. Since detailed descriptions of analyses of single measurements would be very space-demanding, only the expanded uncertainties corresponding to 95% confidence level are presented alongside the measured mean values of particular quantities.

3.1. Basic physical properties

The basic physical properties of studied bio-based materials are summarized in Table 1. The values of bulk density were very low, ranging between 23 kg m^{-3} for FF and 54 kg m^{-3} for WFB. Such low numbers went along with high porosity, in all cases higher than 96%, which is typical for conventional thermal insulating materials.

It can be noticed, that maximal moisture content was significantly lower than porosity of the materials. It could be ascribed to their structure, which was mostly formed by large voids being unable to fully retain the liquid water after saturation.

3.2. Water vapor transport and storage properties

The results of dry-cup and wet-cup methods, i.e. values of $\delta_{m,corr}$ for particular samples, are shown in Fig. 3. While solid bars show results corresponding to the wet cup setup, the cross-hatched bars show the dry cup setup.

The $\delta_{m,\,corr}$ values were then processed according to Eqs. (3) and (4) to obtain water vapor diffusion coefficient, D (m^2·s^{-1}), and water vapor diffusion resistance factor, μ (−). The results are summarized in Table 2.

According to the results presented in Fig. 3 and Table 2, the studied materials exhibited very fast water vapor transport in both dry cup and wet cup modes. FF appeared as the most permeable among the materials investigated, having μ_{dry} and μ_{wet} values equal to 1.31 and 1.03, respectively. All the values are comparable to those measured by other researchers. Korjenic et al. [22] reported very high permeability of flax and jute fibers, determining their water vapor diffusion resistance factors to be 2.9 and 2.0, respectively. In other study, Korjenic et al. [38] concluded that μ-values of sheep wool insulation were between 1 and 5. Studying thermal insulations on hemp basis, Latif et al. [21] reported

Table 1
Basic physical properties.

Material	Bulk density (kg·m^{-3})	Matrix density (kg·m^{-3})	Open porosity (%)	Maximal moisture content (% m^3·m^{-3})
WFB	54.0 ± 1.3	1480 ± 36	96.35 ± 0.20	51.7 ± 1.8
FF	23.0 ± 0.6	1017 ± 22	97.74 ± 0.13	38.2 ± 1.5
HF	38.0 ± 0.8	1036 ± 26	96.33 ± 0.18	45.7 ± 1.7
JF	33.0 ± 0.8	1017 ± 24	96.76 ± 0.17	48.5 ± 1.7
SW	25.0 ± 0.7	1156 ± 27	97.8 ± 0.13	14.0 ± 0.6

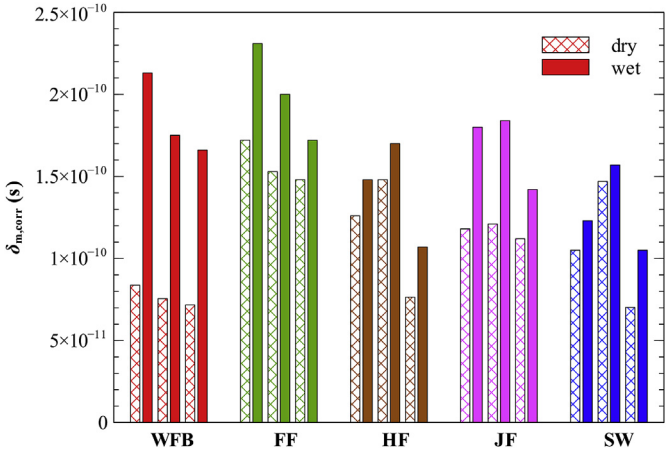

Fig. 3. Water vapor diffusion permeability.

Table 2
Water vapor diffusion coefficient and water vapor diffusion resistance factor.

Material	Water vapor diffusion coefficient ($\times 10^{-5}$ m^{2}s^{-1})		Water vapor diffusion resistance factor (−)	
	Dry cup	Wet cup	Dry cup	Wet cup
WFB	1.06 ± 0.16	2.54 ± 0.64	2.69 ± 0.40	1.12 ± 0.28
FF	2.17 ± 0.32	2.77 ± 0.75	1.31 ± 0.19	1.03 ± 0.28
HF	1.61 ± 0.95	1.95 ± 0.83	1.77 ± 1.05	1.46 ± 0.62
JF	1.61 ± 0.13	2.35 ± 0.59	1.77 ± 0.14	1.23 ± 0.31
SW	1.47 ± 0.99	1.76 ± 0.68	1.93 ± 1.30	1.62 ± 0.62

their μ-values between 1.10 and 2.74, depending on the composition and test mode, which also agreed with the results presented in this paper. Palumbo et al. [39] investigated hemp fibers and wood wool and found their μ-values to be 3.0–2.3 and 2.4–2.1, respectively.

Since all the values of μ obtained using experimental measurements were very low, the insulating materials investigated seem to have optimal predispositions for application on the interior side of buildings. In comparison with calcium silicate and mineral wool, which are typically used as interior thermal insulations and their μ-values are between 2 and 6 [36] and 1.2 and 2.7 [18], respectively, the studied bio-based insulations have comparable or even better water vapor transport properties.

The water vapor storage parameters of studied bio insulations are depicted in Fig. 4, showing gravimetric moisture content, w_m (kg·kg^{-1}) vs. relative humidity, *RH* (%), plots. The adsorption isotherms displayed were obtained at 25 °C. The results obtained for particular *RH* values are completed by error bars and fitted using exponential functions.

All analyzed materials were very hygroscopic. JF showed the highest water vapor sorption properties as it was able to accommodate 37.8% kg·kg^{-1} at 98% relative humidity of air. Such hygroscopic properties were very prospective for materials to be used in buildings' interior as they had good prerequisites to facilitate moderation of indoor air, the humidity in particular [24,40–42]. The water vapor storage properties determined in this research were comparable with the results presented by other researchers. Despite small differences, the found match can be considered as sufficient regarding to the diversity of biomaterials and measurement uncertainties. Investigating alternative thermal insulations based on sheep wool, Zach et al. [23] characterized them by high hygroscopicity values up to 35% kg·kg^{-1}. The hygroscopicity of hemp-based insulation was reported to be 41% in case of untreated samples and between 31 and 34% kg·kg^{-1} after application of various hydrophobic additives [43]. On the other hand Bourdot et al. [44] determined the hygroscopic moisture content of various hemp-based materials to be between 17 and 19% kg·kg^{-1} only. Troppová et al. [19] reported the moisture content of commercially produced wood-based fiberboard to be 22% kg·kg^{-1} at 98% of relative humidity. Finally, the moisture content of jute and flax was slightly over 20% kg·kg^{-1} at 90% according to Korjenic et al. [22].

3.3. Water transport properties

The average results of free water uptake experiment, i.e. cumulative inflow curves as a function of square root of time, are shown in Fig. 5. The presented values are completed by results of uncertainty analysis based on statistical evaluation of series of data (uncertainty of type A).

In general, the free water uptake experiment can be divided into two stages. According to Roels et al. [36], the position of waterfront in the first stage gradually approaches the opposite side of a sample, being governed by capillary and viscous forces. In the second stage, the further increase of the moisture content can be ascribed to dissolution and removal of the air that is entrapped in water, and to a variation at the infiltrating waterfront. According to Eq. (6), the water absorption coefficient, A (kg·m^{-2}·s$^{-0.5}$), is defined as the slope of the first stage of the cumulative inflow curve as a function of square root of time. The apparent moisture diffusivity, κ_{app} (m^2·s^{-1}), is then calculated according to Eq. (8). Here, the capillary moisture content, w_{cap} (kg·m^{-3}), is equal to the moisture content of the specimen at the end of the transition from the first to the second stage of the experiment. The end of transition can be graphically defined as a point, in which a tangent at the right end of particular C_f-$t^{0.5}$ diagram departs from the curve (see Fig. 5). The summary of results is given in Table 3 including $t^{0.5}$ values that correspond to the end of the transition.

All studied insulation materials exhibited enhanced water transport properties as they had relatively high water absorption coefficients and apparent moisture diffusivities. Accounting for 0.14–0.52 kg m^{-2} s$^{-0.5}$ depending on the material type, the values of water absorption coefficient were comparable to other researchers' results only to a limited extent. For instance, Stefanowski et al. [45] measured moisture properties of bio-based materials to determine their susceptibility to mold growth. They investigated hemp, among others, reporting the detailed course of free water uptake experiment. It was shown that mass change after 0.3 h was approximately 27 kg m^{-2} which, according to the methodology used within this research, produced A = 0.82 kg m^{-2} s$^{-0.5}$. Such a value was even higher than 0.39 kg m^{-2} s$^{-0.5}$ reported for HF in this study. However, Stefanowski et al. [45] presented 5.28 kg m^{-2} h^{-1} which was approximately ten times lower than recalculated value of HF in this research (0.39 kg m^{-2} s$^{-0.5}$ = 50.65 kg m^{-2} h^{-1}). Even if the C_f vs. t (or $t^{0.5}$) function agreed well, the difference in the presented A values can be ascribed to different ways of data processing and evaluation [46]. Latif

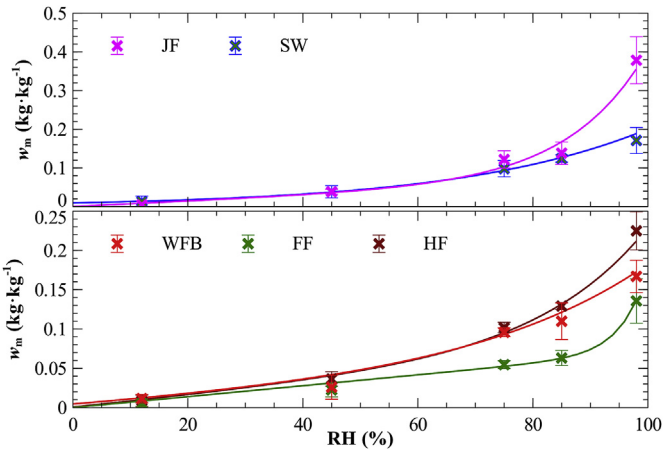

Fig. 4. Adsorption isotherms.

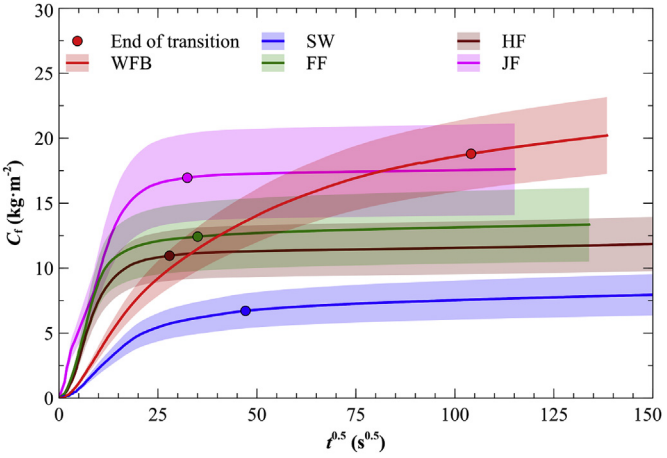

Fig. 5. Experimental results of water absorption test.

et al. [21] analyzed five different hemp samples reporting their A values after 24 h to range between 0.29 and 0.41 kg m^{-2} s$^{-0.5}$. When the evaluation period used in this paper would be extended from the first stage to 24 h, one would obtain $A = 0.045$ kg m^{-2} s$^{-0.5}$ for HF which can be considered as a very good agreement.

Comparing the water transport properties with mineral thermal insulations supposed to be used in the interior (calcium silicate, hydrophilic mineral wool) the enhanced properties of bioinsulations can be pointed out, even if they do not reach such values. Roels et al. [36], Feng and Janssen [16,46] and Feng et al. [47] determined the A values of calcium silicate to be 1.01–1.30 kg m^{-2} s$^{-0.5}$ which was approximately two times higher than A values of JF. On the other hand, the κ_{app} values of all the materials investigated, ranging between 1.14×10^{-6} m^2 s^{-1} (WFB) and 1.20×10^{-5} m^2 s^{-1} (FF), were comparable to both hydrophilic mineral wool (4.1×10^{-5} m^2 s^{-1} [18] (3.0–3.7) $\times 10^{-5}$ m^2 s^{-1} [48]), and calcium silicate (1.99×10^{-6} m^2 s^{-1} [47], 1.97×10^{-6} m^2 s^{-1} [16], 1.78×10^{-6} m^2 s^{-1} [46], 2.32×10^{-6} m^2 s^{-1} [36]). This made the studied biomaterials able to eliminate potential risks of water condensation by fast liquid water redistribution. HF and FF seemed to have the highest predispositions in that respect.

3.4. Heat transport and storage properties

Heat transport and storage properties, thermal conductivity in particular, represent very important material quantities which are considered in most building design approaches. Even if hygric properties are essential as well in case of interior thermal insulations, thermal properties still play the decisive role. The dry state values are summarized in Table 4. According to the extensive review performed by Schiavoni et al. [24], EPS, XPS, stone wool, glass wool or other conventional insulation materials typically have values of thermal conductivity lower than 0.04 W m^{-1} K^{-1}. The thermal conductivities of bio-based materials in Table 4 were ~11–36% higher than those of traditional ones. Nevertheless, their thermal insulating properties could still be considered as very good.

Table 4
Thermal conductivity and specific heat capacity in dry state.

Material	Thermal conductivity (W·m^{-1}·K^{-1})	Specific heat capacity (J·kg^{-1}·K^{-1})
WFB	0.0466 ± 0.0034	2130 ± 338
FF	0.0545 ± 0.0093	1443 ± 260
HF	0.0543 ± 0.0088	1906 ± 312
JF	0.0518 ± 0.0050	1819 ± 303
SW	0.0446 ± 0.0032	1940 ± 331

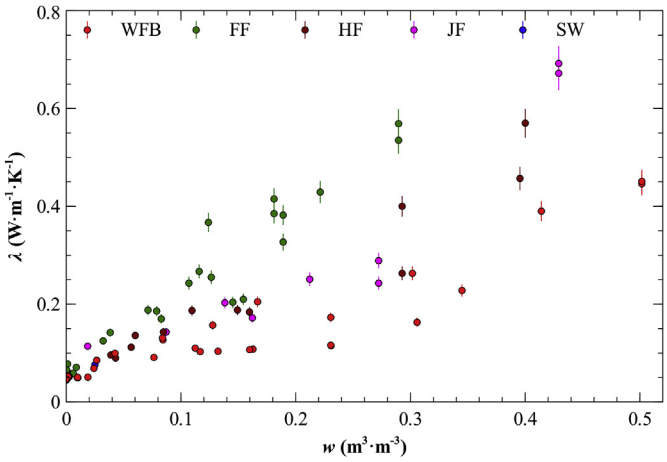

Fig. 6. Moisture-dependent thermal conductivity.

Thermal conductivity of studied materials increased significantly with increasing moisture content (Fig. 6). JF and FF showed to be the most vulnerable as their thermal conductivity in water saturated state reached 0.692 and 0.569 W m^{-1} K^{-1}, respectively. This can be considered as some kind of a tax for their hydrophilic nature and thus enhanced water transport properties which cannot be observed, e.g., in case of polystyrene or hydrophobic mineral wool.

The temperature-dependent values of thermal conductivity at 5–35 °C are summarized in Fig. 7.

The increase of thermal conductivity with increasing temperature was in agreement with findings of other researchers, regarding the variability of biomaterials and uncertainties of measurements. The relatively large error bars displayed in Fig. 7 can be ascribed to variance of data obtained using the needle probe. Since a penetration of the probe into the samples can cause a different sample compression, the changes of the air/body ratio of the material surrounding the probe can be reflected in their heat transport properties.

Studying thermal conductivity of selected bio insulations within the hygroscopic region (~10–90% of RH), Palumbo et al. [39] reported its increase from 0.038 to 0.057 W m^{-1} K^{-1} for hemp fibers and from 0.035 to 0.047 W m^{-1} K^{-1} for wood wool. These values were slightly lower than those reported in this paper. The overhygroscopic region was not investigated in Ref. [36] so a full comparison could not be done. Kymäläinen and Sjöberg [20] studied thermal conductivity in dry state of thermal insulation based on flax (0.035–0.075 W m^{-1} K^{-1}),

Table 3
Liquid water transport properties: experimental data and results.

Material	Cumulative inflow (kg·m^{-2})	Square root of end-of-transition time (s$^{0.5}$)	Water absorption coefficient (kg·m^{-2}·s$^{-0.5}$)	Capillary moisture content (kg·m^{-3})	Apparent moisture diffusivity (× 10^{-6} m^2 s^{-1})
WFB	18.80 ± 2.75	104.08	0.18 ± 0.03	169 ± 25	1.14 ± 0.48
FF	12.43 ± 2.64	35.03	0.35 ± 0.08	102 ± 29	11.98 ± 8.50
HF	10.96 ± 1.93	27.91	0.39 ± 0.07	119 ± 30	10.90 ± 6.66
JF	16.96 ± 3.39	32.41	0.52 ± 0.10	238 ± 58	4.81 ± 3.04
SW	6.71 ± 1.34	47.11	0.14 ± 0.03	94 ± 23	2.28 ± 1.44

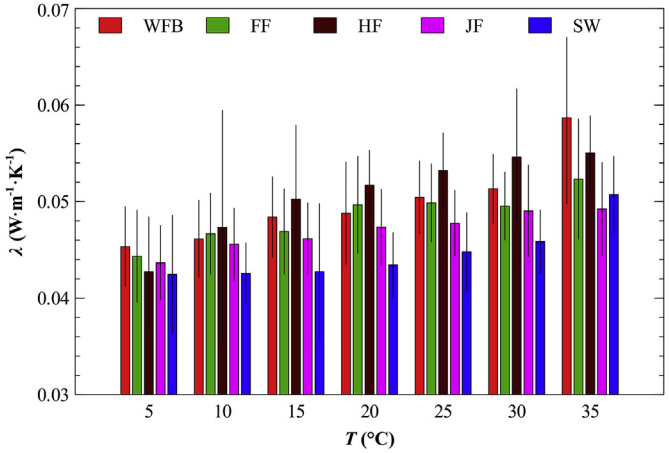

Fig. 7. Temperature-dependent thermal conductivity.

hemp (0.040–0.094 $W\,m^{-1}\,K^{-1}$), and their combination (0.033–0.060 $W\,m^{-1}\,K^{-1}$) in dependence on their bulk density. These λ values were similar to those obtained in this paper. Slightly higher values of thermal conductivity in dry state of hemp (0.062 $W\,m^{-1}\,K^{-1}$), flax (0.065 $W\,m^{-1}\,K^{-1}$), and jute (0.058 $W\,m^{-1}\,K^{-1}$) were reported by Korjenic et al. [49]. The temperature-dependent values of thermal conductivity of SW determined in this paper corresponded with the findings of Zach et al. [23] who identified them between 0.038 $W\,m^{-1}\,K^{-1}$ at 10 °C and 0.049 $W\,m^{-1}\,K^{-1}$ at 40 °C.

4. Conclusions

Meeting standard requirements on thermal protection of buildings is one of the most important tasks of today's building design approaches. This concerns not only new buildings but also the existing ones, including traditional and historical, that should be retrofitted. Preferred solutions consisting in the application of exterior thermal insulation systems are not always possible in this case, thus interior systems are to be used instead. Since using a combination of traditional and modern materials may be understood as controversial by many authorities responsible for the preservation of architectural heritage, the application of natural materials in interior thermal insulation systems seems to be a prospective solution to the problem of thermal retrofitting of historical buildings.

In this paper, the properties of five bio-based materials potentially applicable in interior thermal insulation systems suitable for traditional and historical buildings were studied. The heat transport properties of wood fiber board, flax fibers, hemp fibers, jute fibers, and sheep wool were found quite satisfactory. Even if the measured values of thermal conductivity, ~0.05 $W\,m^{-1}\,K^{-1}$, were slightly higher than those of conventional thermal insulations, they could still be considered as very good thermal insulators. The moisture diffusivity of all studied biomaterials was relatively high, accounting for 1.1×10^{-6} – $1.2 \times 10^{-5}\,m^2\,s^{-1}$, which was comparable with calcium silicate or hydrophilic mineral wool. Their application on the interior side of buildings thus seems to be very promising, allowing using them also in the systems without water vapor barrier. The water vapor diffusion resistance factor of all materials was very low, making possible a fast water vapor removal from the system. All analyzed materials exhibited convenient hygroscopic properties which was a positive feature for materials used in buildings' interior, making them suitable for moderation of indoor air, the humidity in particular.

The detailed experimental analysis of the properties of five prospective biomaterials presented in this study can be considered as a good starting point for further investigations aimed at their practical application for interior thermal insulation systems. Contrary to other experimental studies on biomaterials, the measured sets of heat and moisture transport and storage parameters are complete and prepared for an immediate application in computer simulation tools. Their hygrothermal and energy performance in various traditional and historical construction systems can thus be assessed in a more reliable way than it was common in most previous studies where only a part of the necessary input parameters of computational models was known with a sufficient accuracy.

Acknowledgment

This research has been supported by the Ministry of Culture, Czech Republic, under project No DG16P02H046.

Appendix A. Supplementary data

Supplementary data to this article can be found online at https://doi.org/10.1016/j.buildenv.2019.03.020.

References

[1] J.T. Kim, C.W.F. Yu, Sustainable development and requirements for energy efficiency in buildings - the Korean perspectives, Indoor Built Environ. 27 (6) (2018) 734–751 https://doi.org/10.1177/1420326x18764618.
[2] R. Escandon, S. Silvester, T. Konstantinou, Evaluating the environmental adaptability of a nearly zero energy retrofitting strategy designed for Dutch housing stock to a Mediterranean climate, Energy Build. 169 (2018) 366–378 https://doi.org/10.1016/j.enbuild.2018.03.079.
[3] H.M. Kunzel, Effect of interior and exterior insulation on the hygrothermal behaviour of exposed walls, Mater. Struct. 31 (206) (1998) 99–103 https://doi.org/10.1007/bf02486471.
[4] A.L. Webb, Energy retrofits in historic and traditional buildings: a review of problems and methods, Renew. Sustain. Energy Rev. 77 (2017) 748–759 https://doi.org/10.1016/j.rser.2017.01.145.
[5] E. Vereecken, S. Roels, A comparison of the hygric performance of interior insulation systems: a hot box-cold box experiment, Energy Build. 80 (2014) 37–44 https://doi.org/10.1016/j.enbuild.2014.04.033.
[6] E. Vereecken, L. Van Gelder, H. Janssen, S. Roels, Interior insulation for wall retrofitting - a probabilistic analysis of energy savings and hygrothermal risks, Energy Build. 89 (2015) 231–244 https://doi.org/10.1016/j.enbuild.2014.12.031.
[7] E. Vereecken, S. Roels, Wooden beam ends in combination with interior insulation: the importance of an airtight sealing, 11th Nordic Symposium on Building Physics (Nsb2017), vol. 132, 2017, pp. 664–669 https://doi.org/10.1016/j.egypro.2017.10.003.
[8] D. Watt, S. Sjoberg, P. Wahlgren, Hygrothermal performance of a light weight timber wall assembly with an exterior air barrier, 6th International Building Physics Conference (Ibpc 2015), vol. 78, 2015, pp. 1419–1424 https://doi.org/10.1016/j.egypro.2015.11.164.
[9] T. Stahl, K.G. Wakili, R. Vonbank, S. Brunner, Comparative investigation of energetic refurbishment of half-timbered walls using aerogel based plaster as internal insulation, Bauphysik 38 (5) (2016) 274 https://doi.org/10.1002/bapi.201610029.
[10] G.R. Finken, S.P. Bjarlov, R.H. Peuhkuri, Effect of facade impregnation on feasibility of capillary active thermal internal insulation for a historic dormitory - a hygrothermal simulation study, Constr. Build. Mater. 113 (2016) 202–214 https://doi.org/10.1016/j.conbuildmat.2016.03.019.
[11] J. Carmeliet, D. Derome, Temperature driven inward vapor diffusion under constant and cyclic loading in small-scale wall assemblies: Part 1 experimental investigation, Build. Environ. 48 (2012) 48–56 https://doi.org/10.1016/j.buildenv.2011.08.015.
[12] J.H. Zhao, J. Grunewald, U. Ruisinger, S. Feng, Evaluation of capillary-active mineral insulation systems for interior retrofit solution, Build. Environ. 115 (2017) 215–227 https://doi.org/10.1016/j.buildenv.2017.01.004.
[13] X.H. Zhou, J. Carmeliet, D. Derome, Influence of envelope properties on interior insulation solutions for masonry walls, Build. Environ. 135 (2018) 246–256 https://doi.org/10.1016/j.buildenv.2018.02.047.
[14] A.A. Hamid, P. Wallenten, Hygrothermal assessment of internally added thermal insulation on external brick walls in Swedish multifamily buildings, Build. Environ. 123 (2017) 351–362 https://doi.org/10.1016/j.buildenv.2017.05.019.
[15] E. Vereecken, S. Roels, Capillary active interior insulation systems for wall retrofitting: a more Nuanced story, Int. J. Archit. Herit. 10 (5) (2016) 558–569 https://doi.org/10.1080/15583058.2015.1009575.
[16] C. Feng, H. Janssen, Hygric properties of porous building materials (II): analysis of temperature influence, Build. Environ. 99 (2016) 107–118 https://doi.org/10.1016/j.buildenv.2016.01.016.
[17] M.B. Janetti, T.A. Carrubba, F. Ochs, W. Feist, Heat flux measurements for determination of the liquid water diffusivity in capillary active materials, Int. J. Heat Mass Transf. 97 (2016) 954–963 https://doi.org/10.1016/j.ijheatmasstransfer.2016.02.047.
[18] M. Jerman, R. Cerny, Effect of moisture content on heat and moisture transport and storage properties of thermal insulation materials, Energy Build. 53 (2012) 39–46 https://doi.org/10.1016/j.enbuild.2012.07.002.
[19] E. Troppova, M. Svehlik, J. Tippner, R. Wimmer, Influence of temperature and

moisture content on the thermal conductivity of wood-based fibreboards, Mater. Struct. 48 (12) (2015) 4077–4083 https://doi.org/10.1617/s11527-014-0467-4.
[20] H.-R. Kymalainen, A.-M. Sjoberg, Flax and hemp fibres as raw materials for thermal insulations, Build. Environ. 43 (7) (2008) 1261–1269 https://doi.org/10.1016/j.buildenv.2007.03.006.
[21] E. Latif, S. Tucker, M.A. Ciupala, D.C. Wijeyesekera, D. Newport, Hygric properties of hemp bio-insulations with differing compositions, Constr. Build. Mater. 66 (2014) 702–711 https://doi.org/10.1016/j.conbuildmat.2014.06.021.
[22] A. Korjenic, V. Petranek, J. Zach, J. Hroudova, Development and performance evaluation of natural thermal-insulation materials composed of renewable resources, Energy Build. 43 (9) (2011) 2518–2523 https://doi.org/10.1016/j.enbuild.2011.06.012.
[23] J. Zach, A. Korjenic, V. Petranek, J. Hroudova, T. Bednar, Performance evaluation and research of alternative thermal insulations based on sheep wool, Energy Build. 49 (2012) 246–253 https://doi.org/10.1016/j.enbuild.2012.02.014.
[24] S. Schiavoni, F. D'Alessandro, F. Bianchi, F. Asdrubali, Insulation materials for the building sector: a review and comparative analysis, Renew. Sustain. Energy Rev. 62 (2016) 988–1011 https://doi.org/10.1016/j.rser.2016.05.045.
[25] B. Abediniangerabi, S.M. Shahandashti, B. Bell, S.H. Chao, A. Makhmalbaf, Building energy performance analysis of ultra-high-performance fiber-reinforced concrete (UHP-FRC) facade systems, Energy Build. 174 (2018) 262–275 https://doi.org/10.1016/j.enbuild.2018.06.027.
[26] J.H. Park, Y.J. Kang, J. Lee, S. Wi, J.D. Chang, S. Kim, Analysis of walls of functional gypsum board added with porous material and phase change material to improve hygrothermal performance, Energy Build. 183 (2019) 803–816 https://doi.org/10.1016/j.enbuild.2018.11.023.
[27] L. Havinga, H. Schellen, Applying internal insulation in post-war prefab housing: Understanding and mitigating the hygrothermal risks, Build. Environ. 144 (2018) 631–647 https://doi.org/10.1016/j.buildenv.2018.08.035.
[28] ČSN EN 1602, Thermal Insulating Products for Building Applications - Determination of the Apparent Density, Czech Institute for Standards, Metrology and Testing, Prague, 2013.
[29] ČSN EN 822, Thermal Insulating Products for Building Applications – Determination of Length and Width, Czech Institute for Standards, Metrology and Testing, Prague, 2013.
[30] ČSN EN 823, Thermal Insulating Products for Building Applications – Determination of Thickness, Czech Office for Standards, Metrology and Testing, Prague, 2013.
[31] ČSN EN 12085, Thermal Insulating Products for Building Applications – Determination of Linear Dimensions of Test Specimens, Czech Office for Standards, Metrology and Testing, Prague, 2013.
[32] ČSN EN ISO 12572, Hygrothermal Performance of Building Materials and Products - Determination of Water Vapour Transmission Properties - Cup Method, Czech Office for Standards, Metrology and Testing, Prague, 2017.
[33] E.L. Cussler, Diffusion: Mass Transfer in Fluid Systems, Cambridge University Press, New York, 1997.
[34] ČSN EN ISO 15148, Hygrothermal Performance of Building Materials and Products - Determination of Water Absorption Coefficient by Partial Immersion, Czech Institute for Standards, Metrology and Testing, Prague, 2004.
[35] E. Vejmelkova, M. Pavlikova, M. Jerman, R. Cerny, Free water intake as means of material characterization, J. Build. Phys. 33 (1) (2009) 29–44 https://doi.org/10.1177/1744259109104069.
[36] S. Roels, J. Carmeliet, H. Hens, O. Adan, H. Brocken, R. Cerny, Z. Pavlik, C. Hall, K. Kumaran, L. Pel, R. Plagge, Interlaboratory comparison of hygric properties of porous building materials, J. Therm. Envelope Build. Sci. 27 (4) (2004) 307–325 https://doi.org/10.1177/1097196304042119.
[37] ISO/EIC 98-3, Guide to the Expression of Uncertainty in Measurement, Joint Comittee for Guides in Metrology, France, 2008.
[38] A. Korjenic, J. Zach, J. Hroudova, Sheep wool as alternative heat insulation and their hygrothermal behaviour, Bauphysik 36 (5) (2014) 249–256 https://doi.org/10.1002/bapi.201410037.
[39] M. Palumbo, A.M. Lacasta, N. Holcroft, A. Shea, P. Walker, Determination of hygrothermal parameters of experimental and commercial bio-based insulation materials, Constr. Build. Mater. 124 (2016) 269–275 https://doi.org/10.1016/j.conbuildmat.2016.07.106.
[40] M. Rahim, O. Douzane, A.D.T. Le, G. Promis, B. Laidoudi, A. Crigny, B. Dupre, T. Langlet, Characterization of flax lime and hemp lime concretes: hygric properties and moisture buffer capacity, Energy Build. 88 (2015) 91–99 https://doi.org/10.1016/j.enbuild.2014.11.043.
[41] M. Rahim, O. Douzane, A.D. Tran Le, G. Promis, T. Langlet, Characterization and comparison of hygric properties of rape straw concrete and hemp concrete, Constr. Build. Mater. 102 (2016) 679–687 https://doi.org/10.1016/j.conbuildmat.2015.11.021.
[42] M. Woloszyn, T. Kalamees, M.O. Abadie, M. Steeman, A.S. Kalagasidis, The effect of combining a relative-humidity-sensitive ventilation system with the moisture-buffering capacity of materials on indoor climate and energy efficiency of buildings, Build. Environ. 44 (3) (2009) 515–524 https://doi.org/10.1016/j.buildenv.2008.04.017.
[43] J. Zach, J. Hroudova, J. Brozovsky, Z. Krejza, A. Gailius, Development of thermal insulating materials on natural base for thermal insulation systems, Modern Building Materials, Structures and Techniques 57 (2013) 1288–1294 https://doi.org/10.1016/j.proeng.2013.04.162.
[44] A. Bourdot, T. Moussa, A. Gacoin, C. Maalouf, P. Vazquez, C. Thomachot-Schneider, C. Bliard, A. Merabtine, M. Lachi, O. Douzane, H. Karaky, G. Polidori, Characterization of a hemp-based agro-material: influence of starch ratio and hemp shive size on physical, mechanical, and hygrothermal properties, Energy Build. 153 (2017) 501–512 https://doi.org/10.1016/j.enbuild.2017.08.022.
[45] B.K. Stefanowski, S.F. Curling, G.A. Ormondroyd, A rapid screening method to determine the susceptibility of bio-based construction and insulation products to mould growth, Int. Biodeterior. Biodegrad. 116 (2017) 124–132 https://doi.org/10.1016/j.ibiod.2016.10.025.
[46] C. Feng, H. Janssen, Hygric properties of porous building materials (III): impact factors and data processing methods of the capillary absorption test, Build. Environ. 134 (2018) 21–34 https://doi.org/10.1016/j.buildenv.2018.02.038.
[47] C. Feng, H. Janssen, Y. Feng, Q.L. Meng, Hygric properties of porous building materials: analysis of measurement repeatability and reproducibility, Build. Environ. 85 (2015) 160–172 https://doi.org/10.1016/j.buildenv.2014.11.036.
[48] I. Antepara, Z. Pavlik, J. Zumar, M. Pavlikova, R. Cerny, Properties of hydrophilic mineral wool for desalination of historical masonry, Materials Science-Medziagotyra 22 (1) (2016) 88–93 https://doi.org/10.5755/j01.ms.22.1.7333.
[49] A. Korjenic, J. Zach, J. Hroudova, The use of insulating materials based on natural fibers in combination with plant facades in building constructions, Energy Build. 116 (2016) 45–58 https://doi.org/10.1016/j.enbuild.2015.12.037.

Selected paper 5 – Building and Environment

Jerman, M., Böhm, M., Dušek, J., Černý, R., Effect of steaming temperature on microstructure and mechanical, hygric, and thermal properties of binderless rape straw fiberboards – 2022

To reduce the carbon footprint of construction, it is advisable to use locally available materials. Thermal insulation boards can be made from natural materials, one of which is rapeseed straw. In the last article, the production process is presented. The thermal, moisture, and mechanical properties of the newly developed material are also presented to assess its possible use.

Contribution to practical use

A source of lignocellulose, which is rarely used in practice for the production of building materials, was tested. Rapeseed straw fibers can be used as blown-in insulation or for the production of new thermal insulation boards. In this article, the production process is presented and the characteristics of the material, in particular the thermal and moisture properties, are given.

Knowledge about the effect of temperature on the plasticity and self-adhesive properties of lignin in straw can particularly be used by manufacturers of natural thermal insulation materials. Straw fibers can serve as a partial substitute for wood in fiberboard.

Building and Environment 223 (2022) 109474

Contents lists available at ScienceDirect

Building and Environment

journal homepage: www.elsevier.com/locate/buildenv

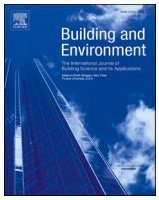

Effect of steaming temperature on microstructure and mechanical, hygric, and thermal properties of binderless rape straw fiberboards

Miloš Jerman *, Martin Böhm, Jaroslav Dušek, Robert Černý

Department of Materials Engineering and Chemistry, Faculty of Civil Engineering, Czech Technical University in Prague, Thákurova 7, 166 29, Prague 6, Czech Republic

ARTICLE INFO

Keywords:
Binderless
Fiberboard
Hygric properties
Mechanical properties
Rape straw
Thermal insulation
Thermal properties

ABSTRACT

Rape straw as a waste product of the oilseed industry is available abundantly in the European Union. In this paper, the utilization of rape straw-based fibers for the preparation of binderless thermal insulation materials is investigated. The effect of steaming temperature, which can be considered as one of the most important parameters of the production process, on microstructure and mechanical, hygric and thermal properties of the insulation boards is analyzed. The experimental results show that the designed binderless rape straw fiberboards achieve the most suitable combinations of mechanical, hygric and thermal properties for the steaming temperatures of 180 °C and higher, which indicates 180 °C as the most promising solution.

1. Introduction

The building industry is considered to be the biggest polluter of the natural environment. One of the reasons is that the materials used are mainly from non-renewable sources. Negative environmental impacts can be addressed by using locally available natural materials with low-embodied energy building materials [1]. The use of natural materials allows for the storage of carbon dioxide in building structures [2–5] and also leads to safeguarding natural resources. The main natural material is wood which provides a wide range of utilization. Traditional particleboards are based on wood and synthetic adhesives, such as urea formaldehyde or phenol formaldehyde, as the binder [6]. Fibers for the production of wood fiberboards are produced by hydro-thermo-mechanical pulping of wood chips. Fiberboards with lower density can be produced without the addition of glue; its cohesiveness is ensured by natural fiber felting and lignin released during thermal treatment. However, the addition of a few weight percent of adhesive is more often used. The boards are produced under pressure, and the higher the pressure, the higher the bulk density of the boards. Fiberboards are used most often in construction as thermal insulation materials. There is a wide range of wood fiber boards, produced with different bulk densities, from very light 30 kg/m^3 boards up to a bulk density of 250 kg m^{-3}. Boards with a higher bulk density can withstand mechanical stress. These boards are manufactured with different modifications for different purposes. The bulk density is usually in the range of 110–160 kg/m^3. The resulting properties of fiberboards without the addition of adhesives are affected by the pressing time, temperature, fiber size, and their treatment [7,8]. Boards with a density of 330–340 kg/m^3 represent thermal conductivity between 0.064 W/(m·K) and 0.066 W/(m·K) [9].

A possibility to reduce the consumption of wood raw materials presents bark utilization. The bark is an outer layer of trees. The wet board was dried in an oven at 103 °C [10]. Insulation boards with densities of 160–300 kg/m^3 were studied by Gößwald et al. [10]. The thermal conductivity of the bark insulation board with a density of 160 kg/m^3 was 0.044 W/(m·K). Thermal conductivity increased with increasing bulk density. From this point of view, it is reasonable to replace the wood, especially because it contains significant amounts of cellulose, hemicellulose, and lignin. Christy et al. [11] studied similar boards from Gelam (Melaleuca viridiflora) bark waste. The effects of four different temperatures (140, 160, 180 and 200 °C) on mechanical and other properties were analyzed. The best physical and mechanical properties were obtained at a pressing temperature of 200 °C. The bulk density was 550 kg/m^3 and the thermal conductivity was 0.14 W/(m·K).

Recently, due to the worldwide shortage of forest resources, as well as economic and environmental considerations, the demand for non-wood lignocellulose fiber has increased [12,13]. Wood particles may be replaced by agriculture residues like stalks, leaves, stems, or straw, which are generated abundantly, annually, by locally available plants for alternative particleboards.

Annual plants represent a good opportunity to reduce the carbon footprint and replace non-renewable materials, because the storage of

* Corresponding author.
E-mail address: milos.jerman@fsv.cvut.cz (M. Jerman).

https://doi.org/10.1016/j.buildenv.2022.109474
Received 31 May 2022; Received in revised form 12 July 2022; Accepted 3 August 2022
Available online 9 August 2022

carbon dioxide in fast growing bio based materials is a key part of sustainable development [3]. The next benefit is their easy biodegradability and nontoxic nature. With increasing concern over health issues and biomass conservation, the fiberboards from agriculture residues with or without adhesives are under intensive investigation [7]. There are many plants that can be used for construction or thermal insulation purposes [1]. Sources of such materials may include, for example, straw, hemp-shive, flax fiber, etc. This biomass is an agricultural by-product and is a significant source of renewable energy. Lignocellulosic materials are widely studied to achieve self-bonding materials. Bonding is caused by lignin plasticization, and consequently lignin polycondensation and hemicellulose reactions, among others, at high temperatures [12,14]. The internal bonding without additional adhesive is mainly due to hydrogen bonding - binding between fibers, condensation reaction in lignin and lignin polysaccharides cross-linking reaction, lignin polycondensation and hemi-reaction among others, at high temperatures and using steam [7,15].

Lignin is a complex phenolic amorphous polymer, an essential element needed in cell wall development, as it is responsible for the rigidity and toughness of the fiber while providing compressive strength. Lignin contains different functional groups, i.e., hydroxyl, methoxyl, and carbonyl groups, which allow its chemical modification to be applied to increase its reactivity. Lignin is a natural adhesive that acts as a binding force between cellulose fibers. When agricultural residues are heated, lignin plasticization and reaction with furfural form a lignin-furfural complex which is believed to participate in self-bonding [7]. The high pressing temperature will increase the lignin fluidity of fibers to help form better interfiber bonds [16].

Manufacturing of particleboards is one way in which to use agricultural waste. It is possible to produce a wide range of boards, according to the bulk density, low density, medium or high density. Domínguez-Robles et al. [17] described the production process and properties of a wheat straw board with a bulk density higher than 1000 kg/m^3. In this case, no glue was added, and yet the board achieved good mechanical properties, in particular flexural strength over 80 MPa. The mechanical properties were influenced mainly by length of the fibers; the shorter the length, the greater the strength. The swelling thickness was approximately 40%.

Thermal insulation materials manufactured from renewable materials can be a good alternative to conventional thermal insulation materials. Mahieu et al. [14] studied sunflower bark and flax particle board self-bound by a thermo-compression process with water. The target density was 350 and 500 kg/m^3. These boards achieved high mechanical properties; however, thickness swelling was more than 60% for the density of 350 kg/m^3 and more than 90% for 500 kg/m^3, which limited the use of this material in building construction. The material was thermo-pressed at 190 °C for 10 min (flax fiber contained a higher proportion of cellulose, 80% and only 6% of lignin). Sunflower straws are by-products of the vegetable-oil industry. Sunflower particleboard without binder was thermo-pressed at 190 °C for 45 min. The bulk density of flax shives was about 100 ± 4 kg/m^3 and 180 ± 5 kg/m^3 for the sunflower bark. The target density of the board was 350 and 500 kg/m^3 and the thermal conductivity was 0.066–70 W/(m·K) for 350 kg/m^3 and 0.074–0.077 W/(m·K) for 500 kg/m^3 [14]. Another possibility presents jute. Jute thermal insulation boards mixed with polyester fibers with a range of 150–230 kg/m^3 were developed and tested by Jin et al. [18]. The thermal conductivity was comparable with synthetic thermal insulation, such as rock wool, mineral wool or polystyrene, e.g., jute board with a density of 152 kg/m^3 achieved a very promising thermal conductivity of 0.0372 W/(m·K).

Binderless insulation with a low density of 250–450 kg/m^3 can also be made from coconut husk. Temperatures of 180 °C, 200 °C and 220 °C were used for hot pressing [19]. It was shown that optimal mechanical properties were achieved by boards made from coconut husk at a pressing temperature 200 °C for 13 min. These binderless boards with a density of 250–350 kg/m^3 had the thermal conductivity in the range of 0.046–0.068 W/(m·K). The thickness swelling (TS) values of the binderless coconut husk insulation boards decreased with increasing temperature and pressing time. At a board density of 350 kg/m^3, the binderless coconut husk insulation board gave the lowest TS value of 21.7% with a pressing temperature of 220 °C/13 min. At a board density of 350 kg/m^3, the binderless bagasse insulation board gave the lowest TS value of 21.7% with a pressing temperature of 200 °C/13 min, whereas the binderless bagasse insulation board gave the lowest TS value of 42.7% with a pressing temperature of 160 °C/7 min [19]. It should be noted that the thickness swelling of both insulation boards exceeded the maximum permitted levels (10%) for insulation boards in JIS A 5905: 2003. Cotton stalk fiber board with a density of 150–450 kg/m^3 had a thermal conductivity in the range of 0.0585–0.0815 W/(m·K) [16]. For preparing binderless particle board, it is also possible to use also rice straw. Kurokochi and Sato [20] investigated the effect of pressing temperature. Water resistance increased significantly with increasing pressing temperature. Fiberboards may also be produced from municipal waste [21]. Municipal waste treated at 180 °C for 2 h had a density of over 800 kg/m^3. Due to its high bulk density, it had higher thermal conductivity compared to thermal insulation materials. The summarized information on binderless boards is given in Table 1.

Rape is an annual plant cultivated as a source of vegetable oil. Rape straw, which contains 19–21% of lignin ([23,24]) and approximately 40% of cellulose [22,23], is a waste product of the oilseed industry. Due to its wide availability (several million tons per annum in the EU), it can play an important role as an alternative sustainable building material, particularly thermal insulation. Therefore, the use of rape straw for the production of resin-bonded fiberboards was studied in various research papers during the last decade. Dukarska et al. [25] developed rape straw particleboards with strength properties comparable to those of particleboards type 5 and OSB/3 boards. The hybrid pMDI/PF applied resin enabled a decrease in the density of the boards to 600–550 kg/m^3. Hýsek et al. [23] developed and tested similar particleboards with different kinds of glue and surface pretreatment but achieved lower mechanical properties while the bulk density was still more than 500 kg/m^3.

The use of rape straw for the preparation of adhesive-free boards was not published yet in common literature sources. However, the high amount of lignin makes good prerequisites for producing boards on rape straw basis without any glue. Therefore, in this paper, the possibility of using rape straw for the production of binderless low-density fiberboards is analyzed. The main aims of the research work are as follows: i) preparation of a board material with low bulk density and low thermal conductivity, ii) investigation of the influence of steaming temperature on material properties, iii) achievement of a low value of wetting-induced volumetric changes.

2. Materials and experimental methods

2.1. Preparation of binderless board samples

Rape straw was obtained from Polepy near the Czech Middle Mountain. The whole straw was washed three times with hot water to remove the impurities and wax layer from the surface [22] in order to achieve a better adherence. The straw was cut in hot water using a pulper with a helical rotor at 3600 rpm for 10 min to ensure good fiber distribution in water. However, due to the size of the pulper and the amount of straw, in addition to the fibers there were also small straw particles. The particles that passed through 4 mesh sized filters were used to make the binderless board. The dimension of the iron forming box was 300 × 300 mm and the thickness of the boards was 40 mm. After the mat was molded, its upper surface was covered with an aluminum sheet. Then the mat was pressed for 1 min at 8 kPa and affixed by clamps. The wet straw was exposed to steam in an oven at 100 °C, 140 °C, 180 °C and 200 °C for 30 min. Then, the board was conditioned via air-drying at a temperature of 60 °C for two days. This wet process was applied without using additives or glue.

Table 1
Binderless boards.

	Steaming Temperature [°C]	Time [min]	Bulk density [kg/m^3]	Thermal conductivity [W/(m·K)]	Thickness swelling [%]	Reference
Rice straw	200–220	10–20	800	not specified	50, 6-12	[20,22]
Bark	103	24	185–277	0.049–0.062	8–19	[10]
Gelem bark	140–200	20	590	not specified	12	[11]
Flax shives and sunflower bark	190	45	350–500	0.042 0.07–0.08	60–95	[14]
Coconut husk	180,200,220	7,10,13	250–450	0.046–0.068	22–43	[19]
Wheat	150–230	30, 5	> 1000	> 0.0867	40–70	[17]
Bagasse	160,180,200	7, 13	250–450	0.049–0.055	21–43	[19]

2.2. Material characterization methods

The microstructural morphology of the fiber surface and adhesively bonded joints was studied by scanning electron microscopy (SEM) using a Phenom XL desktop SEM (ThermoFischer Scientific) with a secondary electron detector operated at an acceleration voltage of 15 kV, and a working distance of 5–15 mm. All the samples for microscopic analysis were vacuum dried at room temperature in order not to affect their properties. Vacuum-dried samples were glued to an aluminum stab using double-sided conductive carbon tape. Sputter coater Quorum SC7620 (Quorum Technologies Ltd, Laughton, United Kingdom) was used to generate an approximately 5–10 nm gold/palladium coating on the samples to make them conductive.

The basic physical properties included the bulk density, water absorption (WA) after 24 h soaking and thickness swelling (TS) after 24 h of soaking. Bulk density was determined according to the EN 1602 standard [26]. For the bulk density test five samples with dimensions of 250 mm × 250 mm × 40 mm were prepared. In the first step the samples were dried, then the average length and width of the boards were measured. Bulk density was calculated according to the common gravimetric formula. The TS 24 h and WA 24 h (ČSN EN 317:1995) [27] values of the boards were determined using test samples of 50 mm × 50 mm. The tests were carried out by immersion of the samples into water for 24 h. At the beginning of the test the weight and thickness of the dried samples were recorded.

2.3. Determination of mechanical and hygrothermal properties

The mechanical properties were represented by the internal bonding strength expressed in terms of tensile strength and modulus of elasticity. The setup of the experiment is given in Fig. 1. The test samples of a 400 cm^2 square cross-section area were cut from the rape fiber boards. The test specimens were dry-cut from the board using a circular saw cutting machine (Brillant 240, ATM, Germany) with fine dynamic cutting to avoid pulling fibers out of the sample. The samples were glued to the frame with flexible couplings using epoxy resin. After the epoxy adhesive had hardened, the sample was affixed in a tensile testing machine. The displacement increase rate was 0.2 mm/s according to the ČSN EN 1607 standard [28].

The water vapor adsorption isotherms were measured using the desiccator method at a temperature of 23 °C. In the first step, the dried samples were placed into a desiccator with different salt solutions to reach various steady relative humidity conditions (Fig. 2). The mass of individual samples was recorded, and the experimental procedure was finished when steady-state values of mass were achieved. Then the gravimetric moisture content was calculated for a particular relative humidity [29].

Thickness swelling in the hygroscopic range was evaluated during the sorption isotherm test. In the overhygroscopic range, it was examined on samples with dimensions of 100 × 100 mm before and after immersion in water for 24 h. The thickness of each sample was measured using a dial indicator with an accuracy of 0.05 mm at four points before and after the experiment. The swelling of the samples during the sorption test was calculated using the following equation:

$$S(-) = \frac{d_1 - d_0}{d_0} \quad (1)$$

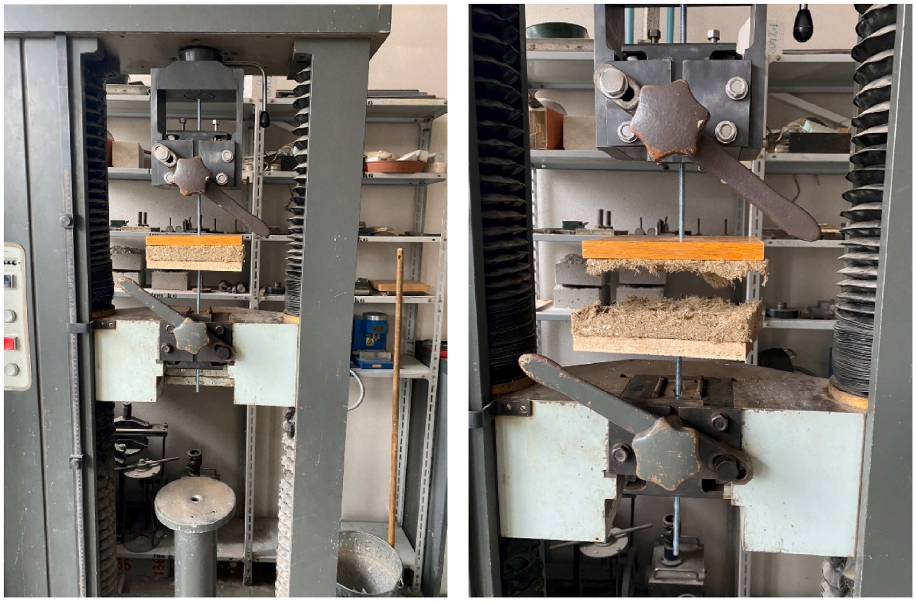

Fig. 1. Internal bonding strength measurement.

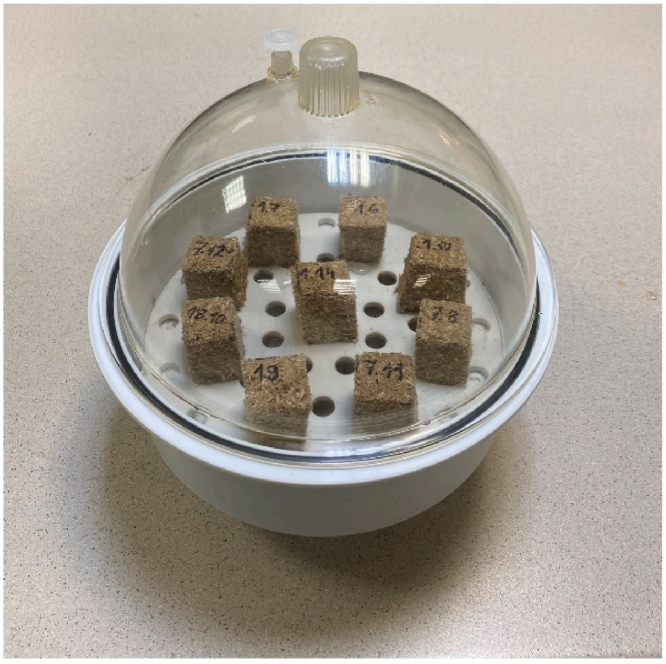

Fig. 2. Determination of sorption isotherms.

where d_1 is thickness of the sample after exposure to the humid environment, d_0 is thickness of sample preconditioned at 11% RH.

The cup method was used to determine the water vapor transport parameters. The measurement was carried out in steady state under isothermal conditions. The dimensions of the tested samples were 100 mm × 100 mm, and the thickness was 40 mm. The lateral sides were sealed to ensure one-dimensional test. Three samples of each material were stored in laboratory conditions (22 ± 2 °C and 50 ± 5% of RH) until they were tested. The measurement of dry cup and wet cup was carried out according to the EN ISO 12572 [30] standard (Fig. 3); it is described in detail, e.g., in Ref. [29]. For the dry cup, the specimens were placed in a metal cup containing silica gel, and for the wet cup distilled water was used. The cups with specimens were then placed into a climatic chamber that maintained a constant temperature of 25 °C and constant relative humidity of 55% during the testing procedure. The mass increase or decrease (wet cup) of the assembly was recorded every 24 h. The water vapor diffusion permeability, δ_m (s), water vapor diffusion coefficient, D ($m^2 \cdot s^{-1}$), and water vapor diffusion resistance factor, μ (−), were calculated according to equations.

$$\delta_m = \frac{\Delta m \cdot d}{t \cdot S \cdot \Delta p_v} \quad (2)$$

$$D = \frac{\delta_m \cdot R \cdot T}{M} \quad (3)$$

$$\mu = \frac{D_a}{D} \quad (4)$$

In Eqs. (2)–(4), Δm (kg) is the mass increase, d (m) is the sample thickness, t (s) is time, S (m^2) is the surface area of the specimen, Δp_v (Pa) is the partial pressure difference, D_a = 2.82 × 10-5 m^2 s^{-1} is the water vapor diffusion coefficient in air at 25 °C, R = 8.314 Pa m^3 $mol^{-1} \cdot K^{-1}$ is the gas constant, T (K) stands for temperature and M = 0.01802 kg mol^{-1} is the molar mass of water. According to the standard EN ISO 12572 [30], for permeable materials the water vapor permeability formula must be corrected with a coefficient depending on the thickness of the air gap between the sample and the salt solution or the silica gel according to the formula

$$\delta_{m,corr} = \frac{d}{\frac{t \cdot S \cdot \Delta p_v}{\Delta m} - \frac{d_a}{\delta_a}} \quad (5)$$

where d_a (m) is the thickness of the air layer and δa = 1.993 × 10^{-10} kg m^{-1} s^{-1} Pa^{-1} is the water vapor permeability in the air at 25 °C. The resistance of the layer above the cup could be neglected because the air in the test chamber was stirred, so that the velocity above each specimen was 2 m s^{-1} or higher which met the requirements prescribed in EN ISO 12572 [30].

Thermal conductivity and specific heat capacity were measured using an Isomet 2104 device. The measurement was based on the evaluation of the temperature response of the analyzed sample to heat flow pulses. Heat flow was induced by an electrical resistor heater having a direct thermal contact with the sample. The thermal conductivity values were determined as a function of moisture content.

MS Excel 2016 (Microsoft Corporation, USA) was used for all calculations. For a more detailed evaluation, basic descriptive statistics, simple linear regression, fixed nonlinear regression, one-way analysis of variance (ANOVA), and Tukey's honestly significant difference (HSD) test were used. All tests were performed at a significance level of α = 0.05 in the Statistica 13.3 Academic software (TIBCO, USA).

3. Results and discussion

The surface of the rape straw fiberboards with fibers steamed at 100–200 °C is shown in Figs. 4–7. It can be seen from the images that with increasing fiber treatment temperature, it was possible to find a larger proportion of lignin on the surface of the fibers and straw

Fig. 3. Determination of water vapor permeability (left) and an example of the manufactured sample (right).

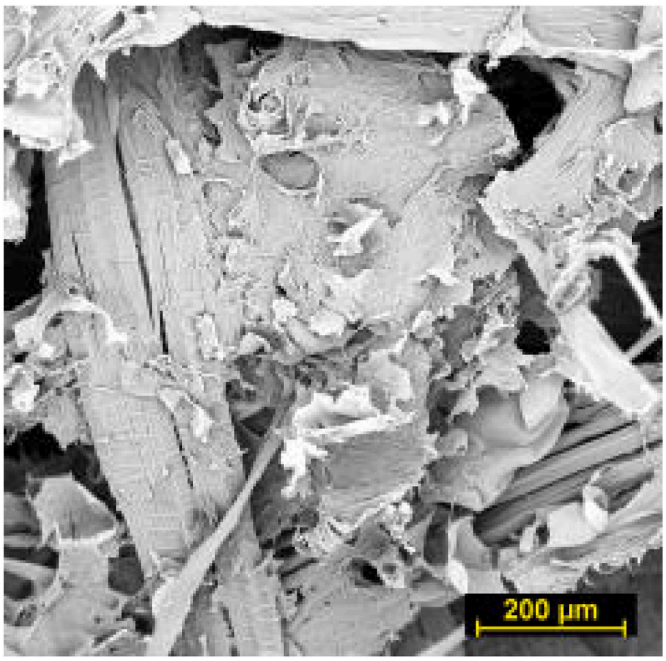

Fig. 4. SEM image of rape straw fiberboard made of fibers steamed at 100 °C.

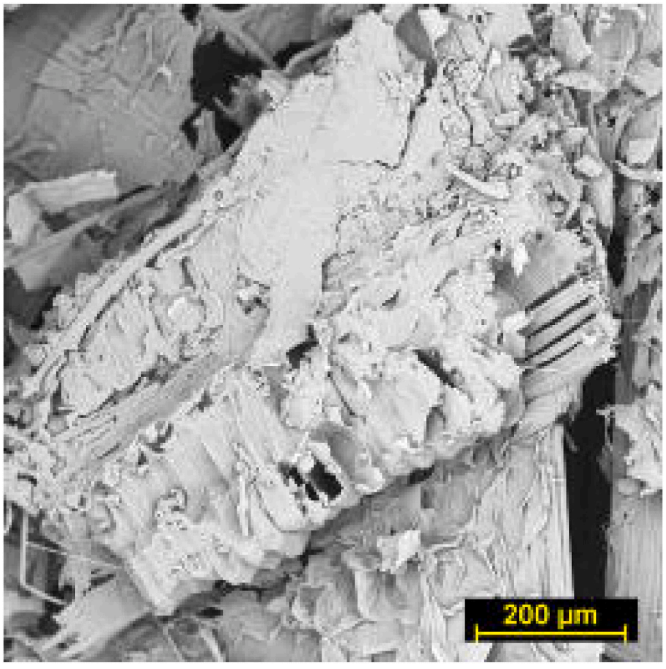

Fig. 5. SEM image of rape straw fiberboard made of fibers steamed at 140 °C.

particles. In particular, lignin plasticized at the temperatures of 180 °C and higher contributed significantly to the cohesiveness of the compressed fibers and particles.

The basic physical properties of the fiberboards studied are summarized in Table 2. The bulk density values of the individual test specimen sets were within the range of 100–110 kg/m^3. They were significantly lower than those of many other binderless organic boards, but higher than inorganic thermal insulation materials, such as EPS or glass wool. WA after 24 h was over 600% for all samples, the differences were within the range of 5%. Thickness swelling decreased substantially with increasing steaming temperature, TS 24 h was almost two times lower for 200 °C in a comparison with 100 °C.

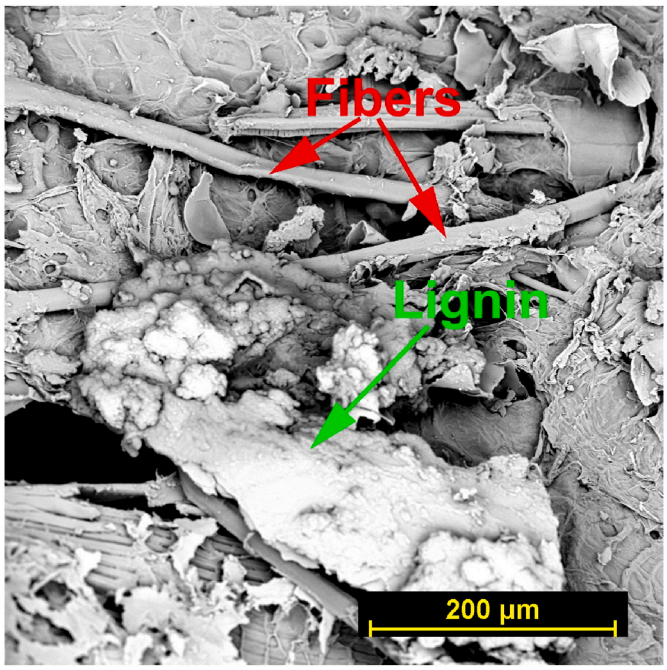

Fig. 6. SEM image of rape straw fiberboard made of fibers steamed at 180 °C.

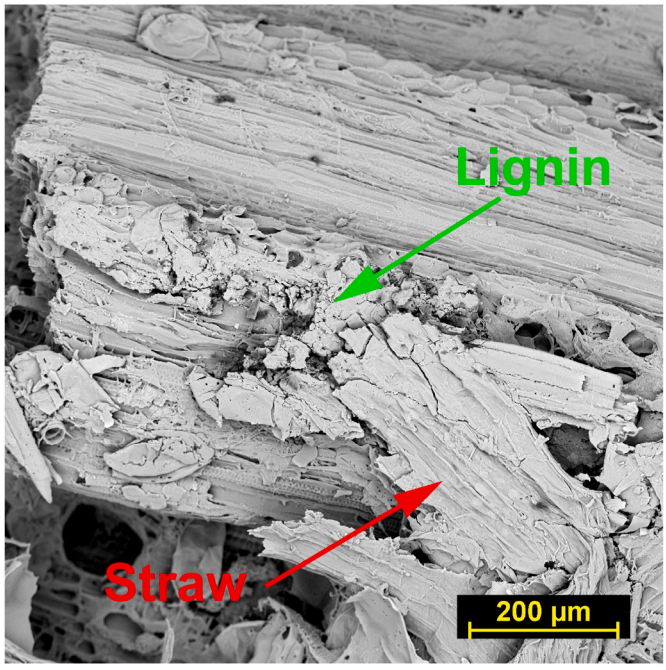

Fig. 7. SEM image of rape straw fiberboard made of fibers steamed at 200 °C.

Table 2
Basic physical properties of rape straw fiberboards (mean ± standard deviation).

Steaming temperature	Bulk density [kg/m^3]	WA 24 h [%kg/kg]	TS 24 h [%]
100 °C	104 ± 4	634 ± 23	6.34 ± 0.18
140 °C	104 ± 4	606 ± 20	4.67 ± 0.20
180 °C	107 ± 5	606 ± 24	4.00 ± 0.28
200 °C	107 ± 4	601 ± 22	3.40 ± 0.29

Table 3
Mechanical properties of rape straw fiberboards.

Steaming temperature	Tensile strength [kPa]	Modulus of elasticity [kPa]
100 °C	$4.6^{a*} \pm 0.37$	$273^{a} \pm 25$
140 °C	$6.3^{b} \pm 0.42$	$373^{b} \pm 35$
180 °C	$12.5^{c} \pm 0.68$	$409^{b,c} \pm 40$
200 °C	$14.0^{d} \pm 0.53$	$442^{c} \pm 32$

*Values with the same index are not statistically significantly different.

The mechanical parameters are presented in Table 3 and Fig. 8. Apparently, both tensile strength and modulus of elasticity increased remarkably with the increasing steaming temperature up to 200 °C. In the case of tensile strength, the highest difference was observed between 140 °C and 180 °C. The enhancement can be explained by the fact that lignin melts better at higher temperatures, as it can be seen in SEM images (Figs. 4–7). This allows lignin to flow over the fiber surface and to establish stronger inter-fiber bonds [31]. In a comparison with some other self-bonded materials e.g., bark fiber boards with a density of ~200 kg/m^3 achieved internal bonding slightly lower than 50 kPa. With increasing bulk density (pressing) increases the tensile strength [10]. The influence of steaming temperature on the tensile strength of the bark fiber board was studied by Christy et al. [11] the best mechanical properties were achieved at the temperature of 200 °C. The tensile strength of self-bonded flax shives board was determined on the samples with a density of 500 kg/m^3 made at the temperature of 190 °C for 45 min [14]. The result was ~20 kPa. Wheat straw self-bonded boards achieved tensile strength much higher, over 800 kPa, enzymatically treated fiber boards ~1.4 MPa. It was mainly due to high bulk density which was in this case over 1000 kg/m^3 [17]. The binderless insulation boards made from bagasse at density of 350 kg/m^3 treated at a hot press temperature of 200 °C for 13 min showed internal bond ~14 kPa [19]. The internal bonding strength of rice straw binderless boards also increased with increasing pressing temperature. At 220 °C only hemicellulose and lignin but also amorphous cellulose were decomposed during the steam treatment. Among the degradation products, 5-hydroxymethylfurfural was supposed to contribute to self-bonding during hot-pressing, while furfural was vaporized from the rice straw [22].

The differences in mechanical properties between the individual steaming temperatures are shown in the ANOVA results in Fig. 8.

The tensile strength values were statistically significantly different for all steaming temperatures ($p < 0.05$). Tukey's HSD test also showed a significant difference in modulus of elasticity for the steaming temperature of 100 °C ($p = 0.0003$). Overall, the value of the modulus of elasticity for the steaming temperature of 200 °C is nearly 62% higher than that for the steaming temperature of 100 °C.

The water vapor storage parameters of the studied rape straw fiberboards are shown in Fig. 9. The moisture content slightly decreased with increasing steaming temperature. The studied fiber insulation material was hygroscopic, but had a lower equilibrium moisture content in comparison with other natural materials, such as hemp, jute, or flax [29]. Similar sorption isotherms of natural thermal insulation materials composed of renewable resources were reported by Korjenic et al. [32]. Slightly higher sorption isotherms were obtained by Fedorik et al. [33] for wood shavings and paper wool. The maximum hygroscopic moisture content reached similar values to those for rape particleboard with bone glue [34].

The thickness swelling in the hygroscopic area was relatively low (Fig. 10). The lowest values (up to 2%) were achieved by the materials steamed at 180 °C and 200 °C, which correlated well with the mechanical properties (Table 3). These results were in a qualitative agreement with Christy et al. [11], where binderless bark boards made at 140 °C swelled by 37% and at 200 °C by only 5%. The swelling in the overhygroscopic range was obviously higher but still significantly lower than for some other binderless fiberboards, e.g., bark fiber boards showed 8–19% [10], Gelam bark 12% [11], flax shives and sunflower bark 60–95% [14], wheat boards 40–70% [17], coconut husk 22–43% [19]. The lower thickness swelling was mainly due to the lower bulk density and lower production pressure.

The water vapor diffusion properties of rape straw fiberboards are presented in Table 4. All studied materials exhibited fast water vapor transport in both dry-cup and wet-cup arrangement which was related to the low density of the samples. The μ-values ranged from 4.3 to 5.6 for the dry cup and from 3.0 to 4.9 for the wet cup and increased with the increasing steaming temperature; this corresponded with the results of the SEM analysis, where for the manufacturing temperatures of 180 °C

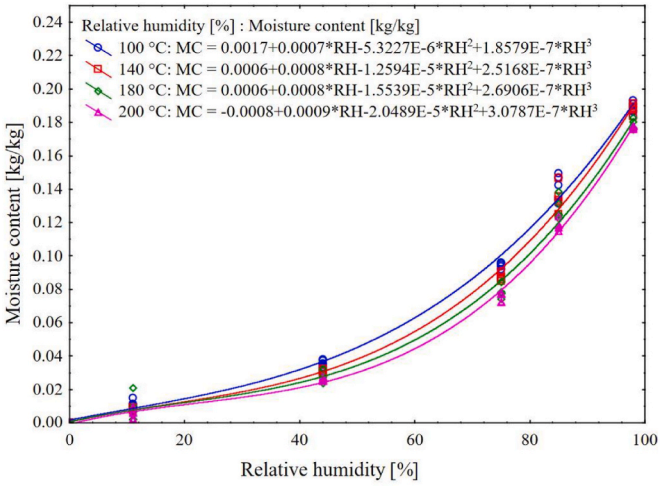

Fig. 9. Sorption isotherms of rape straw fiberboards. The relationship between relative humidity and moisture content corresponds to a cubic polynomial model with coefficients of determination (R^2) of 0.82–0.84.

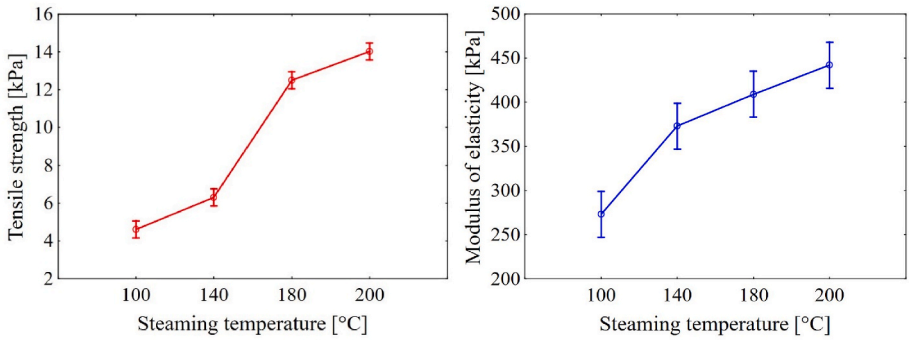

Fig. 8. ANOVA results for tensile strength (left) and modulus of elasticity (right) values according to the steaming temperature. Vertical bars denote 0.95 confidence interval.

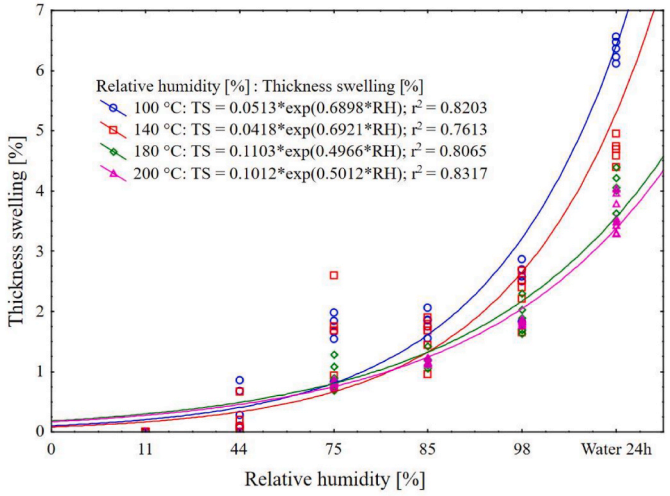

Fig. 10. The effect of steaming temperature on thickness swelling of rape straw fiberboards.

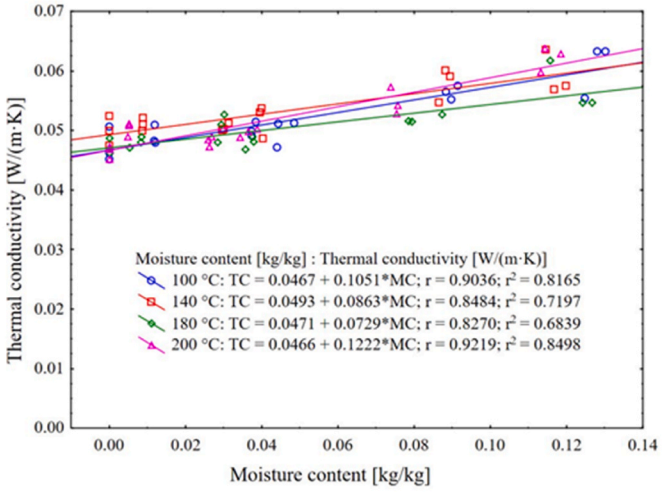

Fig. 11. Moisture dependent thermal conductivity of rape straw fiberboards.

Table 4
Water vapor diffusion properties of rape straw fiberboards with a standard deviation.

Steaming temperature [°C]	Water vapor diffusion permeability [10^{-11} s]		Water vapor diffusion coefficient [10^{-6} m^2 s^{-1}]		Water vapor diffusion resistance factor [−]	
	Dry cup 5–50% RH	Wet cup 75-35% RH	Dry cup 5–50% RH	Wet cup 75-35% RH	Dry cup 5–50% RH	Wet cup 75-35% RH
100	3.87 ± 0.19	5.58 ± 0.52	5.33 ± 0.27	7.68 ± 0.21	4.33 ± 0.23	3.0 ± 0.28
140	3.52 ± 0.22	4.97 ± 0.28	4.84 ± 0.31	6.83 ± 0.17	4.77 ± 0.29	3.4 ± 0.21
180	3.11 ± 0.17	3.40 ± 0.15	4.14 ± 0.23	4.68 ± 0.21	5.59 ± 0.32	4.9 ± 0.22
200	2.97 ± 1.46	3.52 ± 0.33	4.09 ± 2.01	4.84 ± 0.46	5.63 ± 0.23	4.8 ± 0.47

and 200 °C a greater distribution of lignin on the fiber surface was observed. The greater lignin distribution resulted in higher mechanical properties, slightly higher bulk density and affected also the water vapor transport properties. The lignin behavior was summarized in a review article published by Börczök and Pásztory [35]. Under appropriate conditions, the moist lignin incorporated in the wood softens at about 100 °C and allows its molecules to deform in the cell walls. The obtained results were comparable, e.g., with the wood waste particle boards studied by Cetiner et al. [8] and the natural renewable material made from barley straw analyzed by Palumbo et al. [36]. On the other hand, the water vapor diffusion resistance factor of binderless rape straw fiberboards in this paper was much lower than for the particle board produced from rape straw with bone glue [34].

The thermal conductivity of all samples in the dry state (Fig. 11) was within the range of 0.045–0.052 W/(m·K), which was lower than for bark- or coconut binderless fiber boards [10], comparable with resin-bound wood fiberboard [29] or barley straw [36], but somewhat higher than for EPS or mineral wool [37]. The increase of thermal conductivity with the increasing moisture content, u, was very moderate; for u = 0.13 kg/kg the thermal conductivity was in a range of 0.055–0.063 W/(m·K) only, which was several times lower in a comparison with EPS or mineral wool [37]. The specific heat capacity in dry state was for all types of rape straw fiberboards the same, 1380 J/(kg·K), taking into account the error range of the applied measurement method. This value was relatively high compared to mineral wool or polystyrene (770–810 J/(kg·K)) [37] but comparable with some biomaterials, such as the hemp composite analyzed in Ref. [36]. Thermal conductivity increased with increasing moisture content (Fig. 11) and the calculated linear regression models had relatively high coefficients of determination (R^2 = 0.68–0.85). However, in terms of the use of insulating boards in construction, the increase of thermal conductivity in dependence on steaming temperature was not significant.

4. Conclusions

Binderless rape straw fiberboards with a bulk density of ~100 kg/m^3 were designed. The effect of steaming temperature on microstructure and mechanical, hygric and thermal properties were analyzed in the paper. The most important results can be summarized as follows:

- The microstructural analysis showed that with the increasing fiber treatment temperature the proportion of lignin on the surface of fibers and straw particles increased, which was most apparent at the temperatures of 180 °C and higher.
- Both tensile strength and modulus of elasticity of the studied rape straw fiberboards increased remarkably with the increasing steaming temperature up to 200 °C. In the case of tensile strength, the highest difference was observed between 140 °C and 180 °C, which indicated 180 °C as the most effective solution.
- Thickness swelling decreased substantially with increasing steaming temperature.
- The lowest values of thickness swelling in the hygroscopic area (up to 2%) were achieved by the materials steamed at 180 °C and 200 °C, which correlated well with the mechanical properties.
- The thermal conductivity of all samples in the dry state was within the range of 0.045–0.052 W/(m·K), which was only somewhat higher than for EPS or mineral wool. The increase of thermal conductivity with the increasing moisture content was very moderate in the hygroscopic range, up to 0.055–0.063 W/(m·K), which was several times lower in a comparison with EPS or mineral wool.
- Water vapor transport and storage parameters varied only slightly with the changing manufacturing temperature. The relatively low values of water vapor diffusion resistance factor and maximum hygroscopic moisture content implied potential good applicability of

the analyzed fiber boards as thermal insulation materials in the building sector.

Based on the obtained experimental results, it can be concluded that the designed binderless rape straw fiberboards produced at the steaming temperatures of 180 °C and higher achieved the most suitable combination of mechanical, hygric and thermal properties and can be recommended for a potential use as thermal insulation materials in building structures. It should though be noted that while the designed fiberboards can be considered environmentally friendly, as they do not contain synthetic resins, their biodegradability is both a great advantage and disadvantage. Therefore, it is necessary to determine under which conditions they can be used in construction, whether the material is supposed to be impregnated with chemicals or not and, if the impregnation is necessary, which chemicals should be used to maintain the environmental friendliness of the material. These problems need to be addressed in future work.

CRediT authorship contribution statement

Miloš Jerman: Writing – original draft, Resources, Project administration, Methodology, Funding acquisition, Data curation, Conceptualization. **Martin Böhm:** Writing – review & editing, Writing – original draft, Investigation. **Jaroslav Dušek:** Software, Investigation, Data curation. **Robert Černý:** Writing – review & editing, Visualization, Validation, Formal analysis, Conceptualization.

Declaration of competing interest

The authors declare that they have no known competing financial interests or personal relationships that could have appeared to influence the work reported in this paper.

Data availability

Data will be made available on request.

Acknowledgment

This research was supported by the Czech Science Foundation, under project No. 20-12166S.

References

[1] E. Cintura, L. Nunes, B. Esteves, P. Faria, Industrial Crops & Products Agro-industrial wastes as building insulation materials : a review and challenges for Euro-Mediterranean countries, Ind. Crop. Prod. 171 (2021), 113833, https://doi.org/10.1016/j.indcrop.2021.113833.

[2] M. Schulte, Comparative life cycle assessment of bio- based insulation materials : environmental and economic performances. https://doi.org/10.1111/gcbb.12825, 2021, 979-998.

[3] F. Pittau, F. Krause, G. Lumia, G. Habert, Fast-growing bio-based materials as an opportunity for storing carbon in exterior walls, Build. Environ. 129 (2018) 117–129, https://doi.org/10.1016/j.buildenv.2017.12.006.

[4] A. Paiva, S. Pereira, A. Sá, D. Cruz, H. Varum, J. Pinto, A contribution to the thermal insulation performance characterization of corn cob particleboards, Energy Build. 45 (2012) 274–279, https://doi.org/10.1016/j.enbuild.2011.11.019.

[5] M. Palumbo, A.M. Lacasta, M.P. Giraldo, L. Haurie, E. Correal, Bio-based insulation materials and their hygrothermal performance in a building envelope system (ETICS), Energy Build. 174 (2018) 147–155, https://doi.org/10.1016/j.enbuild.2018.06.042.

[6] M. Lee, S. Lee, E. Kang, D. Son, Combustibility and characteristics of wood-fiber insulation boards prepared with four different adhesives, Bioresources 14 (2019) 6316–6330.

[7] M. Nasir, D.P. Khali, M. Jawaid, P.M. Tahir, R. Siakeng, M. Asim, T.A. Khan, Recent development in binderless fiber-board fabrication from agricultural residues : a review, Construct. Build. Mater. 211 (2019) 502–516, https://doi.org/10.1016/j.conbuildmat.2019.03.279.

[8] I. Cetiner, A.D. Shea, Wood waste as an alternative thermal insulation for buildings, Energy Build. 168 (2018) 374–384, https://doi.org/10.1016/j.enbuild.2018.03.019.

[9] F. Segovia, P. Blanchet, N. Auclair, G. Geraud, E. Essoua, Thermo-mechanical properties of a wood fiber insulation board using a bio-based adhesive as a binder, Buildings 10 (2020) 1–15.

[10] J. Gößwald, M.-C. Barbu, A. Petutschnigg, M.E. Tudor, Binderless thermal insulation panels made of spruce bark fibres, Polymers 13 (2021) 1–11, https://doi.org/10.3390/polym13111799.

[11] A.S. Eva Oktoberyani Christy, Soemarno sumardi hadi sumarlan, binderless bark particleboard made from gelem (melaleuce viridiflora sol. Ex geatrtn.) bark waste: the effect of the pressing temperature on its mechanical and physical properties, Bioresources 2 (2021) 4171–4199.

[12] E.M.A. Elbashiry, J. Chen, W. Tuo, Y. Ren, Z. Guo, Review of the pretreatment methods for wheat straw building materials, Reinf. Plast. Compos. 37 (2018) 35–48, https://doi.org/10.1177/0731684417730442.

[13] J.F. Hidalgo-Cordero, T. García-Ortuño, J. García-Navarro, Comparison of binderless boards produced with different tissues of totora (Schoenoplectus californicus (C.A. Mey) Soják) stems, J. Build. Eng. 27 (2020), https://doi.org/10.1016/j.jobe.2019.100961.

[14] A. Mahieu, S. Alix, N. Leblanc, Properties of particleboards made of agricultural by-products with a classical binder or self-bound, Ind. Crop. Prod. 130 (2019) 371–379, https://doi.org/10.1016/j.indcrop.2018.12.094.

[15] X. Zhou, L. Tan, W. Zhang, C. Lv, F. Zheng, R. Zhang, G. Du, B. Tang, X. Liu, Enzymatic hydrolysis lignin derived from corn stover as an intrinstic binder for bio-composites manufacture: effect of fiber moisture content and pressing temperature on boards' properties, Bioresources 6 (2011) 253–264.

[16] X. Zhou, F. Zheng, H. Li, C. Lu, An environment-friendly thermal insulation material from cotton stalk fibers, Energy Build. 42 (2010) 1070–1074, https://doi.org/10.1016/j.enbuild.2010.01.020.

[17] J. Domínguez-Robles, Q. Tarrés, M. Alcalà, N. El Mansouri, A. Rodríguez, P. Mutjé, M. Delgado-aguilar, Development of high-performance binderless fiberboards from wheat straw residue, Construct. Build. Mater. 232 (2020) 1–11, https://doi.org/10.1016/j.conbuildmat.2019.117247.

[18] Z. Jin, J. Li, Q. Wang, W. Su, X. Duan, Z. Tang, Industrial Crops & Products Characterization of multifunctional panels from jute fibers for interior wall covering, Ind. Crop. Prod. 167 (2021), 113530, https://doi.org/10.1016/j.indcrop.2021.113530.

[19] S. Panyakaew, S. Fotios, New thermal insulation boards made from coconut husk and bagasse, Energy Build. 43 (2011) 1732–1739, https://doi.org/10.1016/j.enbuild.2011.03.015.

[20] Y. Kurokochi, M. Sato, Steam treatment to enhance rice straw binderless board focusing hemicellulose and cellulose decomposition products, J. Wood Sci. 66 (2020), https://doi.org/10.1186/s10086-020-1855-8.

[21] M.M. Santos, M.A. Diez, M. Suárez, T.A. Centeno, Innovative particleboard material from the organic fraction of municipal solid waste, J. Build. Eng. 44 (2021), https://doi.org/10.1016/j.jobe.2021.103375.

[22] Y. Kurokochi, M. Sato, Effect of surface structure , wax and silica on the properties of binderless board made from rice straw, Ind. Crop. Prod. 77 (2015) 949–953, https://doi.org/10.1016/j.indcrop.2015.10.007.

[23] Š. Hýsek, M. Gaff, A. Sikora, M. Babiak, New composite material based on winter rapeseed and his elasticity properties as a function of selected factors, Compos. B Eng. 153 (2018) 108–116, https://doi.org/10.1016/j.compositesb.2018.07.042.

[24] M. Viel, F. Collet, C. Lanos, Chemical and multi-physical characterization of agro-resources' by-product as a possible raw building material, Ind. Crop. Prod. 120 (2018) 214–237, https://doi.org/10.1016/j.indcrop.2018.04.025.

[25] D. Dukarska, R. Czarnecki, D. Dziurka, R. Mirski, Construction particleboards made from rapeseed straw glued with hybrid pMDI/PF resin, Eur. J. Wood Wood Prod. 75 (2017) 175–184, https://doi.org/10.1007/s00107-016-1143-x.

[26] ČSN EN 1602, Thermal Insulating Products for Building Application - Determination of the Apparent Density, Czech Office for Standards, Metrology and Testing, Prague, 2013 (n.d).

[27] ČSN EN 317, Particleboards, fibreboards, Determination of Swelling in Thickness after Immersion in Water, Czech Office for Standards, Metrology and Testing, Prague, 1995.

[28] ČSN EN 1607, Thermal Insulating Products for Building Applications – Determination of Tensile Strength Perpendicular to Faces, Czech Office for Standards, Metrology and Testing, Prague, 2013 (n.d).

[29] M. Jerman, I. Palomar, V. Kočí, R. Černý, Thermal and hygric properties of biomaterials suitable for interior thermal insulation systems in historical and traditional buildings, Build. Environ. 154 (2019) 81–88, https://doi.org/10.1016/j.buildenv.2019.03.020.

[30] ČSN EN ISO 12572, Hygrothermal Performance of Building Materials and Products - Determination of Water Vapour Transmission Properties - Cup Method, Czech Office for Standards, Metrology and Testing, Prague, 2017 (n.d).

[31] J. Domínguez-Robles, Q. Tarrés, M. Delgado-Aguilar, A. Rodríguez, F.X. Espinach, P. Mutjé, Approaching a new generation of fiberboards taking advantage of self lignin as green adhesive, Int. J. Biol. Macromol. 108 (2018) 927–935, https://doi.org/10.1016/j.ijbiomac.2017.11.005.

[32] A. Korjenic, V. Petránek, J. Zach, J. Hroudová, Development and performance evaluation of natural thermal-insulation materials composed of renewable resources, Energy Build. 43 (2011) 2518–2523, https://doi.org/10.1016/j.enbuild.2011.06.012.

[33] F. Fedorik, J. Zach, M. Lehto, H. Kymäläinen, R. Kuisma, M. Jallinoja, K. Illikainen, S. Alitalo, Energy & Buildings Hygrothermal properties of advanced bio-based insulation materials, Energy Build. 253 (2021), 111528, https://doi.org/10.1016/j.enbuild.2021.111528.

[34] J. Dušek, M. Jerman, M. Podlena, M. Böhm, C. Robert, Sustainable composite material based on surface-modified rape straw and environment-friendly adhesive,

Construct. Build. Mater. 300 (2021), https://doi.org/10.1016/j.conbuildmat.2021.124036.

[35] Z. Börcsök, Z. Pásztory, The role of lignin in wood working processes using elevated temperatures: an abbreviated literature survey, Eur. J. Wood Wood Prod. 79 (2021) 511–526, https://doi.org/10.1007/s00107-020-01637-3.

[36] M. Palumbo, A.M. Lacasta, N. Holcroft, A. Shea, P. Walker, Determination of hygrothermal parameters of experimental and commercial bio-based insulation materials, Construct. Build. Mater. 124 (2016) 269–275, https://doi.org/10.1016/j.conbuildmat.2016.07.106.

[37] M. Jerman, R. Černý, Effect of moisture content on heat and moisture transport and storage properties of thermal insulation materials, Energy Build. 53 (2012) 39–46, https://doi.org/10.1016/j.enbuild.2012.07.002.

7. Conclusions and direction of future research

This list of articles provides information on the determination of a complete set of material transport and accumulation parameters. The effect of the pore size distribution curve on moisture, and subsequently on thermal properties, has been demonstrated. Pore size also influences freeze-thaw resistance. The freezing resistance and cyclic behavior of the material during wetting and drying are also discussed. The knowledge gained can be applied in materials engineering, particularly in the research and development of new materials and in the evaluation of building structures. In the final paper presented, a new eco-friendly thermal insulation material has been developed, with further advancements expected. It is anticipated that the knowledge gained from this theoretical research will be applied in practical research, eventually leading to the introduction of new products to the market.

- The theoretical research will deal with the development and quality of the self-adhesive properties of lignin contained in fibers from post-harvest residues, specifically rapeseed straw. These are influenced by several factors. The first is the interfacial interface of the fibers, which is influenced by straw pulping technology. In particular, temperature, humidity during the pulping process, and the distance between the discs are important factors influencing fiber size and surface properties. The fibers obtained will be analyzed using microscopic and chemical techniques. The sub-objectives will be:
    - Development and research of thermal insulation boards from secondary agricultural production such as straw. This biomass contains lignin, which acts as a binder under certain conditions. The effect of temperature, humidity, and pressure on the morphology and self-adhesive properties of lignin will be investigated.
- The practical research will build on the findings obtained within the framework of the GACR grant 20-12166S, during which cooperation was established with the German institute IHD Dresden, where thin fibers from rapeseed straw were produced. The possibilities of their use will be the subject of further research. The aim is to use the theoretical knowledge in practice. CIUR a.s. was approached

and several applied projects were submitted through the TACR agency. The main topics are:

- Research and development of new blown-in thermal insulation made of rapeseed fibers obtained in connection with the solution of GACR 20-12166S.
- Development of new blown-in thermal insulation from renewable raw materials from agriculture and forestry. This will be insulation with a predominant share of cellulose from different types of cereals and similar plant residues and wood pulp.
- Further developments could focus on the development of blown-in thermal insulation from difficult-to-process municipal waste based on cardboard.
- Newly developed insulations would need to be chemically treated to have the required reaction to fire and be resistant to biocorrosion. Chemical treatment will be part of further development.
- An important issue is the recycling of natural materials at the end of their useful life. One solution is to convert this material into biochar that can be reused in agriculture or for water purification. This would complete the life cycle of the product in the sense of a circular economy. Biochar can be produced by pyrolysis.

References

[1] J.F. Luhr, Earth, Dorling Kindersley Limited, London, 2005.

[2] S. Stanca, Improving energy efficiency in a building using passiva energy-saving measures, J. Appl. Eng. Sci. 13 (2023) 269–274. https://doi.org/10.2478/jaes-2023-0034.

[3] I. Cetiner, A.D. Shea, Wood waste as an alternative thermal insulation for buildings, Energy Build. 168 (2018) 374–384. https://doi.org/10.1016/j.enbuild.2018.03.019.

[4] W. Liang, X. Di, S. Zheng, L. Wu, J. Zhang, A study on thermal bridge effect of vacuum insulation panels (VIPs), J. Build. Eng. 71 (2023) 106492. https://doi.org/10.1016/j.jobe.2023.106492.

[5] F. Gubbels, D.D. Santi, V. Baily, Durability of vacuum insulation panels in the cavity of an insulating glass unit, Build. Phys. 38(6) (2015) 485–499. https://doi.org/10.1177/1744259114522118.

[6] P.B. Jelle, Traditional, state-of-the-art and future thermal building insulation materials and solutions – Properties, requirements and possibilities, Energy Build. 43 (2011) 2549–2563. https://doi.org/10.1016/j.enbuild.2011.05.015.

[7] J. Laskowski, B. Milow, L. Ratke, Aerogel – aerogel composites for normal temperature range thermal insulations, J. Non. Cryst. Solids. 441 (2016) 42–48. https://doi.org/10.1016/j.jnoncrysol.2016.03.020.

[8] F. Pittau, F. Krause, G. Lumia, G. Habert, Fast-growing bio-based materials as an opportunity for storing carbon in exterior walls, Build. Environ. 129 (2018) 117–129. https://doi.org/10.1016/j.buildenv.2017.12.006.

[9] M. Jerman, Utilization of natural materials in building engineering, Habilitation thesis, CTU, Prague, 2020.

[10] B.K. Stefanowski, S.F. Curling, G.A. Ormondroyd, Assessment of lignocellulosic nut wastes as an absorbent for gaseous formaldehyde, Ind. Crop. Prod. 98 (2017) 25–28. https://doi.org/10.1016/j.indcrop.2017.01.012.

[11] L. Svoboda, Stavební hmoty, Jaga Group s.r.o., 2007.

[12] Y. Wang, K. Liu, Y. Liu, D. Wang, J. Liu, The impact of temperature and relative humidity dependent thermal conductivity of insulation materials on heat transfer through the building envelope, J. Build. Eng. 46 (2022) 103700. https://doi.org/10.1016/j.jobe.2021.103700.

[13] G.G. Akkurt, N. Aste, J. Borderon, A. Buda, M. Calzolari, D. Chung, V. Costanzo, C. Del Pero, G. Evola, H.E. Huerto-cardenas, F. Leonforte, A. Lo Faro, E. Lucchi, L. Marletta, F. Nocera, V. Pracchi, C. Turhan, Dynamic thermal and hygrometric simulation of historical buildings : Critical factors and possible solutions, Renew. Sustain. Energy Rev. 118 (2020) 109509. https://doi.org/10.1016/j.rser.2019.109509.

[14] M. Caniato, A. Marzi, S. Monteiro, A. Gasparella, A review of the thermal and acoustic properties of materials for timber building construction, J. Build. Eng. 43 (2021) 103066. https://doi.org/10.1016/j.jobe.2021.103066.

[15] ČSN 73 1353 Determination of thermal conductivity of autoclaved aerated concrete, Czech Office for Standards, Metrology and Testing, Prague, 2010.

[16] ČSN EN 678, Determination of the dry density of autoclave aerated concrete, Czech Office for Standards, Metrology and Testing, Prague, 1995.

[17] ČSN EN 12390-7:2009 Testing hardened concrete – Part 7: Density of hardened concrete, Czech Office for Standards, Metrology and Testing, Prague 2009.

[18] ČSN EN 772-4 Methods of test for masonry units - Part 4: Determination of real and bulk density and of total and open porosity for natural stone masonry units, Czech Office for Standards, Metrology and Testing, Prague 1999.

[19] M. Jerman, R. Černý, Effect of moisture content on heat and moisture transport and storage properties of thermal insulation materials ˇ, Energy Build. 53 (2012)

39–46. https://doi.org/10.1016/j.conbuildmat.2017.06.087.

[20] M. Jerman, M. Keppert, J. Výborný, R. Černý, Hygric, thermal and durability properties of autoclaved aerated concrete, Construction and Building Materials, 41 (2013) 352–359. https://doi.org/10.1016/j.conbuildmat.2012.12.036.

[21] ČSN EN ISO 1183-3, Plastics - Methods for determining the density of non-cellular plastics - Part 3: Gas pyknometer method, Czech Office for Standards, Metrology and Testing, Prague, 2000.

[22] M. Jerman, L. Scheinherrová, I. Medved, J. Krejsová, M. Doleželová, P. Bezdička, R. Černý, Effect of cyclic wetting and drying on microstructure, composition and length changes of lime-based plasters, Cem. Concr. Compos. 104 (2019). https://doi.org/10.1016/j.cemconcomp.2019.103411.

[23] ČSN EN 680 Determination of the drying shrinkage of autoclaved aerated concrete, Czech, 2006.

[24] Jerman, M.; Výborný, J.; Černý, R. Drying shrinkage of autoclaved aerated concrete, Thermophysics 2011. Brno: VUT Brno, 2011. pp. 72-76. ISBN 978-80-214-4345-7.

[25] M. Jerman, I. Medved, R. Černý, Length changes of autoclaved aerated concrete exposed to cyclic wetting and drying, Cem. Wapno Bet. 20 (2015) 139.

[26] ČSN 73 1322 Stanovení mrazuvzdornosti betonu, Czech Office for Standards, Metrology and Testing, Prague, 1969.

[27] ČSN EN 15304 Determination of the freeze-thaw resistance of autoclaved aerated concrete, Czech Office for Standards, Metrology and Testing, Prague, 2010.

[28] ČSN EN 679 Determination of the compressive strength of autoclaved aerated concrete, Czech Office for Standards, Metrology and Testing, Prague, 2006.

[29] R. Drochytka, Pórobeton, VUTIUM, Brno, 1999.

[30] ČSN EN 1015-18 Methods of test for mortar for masonry - Part 18: Determination of water absorption coefficient due to capillarity action of

hardened mortar, Czech Office for Standards, Metrology and Testing, Prague, 2003.

[31] ČSN EN ISO 15148 Hygrothermal performance of building materials and products - Determination of water absorption coefficient by partial immersion, Czech Office for Standards, Metrology and Testing, Prague, 2004.

[32] J. Lu, K. Wang, M. Qu, Experimental determination on the capillary water absorption coefficient of porous building materials : A comparison between the intermittent and continuous absorption tests, J. Build. Eng. 28 (2020) 101091. https://doi.org/10.1016/j.jobe.2019.101091.

[33] R. Černý et. al., Počítačové a experimentální metody pro stanovení vlivu proměnlivého prostředí na degradaci historického zdiva, České vysoké učení technické v Praze, 2013.

[34] ČSN EN ISO 12572, Hygrothermal performance of building materials and products - Determination of water vapor transmission properties - Cup method, Czech Office for Standards, Metrology and Testing, Prague, 2017., n.d.

[35] M. Jerman, I. Palomar, V. Kočí, R. Černý, Thermal and hygric properties of biomaterials suitable for interior thermal insulation systems in historical and traditional buildings, Build. Environ. 154 (2019) 81–88. https://doi.org/10.1016/j.buildenv.2019.03.020.

[36] M. Jerman, M. Böhm, J. Dušek, R. Černý, Effect of steaming temperature on microstructure and mechanical, hygric, and thermal properties of binderless rape straw fiberboards, 223 (2022). https://doi.org/10.1016/j.buildenv.2022.109474.

[37] ČSN EN ISO 16536 Thermal insulating products for building applications – Determination of long-term water absorption by diffusion, Czech Office for Standards, Metrology and Testing, Prague, 2020.

[38] Z. Pavlík, J. Žumár, I. Medveď, R. Černý, Water vapor adsorption in porous building materials: Experimental measurement and theoretical analysis., Transp. Porous Media. 19 (2012) 939–954.

[39] M.E.L. Assaad, T. Colinart, T. Lecompte, Thermal conductivity assessment of moist building insulation material using a Heat Flow Meter apparatus, Build. Environ. 234 (2023) 110184. https://doi.org/10.1016/j.buildenv.2023.110184.

[40] ČSN EN ISO 10456 Building materials and products – Hygrothermal properties – Tabulated design values and procedures for determining declared and design thermal values (ISO 10456:2007), 2009.

[41] M. Ayadi, C. Segovia, A. Baffoun, R. Zouari, V. Fierro, A. Celzard, S. Msahli, N. Brosse, Influence of Anatomy, Microstructure, and Composition of Natural Fibers on the Performance of Thermal Insulation Panels, (2023). https://doi.org/10.1021/acsomega.3c02481.

[42] ČSN EN 12667 Thermal performance of building materials and products - Determination of thermal resistance by means of guarded hot plate and heat flow meter methods - Products of high and medium thermal resistance, Czech Office for Standards, Metrology and Testing, Prague, 2001.

[43] ČSN 72 7012-2 (727012) Determination of Steady State Thermal Conductivity of Materials. Hot Plate Methods. Guarded Hot Plate Method, Czech Office for Standards, Metrology and Testing, Prague, 1994.

[44] ISO 10051:1996 Thermal insulation — Moisture effects on heat transfer — Determination of thermal transmissivity of a moist material, 1996.

[45] L. Fiala, M. Jerman, P. Reiterman, R. Cerný, Determination of Thermal Conductivity of Silicate Matrix for Applications in Effective Media Theory, Int. J. Thermopysics. 39 (2018) 1–12. https://doi.org/10.1007/s10765-017-2347-y.

[46] F. Pittau, F. Krause, G. Lumia, G. Habert, Fast-growing bio-based materials as an opportunity for storing carbon in exterior walls, Build. Environ. 129 (2018) 117–129. https://doi.org/10.1016/j.buildenv.2017.12.006.

[47] S. Pereira, M. Correia, J. Pinto, A. Ramos, A. Briga-s, I. Bentes, C.A. Teixeira, Thermal performance and life cycle assessment of corn cob particleboards, J. Build. Eng. 44 (2021) 102998. https://doi.org/10.1016/j.jobe.2021.102998.

[48] K. Zhang, S. Zheng, Y. Liu, J. Lin, Isolation of hierarchical cellulose building blocks from natural flax fibers as a separation membrane barrier, Int. J. Biol. Macromol. 155 (2020) 666–673. https://doi.org/10.1016/j.ijbiomac.2020.03.225.

[49] P. Raja, V. Murugan, S. Ravichandran, L. Behera, R.A. Mensah, S. Mani, A. Kasi, K. Babu, N. Balasubramanian, G. Sas, H. Vahabi, O. Das, A Review of Sustainable Bio-Based Insulation Materials for Energy-Efficient Buildings, Macro Molecular. 2300086 (2023) 1–11. https://doi.org/10.1002/mame.202300086.

[50] Z. Moujoud, S. Sair, H. Ait, I. Ayouch, A. El, O. Tanane, Geopolymer composites reinforced with natural fibers: A review of recent advances in processing and properties, Constr. Build. Mater. 388 (2023) 131666. https://doi.org/10.1016/j.conbuildmat.2023.131666.

[51] J. Chybík, Přírodní stavební materiály, Grada Publishing, a.s., 2009.

[52] H. Kymäläinen, A. Sjöberg, Flax and hemp fibers as raw materials for thermal insulations, Build. Environ. 43 (2008) 1261–1269. https://doi.org/10.1016/j.buildenv.2007.03.006.

[53] M.P. Sáez-Pérez, M. Brümmer, J.A. Durán-Suárez, A review of the factors affecting the properties and performance of hemp aggregate concretes, J. Build. Eng. 31 (2020). https://doi.org/10.1016/j.jobe.2020.101323.

[54] S.L. Platt, P. Walker, D. Maskell, A. Shea, F. Bacoup, A. Mahieu, H. Zmamou, R. Gattin, Sustainable bio & waste resources for thermal insulation of buildings, Constr. Build. Mater. 366 (2023) 130030. https://doi.org/10.1016/j.conbuildmat.2022.130030.

[55] A.Y. Oumeziane, S. Moissette, M. Bart, C. Lanos, Influence of temperature on sorption process in hemp concrete, Constr. Build. Mater. 106 (2016) 600–607. https://doi.org/10.1016/j.conbuildmat.2015.12.117.

[56] S. Pantawee, T. Sinsiri, C. Jaturapitakkul, P. Chindaprasirt, Utilization of hemp concrete using hemp shiv as coarse aggregate with aluminium sulfate [Al2(SO4)3] and hydrated lime [Ca(OH)2] treatment, Constr. Build. Mater. 156 (2017) 435–442. https://doi.org/10.1016/j.conbuildmat.2017.08.181.

[57] J. Dušek, M. Jerman, M. Podlena, M. Böhm, R. Černý, Sustainable composite material based on surface-modified rape straw and environment-friendly adhesive, Constr. Build. Mater. 300 (2021). https://doi.org/10.1016/j.conbuildmat.2021.124036.

[58] S. Elfordy, F. Lucas, F. Tancret, Y. Scudeller, L. Goudet, Mechanical and thermal properties of lime and hemp concrete ("hempcrete") manufactured by a projection process, Constr. Build. Mater. 22 (2008) 2116–2123. https://doi.org/10.1016/j.conbuildmat.2007.07.016.

[59] S. Baladivakar, M. Starvin, J. Raj, Mechanical and Thermal Characteristics of Hybrid Composites Fortified with Flax, Banyan, and Glass Fibers for Automobile Safety Applications, J. Nat. Fibers. 19 (2022). https://doi.org/10.1080/15440478.2022.2125923.

[60] F. Fedorik, J. Zach, M. Lehto, H. Kymäläinen, R. Kuisma, M. Jallinoja, K. Illikainen, S. Alitalo, Energy & Buildings Hygrothermal properties of advanced bio-based insulation materials, Energy Build. 253 (2021) 111528. https://doi.org/10.1016/j.enbuild.2021.111528.

[61] R.K. Cheedarala, K.V. Chalapathi, J. Il Song, Delayed Flammability for Natural Fabrics by Deposition of Silica Core-Amine Shell Microspheres through Dip-Coating Process, Chem. Eng. J. Adv. 8 (2021) 100164. https://doi.org/10.1016/j.ceja.2021.100164.

[62] N.M. Aly, H.S. Seddeq, K. Elnagar, T. Hamouda, Acoustic and thermal performance of sustainable fiber reinforced thermoplastic composite panels for insulation in buildings, J. Build. Eng. 40 (2021). https://doi.org/10.1016/j.jobe.2021.102747.

[63] A. Majumder, M. Achenza, C. Carlo, R. Baccoli, A. Frattolillo, Energy & Buildings Thermo-acoustic building insulation materials fabricated with recycled fibers – Jute, Wool and Loofah, Energy Build. 293 (2023) 113211. https://doi.org/10.1016/j.enbuild.2023.113211.

[64] CSO [Czech Statistical Office] Inventory of farm animals - 2022 In: Czech

Statistical Office [online]. [Prague]: Czech Statistical Office. Generated 16.05.2024 [vid. 2024-05-16]. Available: https://www.czso.cz/documents/10180/165456702/2701422209.pdf/739b, (n.d.).

[65] J. Zach, A. Korjenic, V. Petránek, J. Hroudová, T. Bednar, Performance evaluation and research of alternative thermal insulations based on sheep wool, Energy Build. 49 (2012) 246–253. https://doi.org/10.1016/j.enbuild.2012.02.014.

[66] Z. Ye, C.M. Wells, C.G. Carrington, N.J. Hewitt, Thermal conductivity of wool and wool – hemp insulation, (2006) 37–49. Internatioal J. Energy Res.(2006) 30: 37–49 https://doi.org/10.1002/er.1123.

[67] D. Kumar, M. Alam, P.X.W. Zou, J.G. Sanjayan, R. Ahmed, Comparative analysis of building insulation material properties and performance, Renew. Sustain. Energy Rev. 131 (2020) 110038. https://doi.org/10.1016/j.rser.2020.110038.

[68] E.M.A. Elbashiry, J. Chen, W. Tuo, Y. Ren, Z. Guo, Review of the pretreatment methods for wheat straw building materials, Reinf. Plast. Compos. 37 (2018) 35–48. https://doi.org/10.1177/0731684417730442.

[69] J.F. Hidalgo-Cordero, T. García-Ortuño, J. García-Navarro, Comparison of binderless boards produced with different tissues of totora (Schoenoplectus californicus (C.A. Mey) Soják) stems, J. Build. Eng. 27 (2020). https://doi.org/10.1016/j.jobe.2019.100961.

[70] G.I. Mantanis, E.T. Athanassiadou, M.C. Barbu, K. Wijnendaele, Adhesive systems used in the European particleboard, MDF and OSB industries, Wood Mater. Sci. Eng. 13 (2018) 104–116. https://doi.org/10.1080/17480272.2017.1396622.

[71] M. Nasir, D.P. Khali, M. Jawaid, P.M. Tahir, R. Siakeng, M. Asim, T.A. Khan, Recent development in binderless fiber-board fabrication from agricultural residues: A review, Constr. Build. Mater. 211 (2019) 502–516. https://doi.org/10.1016/j.conbuildmat.2019.03.279.

[72] E. Cintura, L. Nunes, B. Esteves, P. Faria, Industrial Crops & Products Agro-

industrial wastes as building insulation materials : A review and challenges for Euro-Mediterranean countries, Ind. Crop. Prod. 171 (2021) 113833. https://doi.org/10.1016/j.indcrop.2021.113833.

[73] C. Cosereanu, C. Cerbu, Morphology, Physical, and Mechanical Properties of Particleboard Made from Rape Straw and Wood Particles Glued with Urea-Formaldehyde Resin, BioResources. 14 (2019) 2903–2918.

[74] R. Mirski, A. Derkowski, D. Dziurka, M. Wieruszewski, D. Dukarska, Effects of chip type on the properties of chip-sawdust boards glued with polymeric diphenyl methane diisocyanate, Materials (Basel). 13 (2020). https://doi.org/10.3390/ma13061329.

[75] Sunardi, M. Fawaid, R. Lusiani, S.B. Aji Kesworo, T.D. Widodo, The Effect of Wood Sawdust Mesh Combination on Mechanical Behavior of Particle Board, IOP Conf. Ser. Mater. Sci. Eng. 494 (2019). https://doi.org/10.1088/1757-899X/494/1/012089.

[76] M. Budakci, The determination of adhesion strength of wood veneer and synthetic resin panel (laminate) adhesives, Wood Res. 55 (2010) 125–136.

[77] A. Mahieu, S. Alix, N. Leblanc, Properties of particleboards made of agricultural by-products with a classical binder or self-bound, Ind. Crops Prod. 130 (2019) 371–379. https://doi.org/10.1016/j.indcrop.2018.12.094.

[78] CSO [Czech Statistical Office]Sown areas of winter crops for harvest in 2024 In: Czech Statistical Office [online]. [Prague]: Czech Statistical Office. Generated 16.05.2024 [vid. 2024-05-16]. Available:https://www.czso.cz/csu/czso/osevni-plochy-ozimych-pl, n.d.

[79] R. Mirski, D. Dziurka, R. Czarnecki, The Possibility of Replacing Strands in the Core Layer of Oriented Strand Board by Particles from the Stems of Rape (Brassica napus L. var. napus), BioResources. 11 (2016) 9273–9279. https://doi.org/10.15376/biores.11.4.9273-9279.